

PSD v 2.0

September 22, 2020

Contents

1	Introduction	3
1.1	Introduction	3
1.2	PSD evolution	3
1.2.1	Version 2.1 (currently under development)	3
1.2.2	Version 2.0 - 2020-08-18	3
1.2.3	Version 1.8 - 2020-01-21	5
1.2.4	Version 1.7 - 2019-11-08	5
1.2.5	Version 1.6 - 2019-06-11	6
1.2.6	Version 1.5 - 2019-05-29	6
1.2.7	Version 1.4 - 2019-05-14	6
1.2.8	Version 1.3 - 2019-04-08	7
1.2.9	Version 1.2 - 2019-03-18	7
1.2.10	Version 1.1 - 2019-03-04	8
1.2.11	Version 1.0 - 2019-02-15	8
1.2.12	Version git tags	8
2	Installation	9
2.1	Dependencies	9
2.2	PSD installation steps	9
2.3	Update PSD to the latest version	10
2.4	PSD developers version	10
3	Theoretical background	11
3.1	Elastostatics	11
3.2	Elastodynamics	12
3.3	Time discretization	13
3.3.1	Generalized- α method	13
3.3.2	Time discretized variational problem (no damping)	14
3.3.3	Time discretized variational problem (Rayleigh damping)	15
3.3.4	Implicit N- β and HHT- α method as special cases	17
3.3.5	Considerations on methods based upon operator splitting	17
3.4	Space discretization	17
3.5	Linear and nonlinear dynamic solvers	18
3.5.1	Linear case - linear elastic material behavior	18
3.5.2	Nonlinear case - inelastic material behaviors (under implementation)	18
3.6	Paraxial formulation for absorbing layers	19
3.6.1	Standard formulation	20
3.6.2	Accounting for incident waves	21
4	Tutorials	22
4.1	Linear Elasticity	22
4.1.1	PSD simulation of 2D bar problem bending under own body weight	23

4.1.2	PSD simulation of 2D bar problem clamped at both ends	24
4.1.3	PSD simulation of 2D bar problem clamped at one end while being pulled at the other end (Dirichlet-Dirichlet case)	25
4.1.4	PSD simulation of 2D bar problem clamped at one end while being pulled at the other end (Dirichlet-Neumann case)	26
4.1.5	PSD simulation of 2D bar problem clamped at one end while being pulled at the other end (Dirichlet-Neumann-Point boundary conditions case)	27
4.1.6	PSD simulation of 3D bar problem clamped at one end while being pulled at the other end (Dirichlet-Neumann case)	28
4.1.7	PSD simulation of 3D mechanical piece (Dirichlet-Neumann case) with complex mesh	29
4.2	Damage mechanics	31
4.2.1	Hybrid phase-field for damage	31
4.3	Elastodynamics	32
4.4	Soil dynamics	33
4.5	General list of examples	34
5	Validation	41
5.1	Linear elasticity solver validation and verification using method of manufactured solutions	41
5.1.1	Introduction	41
5.1.2	Verification tests with the method of manufactured solutions	42
5.1.3	FEM solving model	43
5.1.4	The FEM solver	43
5.2	Damage mechanics solver validation	45
5.3	Validating the PSD soil-dynamic solver with paraxial boundary conditions	48
5.3.1	Numerical experiment 1: A two-dimensional square	48
5.3.2	Test 1: top loading of the square	49
5.3.3	Test 2: bottom loading of the square	49
5.3.4	Numerical experiment 2: 3D case with complex geometry	49
6	Functions and descriptions	58
6.1	Flags for PSD_PreProcess	58
6.1.1	Integer type flags used for PSD_PreProcess	58
6.1.2	String type flags used for PSD_PreProcess	58
6.1.3	Bool type flags used for PSD_PreProcess	59
6.2	Flags as per physics	59
6.3	Functions in gofastplugins.cpp	59
6.3.1	GFPeigen	59
6.3.2	GFPeigenAlone	60
6.3.3	GFPmaxinttwoFEfields	60
7	Gallery	61

Chapter 1

Introduction

1.1 Introduction

PSD acronym for Parallel Solid/Structural/Seismic Dynamics, is a finite elements-based solid mechanics solver with capabilities of performing High Performance Computing (HPC) simulations with billions of unknowns. The kernel of PSD is wrapped around FreeFEM for finite element discretization, and PETSc for linear algebra/Preconditioning. PSD solver contains straightforward supports for static or dynamic simulations with linear and nonlinear solid mechanics problems. Besides these hybrid-phase field fracture mechanics models have also been incorporated within PSD. For dynamics the generalized- α model for time discretization is used, this models enable straightforward use of Newmark- β , central difference, or HHT as time discretization. PSD uses state-of-the art domain-decomposition paradigm via vectorial finite elements for parallel computing and all solvers are proven to scale quasi-optimally. PSD has proven scalability up to 13,000 cores with largest problem solved containing over 5 Billion unknowns.

1.2 PSD evolution

PSD has been maturing and evolving with time, following subsections present the highlights of some key changes made to each PSD version.

1.2.1 Version 2.1 (currently under development)

Added

- New accurate force calculations via matrix-vector product: new flag `-getreactionforce`.
- New flag `-reactionforce` variational-based | stress-based to get reaction force on a surface.
- New flag `-plotreactionforce` to activate real time pipe plotting using GnuPlot.

Removed

- Flag `-pipegnu` not supported for damage mechanics (to be further deprecated from elsto/soildynamics)

1.2.2 Version 2.0 - 2020-08-18

Added

- New preprocessing via C++, `PSD_PreProcess` binary.
- New solving via shell wrapper `PSD_Solve` instead of `FreeFem++` or `FreeFem++-mpi`.
- Scripting is now handled in `.hpp` files.

- New time discretization option `-timediscretization [string]` for dynamic simulation, with `[string]` choose between the following options `generalized-alpha`, `newmark-beta`, and `hht`.
- New Dirichlet point boundary conditions by `-dirichletpointconditions [int]` flag, with `[int]` number of Dirichlet point conditions.
- Paraxial element support for solidynamics extended to 3D.
- New point boundary conditions.
- New dummy city mesh and analysis 2D for soil dynamics.
- Automatic identification of FreeFEM and Gmsh during `./configure`.
- New flags for `-with-FreeFEM=` and `-with-Gmsh=` during `./configure`.
- New flag `-problem linear-elasticity|damage|elastodynamics|soildynamics` to define physics.
- New flag `-model` to set approximation for damage mechanics `hybrid-phase-field|Mazar`.
- Better energy splitting included Hybrid phase-field compressibility vs tensile energy condition.
- Introduce boundary conditions via `-dirichletconditions [int]` flag.
- Introduce point boundary conditions via `-dirichletpointcondition [int]` flag.
- Introduce traction boundary conditions via `-tractionconditions [int]` flag.
- New folder `tests` containing unit-tests for modules.
- New Hujeux law (nonlinear soil law) coupling using C++ class (Thanks to Evelyne Foerster).
- New pseudo-nonlinear model for solving elastodynamics and soildynamics with nonlinear Newton-Raphsons.
- New option `-nonlinearmethod Picard | Newton-Raphsons | pseudo-nonlinear`.
- Introduced double couple earthquake source boundary condition for soildynamics.
- New flag `-doublecouple force-based | displacement-based` to use double couple source for soil-dynamics.
- New top-ii-vol parallel meshing via `-top2vol-meshing` flag (compatible with soildynamics).

Changed

- Moved to FreeFEM 4.6.
- Moved to PETSc 13.13.
- Moved to C++ for preprocessing.
- Dirichlet conditions handled now by `-dirichletconditions [int]` flag, with `[int]` number of Dirichlet conditions.
- Traction conditions handled now by `-tractionconditions [int]` flag, with `[int]` number of traction conditions.
- Body force conditions handled now by `-bodyforceconditions [int]` flag, with `[int]` regions under bodyforce.
- Changes to GFP energydecoposition plugin `DecompEnergy_0p`, now includes compressibility history.
- Replaced GFPDecompEnergy2D/GFPDecompEnergy3D by a generic 2D/3D function `GFPSSplitEnergy`.
- Postprocessing flag `-postprocess` options now support `u , v, a , uv, ua, av, uav, d or ud`.

Removed

- No more `FFINSTALLDIR` and `GMSH` variables during `make` and `make check`.
- Deprecated PSD flag `plot` flag now handled by `postprocess`.
- Deprecated PSD flag `nonlinear` flag now handled by `problem` and `model`.
- Deprecated PSD flag `bodyforce` flag now handled by an `int` valued `bodyforceconditions`.
- Deprecated PSD flag `dynamic` flag now handled by `problem` and `model`.
- Deprecated PSD flag `soildynamic` flag now handled by `problem` and `model`.
- Deprecated PSD flag `quasistatic` flag now handled by `problem` and `model`.
- Deprecated PSD flag `dirichletbc` flag now handled by `dirichletconditions`.

1.2.3 Version 1.8 - 2020-01-21

Added

- New soil dynamic module `-soildynamics`
- New paraxial element support in 2D.
- New timeplotting support `timepv`
- New `-postprocess` option for postprocessing `u`, `v`, `a`, or `uav`.

Changed

- Moved to FreeFEM 4.4.2.
- Moved to PETSc 13.12.
- New simpler way of plotting `savevtk` in parallel with `append` flag for iterative solutions.
- VTU files get stored with a date and time stamp.
- New way of maintaining a logfile for all simulations (date,time,case,...) in `simulation-log.csv`.

1.2.4 Version 1.7 - 2019-11-08

Added

- New mesh reordering via Reverse Cuthill-Mackee via `-useRCM`.
- New quasi-static parallel solver (Extension of B.Masseran & G.Rastiello sequential version).
- New GFP plugin for Mazar's damage update for 2D/3D problems `GFPMazarsDamageUpdate(...)`.
- New MPI plotting routine `plotJustMeshMPI()`.
- New option `-fastmethod` to switch back to default variational formulation.
- New make flag for compiling on supercomputer.

Changed

- Changed variational formulation now using $\epsilon(u) : A : \epsilon(v)$.
- Using GFP becomes optional `-useGFP`.
- Better documentation via `.md` and `.html` files.
- Better plotting support for `PlotMPI()`.
- Moved to FreeFEM 4.4.

1.2.5 Version 1.6 - 2019-06-11

Added

- Dynamic linear solver in 2D and 3D parallel/sequential.
- New finite element variable for partition of unity for fixing integrals.

Changed

- Better documentation via .md and .html files.
- Correct quadrature order for faster computations.
- Major changes/splitting of .script files.

Removed

- Removed the `BoundaryAndSourceConditions.script` merged with `ControlParameters.script`.

Bugs

- Bug in integrals fixed.

1.2.6 Version 1.5 - 2019-05-29

Added

- Dynamic linear solver in 2D and 3D sequential.
- New meshes for dynamics tests `bar-dynamic.msh`.
- Checking modules `make check`.
- Faster sparsity pattern calculations.

Changed

- Better documentation via .md and .html files.
- Major restructuring of the codes.
- Moved to `automake` for solver installation.
- Mesh building via `make`.

Removed

- Removed the manufactured solution codes.

1.2.7 Version 1.4 - 2019-05-14

Added

- Fully vectorial finite element solver for phase-field `-vectorial`.
- New `-supercomp` for avoiding xterm issues on super computers.
- New `MatViz()` function for matrix sparsity visualization.
- Introduced GFP plugin support (Go Fast Plugins).

Changed

- Elastic energy decomposition is now optional `-energydecomp`.
- Force calculation using integrals (Thanks to G.Rastiello).

1.2.8 Version 1.3 - 2019-04-08

Added

- New meshes in 2D/3D Notched-plate , square-crack, etc.
- New fracture mechanics module.
- New `-nonlinear` flag to activate phase-field model for brittle fracture.
- New `-timelog` for time logging the solver.
- New `-pipegnu` for GNUMplot piping.

Changed

- Scripting now performed using `.script` files:
 - `BoundaryAndSourceConditions.script`
 - `LinearFormBuilderAndSolver.script`
 - `Macros.script`
 - `Main.script`
 - `VariationalFormulation.script`
 -
- Move to FreeFEM version 4.0.
- Move to PETSc version 3.11.

1.2.9 Version 1.2 - 2019-03-18

Added

- Support for Gmsh's `.msh` or Medit's `.mesh` meshes in folder `Meshes`.
- Advance to 3D physics.
- New MPI based parallel solver linear elasticity.
- New approach for solver generation via scripting (PhD thesis MA Badri) with `scriptGenerator.edp`.
- Integrated Domain decomposition macro (PhD thesis MA Badri).
- Customized `.vtk` support for ParaView post-processing.
- New point boundary condition macro `pointbc(Real[int], fespace, matrix)`.
- New flags for communicating with the solver: `-dimension`, `-plot`, `-bodyforce`, `-lagrange`, etc.

Changed

- More advance README.MD.
- Sequential solver now merged within scripting via flag `-sequential`.
- Move to FreeFEM version 3.62.
- Moved manufactured solutions to `validation-test` folder.

1.2.10 Version 1.1 - 2019-03-04

Added

- Initial FreeFEM files for sequential linear elasticity in 2D (case of constrained bar).
- More cases of manufactured solution for linear elasticity in 2D.
- Added **README.MD** for explaining the solver.
- ParaView plotting activated.

Changed

- Moved to Tuleap git hosting from CEA.
- Separate folder of manufactured solutions and the linear elastic solver.
- Move to FreeFEM version 3.61.

1.2.11 Version 1.0 - 2019-02-15

Added

- Initial FreeFEM files Method of manufactured solution for linear elasticity in 2D.

1.2.12 Version git tags

- | [1.0] |8a8ecb2746b7da792073358c60df33bae647f788 |
- | [1.1] |a667e6085ba1f92f8dd619bd40e18f85c593bc0a |
- | [1.2] |e48b7b3a30c05ad4c343efa6a17fee386031f437 |
- | [1.3] |39f4324550365849852c5264b8d4535aae05e30d |
- | [1.4] |f51f678630eb9b2fed355e5cedf976ce8b5fa341 |
- | [1.5] |07293ba09a69d3d6a16278220a0b4a7a9f318f96 |
- | [1.6] |f359dd049fb1ddde376e8ad8e5177c663e430418 |
- | [1.7] |aee9bfec868a70b3d9974d7692bc19f9739ab7dc |
- | [1.8] |2f26292636c7248133e31ae912ee58113de2ef71 |
- | [2.0] |1e1a4d7f10df30d106b52eba1c5caf69e8bc0f36 |

Chapter 2

Installation

PSD is cross-platform solver built to work with Linux, MacOs, and Windows platforms.

2.1 Dependencies

To install and work with PSD first check that you have installed all the dependencies. PSD depends on the following:

- C++ (g++ version 4.8 or greater) (or Intel compiler)
- automake
- FreeFEM
- PETSc (optional)
- Gmsh
- gnuplot (optional)
- git

2.2 PSD installation steps

Now that I have all the dependencies what next ?

- Go ahead and grab the latest copy of PSD. The code is hosted on CEA's internal git repository.

```
git clone https://codev-tuleap.intra.cea.fr/plugins/git/hpcseism/freefem.git PSD-Sources
```

- Now goto the PSD-Sources folder and autoconf PSD within the cloned folder

```
autoreconf -i
```

- Configure PSD within the cloned folder

```
./configure
```

Note: `./configure` will install PSD in `$HOME/PSD` to change this directory use `-prefix=Your/Own/Path` with `./configure`.

Note: `./configure` will try to look for installation of FreeFEM and Gmsh in `usr/bin/` or `usr/local/bin/` directories. If you have these packages installed in some other directory this should be specified during

./configure by using flags `-with-FreeFEM=` and `-with-Gmsh=`. For example, if FreeFEM is installed at `home/FreeFem/bin` and Gmsh in `home/Gmsh/bin` then one should use

Note: Please use the new version of Gmsh (greater than version 4.3.0) from their official website.

```
./configure --with-FreeFEM=home/FreeFem/bin --with-Gmsh=home/Gmsh/bin
```

- Make PSD directives

```
make
```

- Install PSD

```
make install
```

Note: To install a copy of PSD for developers use `make install-devel` instead of `make install`

- Check if installation is correct

```
make check
```

Now you should have the solver at `$HOME/PSD`. To use the solver please go to `$HOME/PSD`.

2.3 Update PSD to the latest version

If you are a PSD user and would like to update your old PSD source to a new one. Go to your `PSD-Sources` folder and

```
git pull origin master
```

After this step simply

```
./reconfigure; make; make install; make check
```

2.4 PSD developers version

If you would like to install a developers copy of PSD use:

```
make install-devel;
```

Chapter 3

Theoretical background

3.1 Elastostatics

Let us consider d -dimensional domain $\Omega \in \mathbb{R}^d$ in a Euclidean referential $R(O, \mathbf{e}_i)$ (with $i = 1, \dots, d$) submitted to a system of body forces \mathbf{b} . We denote $\partial\Omega$ the boundary of Ω and indicate with $\mathbf{n} = \mathbf{n}(\mathbf{x}) = n_i(\mathbf{x})\mathbf{e}_i$ its outer normal in any point $\mathbf{x} = x_i\mathbf{e}_i \in \partial\Omega$.

The problem to solve in order to characterize the dynamics equilibrium thus consists in finding a vector-valued displacement field $\mathbf{u} = \mathbf{u}(\mathbf{x}, t) : \Omega \times [0, T] \rightarrow \mathbb{R}^d$ regular “enough” and such that:

$$\begin{cases} \operatorname{div}\boldsymbol{\sigma} + \mathbf{b} = 0 & (\mathbf{x}, t) \in \Omega \times [0, T] \\ \boldsymbol{\sigma} = \boldsymbol{\sigma}(\mathbf{u}) & (\mathbf{x}, t) \in \Omega \times [0, T] \\ \mathbf{u} = \mathbf{u}^* & (\mathbf{x}, t) \in \partial_u\Omega \times [0, T] \\ \boldsymbol{\sigma} \cdot \mathbf{n} = \mathbf{t} & (\mathbf{x}, t) \in \partial_t\Omega \times [0, T] \end{cases} \quad (3.1)$$

where “div” denotes the divergence operator, symbol “.” denotes the single contraction operation between tensors, $\rho = \rho(\mathbf{x}) : \Omega \rightarrow \mathbb{R}$ is the material density and $\boldsymbol{\sigma} = \boldsymbol{\sigma}(\mathbf{u})$ denotes a constitutive equation expressing the relationship between the second order Cauchy’s stress tensor $\boldsymbol{\sigma} : \Omega \times [0, T] \rightarrow \mathbb{R}^{d \times d}$ and the displacement. Moreover, $\mathbf{u}^* = \mathbf{u}^*(\mathbf{x}, t) : \partial_u\Omega \times [0, T] \rightarrow \mathbb{R}^d$ is the imposed displacement field on $\partial_u\Omega$ (Dirichlet boundary condition) and $\mathbf{t} = \mathbf{t}(\mathbf{x}, t) : \partial_t\Omega \times [0, T] \rightarrow \mathbb{R}^d$ is the imposed traction vector on $\partial_t\Omega$ (Neumann boundary condition). The split of $\partial\Omega$ is such that $\partial\Omega = \overline{\partial_u\Omega \cup \partial_t\Omega}$ and $\partial_u\Omega \cap \partial_t\Omega = \emptyset$, with overline $\overline{\bullet}$ denoting the closure of set \bullet .

Let us now introduce the spaces of the admissible displacements fields (\mathcal{U}) and test functions (\mathcal{V}):

$$\begin{aligned} \mathcal{U} &= \left\{ \mathbf{u} = \mathbf{u}(\mathbf{x}, t) : \partial_u\Omega \times [0, T] \rightarrow \mathbb{R}^d \mid \mathbf{u} \in H^1(\Omega), \mathbf{u} = \mathbf{u}^* \text{ on } \partial_u\Omega \times [0, T] \right\} \\ \mathcal{V} &= \left\{ \mathbf{v} = \mathbf{v}(\mathbf{x}, t) : \partial_u\Omega \times [0, T] \rightarrow \mathbb{R}^d \mid \mathbf{v} \in H^1(\Omega), \mathbf{v} = 0 \text{ on } \partial_u\Omega \times [0, T] \right\} \end{aligned} \quad (3.2)$$

The weak form of previous boundary value problem can be easily obtained by integrating by part the linear momentum balance equation using a test function $\mathbf{v} \in \mathcal{V}$, and imposing the Neumann boundary condition:

$$\underbrace{\int_{\Omega} \boldsymbol{\sigma}(\mathbf{u}) : \boldsymbol{\epsilon}(\mathbf{v}) \, dV}_{:=K(\mathbf{u}, \mathbf{v})} = \underbrace{\int_{\Omega} \mathbf{b} \cdot \mathbf{v} \, dV + \int_{\partial_t\Omega} \mathbf{t} \cdot \mathbf{v} \, dS}_{:=b(\mathbf{v}; \mathbf{b}) + b(\mathbf{v}; \mathbf{t})_{\partial_t\Omega}} \quad \forall \mathbf{v} \in \mathcal{V} \quad (3.3)$$

where symbol “:.” is the double contraction operation between tensors, $K(\mathbf{u}, \mathbf{v})$ is the bi-linear symmetric form associated with the stiffness matrix and $b(\mathbf{v}; \mathbf{b}) + b(\mathbf{v}; \mathbf{t})_{\partial_t\Omega}$ are the linear forms associated with the external loading.¹

¹In the following of this document, given a known field \mathbf{a} , symbol $b(\mathbf{v}; \mathbf{a})$ will be used to denote the linear form $\int_{\Omega} \mathbf{a} \cdot \mathbf{v} \, dV$, whereas $b(\mathbf{v}; \mathbf{a})_{Surf}$ will denote the linear form obtained from the surface integral $\int_{Surf} \mathbf{a} \cdot \mathbf{v} \, dS$. Any linear form without down-script has to be interpreted as an integral over Ω . Only surface integrals will be defined explicitly.

The problem to solve can be finally written as:

Find $\mathbf{u} \in \mathcal{U}$ such that : $K(\mathbf{u}, \mathbf{v}) = b(\mathbf{v}; \mathbf{b}) + b(\mathbf{v}; \mathbf{t})_{\partial_t \Omega} \quad \forall \mathbf{v} \in \mathcal{V}$	(3.4)
---	-------

3.2 Elastodynamics

The problem to solve in order to characterize the dynamics equilibrium thus consists in finding a vector-valued displacement field $\mathbf{u} = \mathbf{u}(\mathbf{x}, t) : \Omega \times [0, T] \rightarrow \mathbb{R}^d$ regular “enough” and such that:

$$\begin{cases} \operatorname{div} \boldsymbol{\sigma} + \mathbf{b} = \rho \ddot{\mathbf{u}} & (\mathbf{x}, t) \in \Omega \times [0, T] \\ \boldsymbol{\sigma} = \boldsymbol{\sigma}(\mathbf{u}) & (\mathbf{x}, t) \in \Omega \times [0, T] \\ \mathbf{u} = \mathbf{u}^* & (\mathbf{x}, t) \in \partial_u \Omega \times [0, T] \\ \boldsymbol{\sigma} \cdot \mathbf{n} = \mathbf{t} & (\mathbf{x}, t) \in \partial_t \Omega \times [0, T] \\ \mathbf{u} = \mathbf{u}_0 & \mathbf{x} \in \Omega, t = 0 \\ \dot{\mathbf{u}} = \dot{\mathbf{u}}_0 & \mathbf{x} \in \Omega, t = 0 \end{cases} \quad (3.5)$$

where “div” denotes the divergence operator, symbol “.” denotes the single contraction operation between tensors, $\rho = \rho(\mathbf{x}) : \Omega \rightarrow \mathbb{R}$ is the material density, $\ddot{\mathbf{u}} = \ddot{\mathbf{u}}(\mathbf{x}, t) = \mathbf{u}_{tt} : \Omega \times [0, T] \rightarrow \mathbb{R}^d$ is the acceleration field (i.e., the second time derivative of the field \mathbf{u}) and $\boldsymbol{\sigma} = \boldsymbol{\sigma}(\mathbf{u})$ denotes a constitutive equation expressing the relationship between the second order Cauchy’s stress tensor $\boldsymbol{\sigma} : \Omega \times [0, T] \rightarrow \mathbb{R}^{d \times d}$ and the displacement. Moreover, $\mathbf{u}^* = \mathbf{u}^*(\mathbf{x}, t) : \partial_u \Omega \times [0, T] \rightarrow \mathbb{R}^d$ is the imposed displacement field on $\partial_u \Omega$ (Dirichlet boundary condition) and $\mathbf{t} = \mathbf{t}(\mathbf{x}, t) : \partial_t \Omega \times [0, T] \rightarrow \mathbb{R}^d$ is the imposed traction vector on $\partial_t \Omega$ (Neumann boundary condition). The split of $\partial \Omega$ is such that $\partial \Omega = \overline{\partial_u \Omega \cup \partial_t \Omega}$ and $\partial_u \Omega \cap \partial_t \Omega = \emptyset$, with overline $\overline{\bullet}$ denoting the closure of set \bullet . Finally, $\mathbf{u}_0 = \mathbf{u}_0(\mathbf{x}, 0) : \Omega \rightarrow \mathbb{R}^d$ and $\dot{\mathbf{u}}_0 = \dot{\mathbf{u}}_0(\mathbf{x}, 0) : \Omega \rightarrow \mathbb{R}^d$ are the displacement and velocity fields at time $t = 0$ (initial conditions).

Let us now introduce the spaces of the admissible displacements fields (\mathcal{U}) and test functions (\mathcal{V}):

$$\begin{aligned} \mathcal{U} &= \left\{ \mathbf{u} = \mathbf{u}(\mathbf{x}, t) : \partial_u \Omega \times [0, T] \rightarrow \mathbb{R}^d \mid \mathbf{u} \in H^1(\Omega), \mathbf{u} = \mathbf{u}^* \text{ on } \partial_u \Omega \times [0, T], \mathbf{u}(\mathbf{x}, 0) = 0, \dot{\mathbf{u}}(\mathbf{x}, 0) = \dot{\mathbf{u}}_0 \right\} \\ \mathcal{V} &= \left\{ \mathbf{v} = \mathbf{v}(\mathbf{x}, t) : \partial_u \Omega \times [0, T] \rightarrow \mathbb{R}^d \mid \mathbf{v} \in H^1(\Omega), \mathbf{v} = 0 \text{ on } \partial_u \Omega \times [0, T], \right\} \end{aligned} \quad (3.6)$$

The weak form of previous boundary value problem can be easily obtained by integrating by part the linear momentum balance equation using a test function $\mathbf{v} \in \mathcal{V}$, and imposing the Neumann boundary condition:

$$\underbrace{\int_{\Omega} \rho \ddot{\mathbf{u}} \cdot \mathbf{v} \, dV}_{:= M(\ddot{\mathbf{u}}, \mathbf{v})} + \underbrace{\int_{\Omega} \boldsymbol{\sigma}(\mathbf{u}) : \boldsymbol{\epsilon}(\mathbf{v}) \, dV}_{:= K(\mathbf{u}, \mathbf{v})} = \underbrace{\int_{\Omega} \mathbf{b} \cdot \mathbf{v} \, dV}_{:= b(\mathbf{v}; \mathbf{b})} + \underbrace{\int_{\partial_t \Omega} \mathbf{t} \cdot \mathbf{v} \, dS}_{:= b(\mathbf{v}; \mathbf{t})_{\partial_t \Omega}} \quad \forall \mathbf{v} \in \mathcal{V} \quad (3.7)$$

where symbol “:.” is the double contraction operation between tensors, $M(\ddot{\mathbf{u}}, \mathbf{v})$ is the bi-linear symmetric form associated with inertial terms (i.e., dependent on the mass matrix), $K(\mathbf{u}, \mathbf{v})$ is the bi-linear symmetric form associated with the stiffness matrix and $b(\mathbf{v}; \mathbf{b}) + b(\mathbf{v}; \mathbf{t})_{\partial_t \Omega}$ are the linear forms associated with the external loading.²

The problem to solve can be finally written as:

Find $\mathbf{u} \in \mathcal{U}$ such that : $M(\ddot{\mathbf{u}}, \mathbf{v}) + K(\mathbf{u}, \mathbf{v}) = b(\mathbf{v}; \mathbf{b}) + b(\mathbf{v}; \mathbf{t})_{\partial_t \Omega} \quad \forall \mathbf{v} \in \mathcal{V}$	(3.8)
--	-------

²In the following of this document, given a known field \mathbf{a} , symbol $b(\mathbf{v}; \mathbf{a})$ will be used to denote the linear form $\int_{\Omega} \mathbf{a} \cdot \mathbf{v} \, dV$, whereas $b(\mathbf{v}; \mathbf{a})_{Surf}$ will denote the linear form obtained from the surface integral $\int_{Surf} \mathbf{a} \cdot \mathbf{v} \, dS$. Any linear form without down-script has to be interpreted as an integral over Ω . Only surface integrals will be defined explicitly.

The only way for accounting form dumping effects in this formulation is through a proper definition of a constitutive law $\boldsymbol{\sigma} = \boldsymbol{\sigma}(\mathbf{u})$ modeling dissipative processes occurring at the material level. In some cases, however, it can be useful to account for damping effects in a more global way. This can be done by modifying the variational problem as follows:

Find $\mathbf{u} \in \mathcal{U}$ such that :

$$M(\ddot{\mathbf{u}}, \mathbf{v}) + C(\dot{\mathbf{u}}, \mathbf{v}) + K(\mathbf{u}, \mathbf{v}) = b(\mathbf{v}; \mathbf{b}) + b(\mathbf{v}; \mathbf{t})_{\partial_t \Omega} \quad \forall \mathbf{v} \in \mathcal{V}$$

(3.9)

where $C(\dot{\mathbf{u}}, \mathbf{v})$ is an additional bi-linear symmetric form associated with damping/viscous effects.

3.3 Time discretization

Time discretized variational formulations are illustrate in this subsection, considering several implicit time integration schemes. Representative members of these algorithms are, among others, the N- β method [20], the HHT- α method [12], the WBZ- α method [24], the HP- θ_1 method [14] and the CH- α method [5]. These methods exhibit second order accuracy in linear dynamics and permit efficient variable step size techniques, being one-step methods. The CH- α , the HHT- α and the WBZ- α methods, the so called α -methods, are one-parameter schemes which can be considered as particular cases of a more general class of methods named generalized - α (G - α). This class of methods corresponds to the CH- α scheme [5], where the algorithmic parameters α_m , α_f , β and γ are assumed to be independent of each other.

3.3.1 Generalized- α method

The Generalized - α (G - α) is an implicit method that allows for high frequency energy dissipation, reduced unwanted low-frequency dissipation, and second order accuracy (i.e., Δt^2), both in linear and nonlinear regimes. Depending on choices of input parameters, unconditionally stability can be achieved for linear problems (as for all implicit schemes). Stability properties for nonlinear problem were studied in [9]. In the latter work, the second-order accuracy of this class of algorithms was proved also in the non-linear regime, independently of the quadrature rule for non-linear internal forces. Conversely, the G-stability notion which is suitable for linear multi-step schemes devoted to non-linear dynamic problems cannot be applied, as the non-linear structural dynamics equations are not contractive. Nonetheless, [9] proved that the G - α methods are stable in an energy sense, and guarantee energy decay for high-frequencies and asymptotic cancellation. However, overshoot and heavy energy oscillations in the intermediate-frequency range are exhibited.

Problem setting

Let introduce a time discretization of the time interval $[0, T]$ in an ordered sequence of $N+1$ time increments $(0, \dots, t_i, t_{i+1}, \dots, T)$ such that $t_{i+1} = t_i + \Delta t$, with $\Delta t = T/N$ denoting the time step (here supposed constant). According to the (G - α) method, the dynamic evolution equation is solved at intermediate time $t_{n+1-\alpha} \in [t_n, t_{n+1}]$. The following notation is used to denote the value of a generic variable z at time $t_{n+1-\alpha}$:

$$z_{n+1-\alpha} = (1-\alpha)z_{n+1} + \alpha z_n \quad \text{with } \alpha \in [0, 1] \quad (3.10)$$

Furthermore, the following approximations (standard for Newmark schemes) for the displacement and velocity fields at time t_{n+1} are used [20]:

$$\begin{aligned} \mathbf{u}_{n+1} &= \bar{\mathbf{u}}_{n+1} + \beta \Delta t^2 \ddot{\mathbf{u}}_{n+1} \\ \dot{\mathbf{u}}_{n+1} &= \dot{\bar{\mathbf{u}}}_{n+1} + \gamma \Delta t \ddot{\mathbf{u}}_{n+1} \end{aligned} \quad (3.11)$$

where $\bar{\mathbf{u}}_{n+1}$ and $\dot{\bar{\mathbf{u}}}_{n+1}$ are the following known contributions (predictions in predictor-corrector schemes):

$$\begin{aligned} \bar{\mathbf{u}}_{n+1} &= \mathbf{u}_n + \Delta t \dot{\mathbf{u}}_n + \Delta t^2 \left(\frac{1}{2} - \beta \right) \ddot{\mathbf{u}}_n \\ \dot{\bar{\mathbf{u}}}_{n+1} &= \dot{\mathbf{u}}_n + \Delta t (1 - \gamma) \ddot{\mathbf{u}}_n \end{aligned} \quad (3.12)$$

and (β, γ) are algorithmic parameters. By inverting the first equation of (3.11), one can express $\ddot{\mathbf{u}}_{n+1}$ as a function of \mathbf{u}_{n+1} as:

$$\ddot{\mathbf{u}}_{n+1} = \frac{1}{\beta \Delta t^2} (\mathbf{u}_{n+1} - \bar{\mathbf{u}}_{n+1}) \quad (3.13)$$

3.3.2 Time discretized variational problem (no damping)

Neglecting damping effects, the problem to solve is written as:

Find $\mathbf{u}_{n+1} \in \mathcal{U}$ such that :

$$M(\ddot{\mathbf{u}}_{n+1-\alpha_m}, \mathbf{v}) + K(\mathbf{u}_{n+1-\alpha_f}, \mathbf{v}) = b(\mathbf{v}; \mathbf{b}) + b(\mathbf{v}; \mathbf{t}_{n+1-\alpha_f})_{\partial_t \Omega} \quad \forall \mathbf{v} \in \mathcal{V}$$

(3.14)

where $\ddot{\mathbf{u}}_{n+1-\alpha_m}$ and $\mathbf{u}_{n+1-\alpha_f}$ can be written according to (3.10):

$$\begin{aligned} \ddot{\mathbf{u}}_{n+1-\alpha_m} &= \frac{1 - \alpha_m}{\beta \Delta t^2} (\mathbf{u}_{n+1} - \bar{\mathbf{u}}_{n+1}) + \alpha_m \ddot{\mathbf{u}}_n \\ \mathbf{u}_{n+1-\alpha_f} &= (1 - \alpha_f) \mathbf{u}_{n+1} + \alpha_f \mathbf{u}_n \end{aligned} \quad (3.15)$$

Furthermore, parameters β and γ read:

$$\gamma = \frac{1}{2} + \alpha_f - \alpha_m \quad \beta = \frac{1}{4} \left(\gamma + \frac{1}{2} \right)^2 \quad (3.16)$$

Bilinear and linear operators. Using equation (3.13), one can easily write the bi-linear part associated with the mass matrix in terms of the unknown displacement \mathbf{u}_{n+1} as follows:

$$M(\ddot{\mathbf{u}}_{n+1-\alpha_m}, \mathbf{v}) = \frac{1 - \alpha_m}{\beta \Delta t^2} M(\mathbf{u}_{n+1}, \mathbf{v}) - \frac{1 - \alpha_m}{\beta \Delta t^2} m(\mathbf{v}; \bar{\mathbf{u}}_{n+1}) + \alpha_m m(\mathbf{v}; \ddot{\mathbf{u}}_n) \quad (3.17)$$

where linear forms $m(\mathbf{v}; \bar{\mathbf{u}}_{n+1})$ and $m(\mathbf{v}; \ddot{\mathbf{u}}_n)$ read:³

$$m(\mathbf{v}; \bar{\mathbf{u}}_{n+1}) = \int_{\Omega} \rho \bar{\mathbf{u}}_{n+1} \cdot \mathbf{v} \, dV \quad m(\mathbf{v}; \ddot{\mathbf{u}}_n) = \int_{\Omega} \rho \ddot{\mathbf{u}}_n \cdot \mathbf{v} \, dV \quad (3.19)$$

Term $m(\mathbf{v}; \bar{\mathbf{u}}_{n+1})$ figuring in equation (3.17) can also be expanded as:

$$m(\mathbf{v}; \bar{\mathbf{u}}_{n+1}) = m(\mathbf{v}; \mathbf{u}_n) + \Delta t m(\mathbf{v}; \dot{\mathbf{u}}_n) + \Delta t^2 \left(\frac{1}{2} - \beta \right) m(\mathbf{v}; \ddot{\mathbf{u}}_n) \quad (3.20)$$

As a consequence (3.17) can be rewritten as:⁴

$$M(\ddot{\mathbf{u}}_{n+1-\alpha_m}, \mathbf{v}) = \frac{1 - \alpha_m}{\beta \Delta t^2} M(\mathbf{u}_{n+1}, \mathbf{v}) - \frac{1 - \alpha_m}{\beta \Delta t^2} m(\mathbf{v}; \mathbf{u}_n) - \frac{1 - \alpha_m}{\beta \Delta t} m(\mathbf{v}; \dot{\mathbf{u}}_n) + \left(1 - \frac{1 - \alpha_m}{2\beta} \right) m(\mathbf{v}; \ddot{\mathbf{u}}_n) \quad (3.22)$$

In a similar way, we can rewrite the bi-linear form associated with the stiffness matrix as:

$$K(\mathbf{u}_{n+1-\alpha_f}, \mathbf{v}) = (1 - \alpha_f) K(\mathbf{u}_{n+1}, \mathbf{v}) + \alpha_f k(\mathbf{v}; \mathbf{u}_n) \quad (3.23)$$

³More in general, given a field $\mathbf{a} = \mathbf{a}(\mathbf{x}) : \Omega \rightarrow \mathbb{R}^d$, $m(\mathbf{v}; \mathbf{a})$ denotes the linear form:

$$m(\mathbf{v}; \mathbf{a}) = \int_{\Omega} \rho \mathbf{a} \cdot \mathbf{v} \, dV \quad (3.18)$$

⁴When summing up the terms depending on $\ddot{\mathbf{u}}_n$, coming from the definition of $\bar{\mathbf{u}}_{n+1}$ and from equation (3.17), we have:

$$-\left[(1 - \alpha_m) \left(\frac{1 - 2\beta}{2\beta} \right) - \alpha_m \right] = -\frac{(1 - \alpha_m)(1 - 2\beta) - 2\beta\alpha_m}{2\beta} = -\frac{1 - 2\beta - \alpha_m + 2\beta\alpha_m - 2\beta\alpha_m}{2\beta} = 1 - \frac{1 - \alpha_m}{2\beta} \quad (3.21)$$

where $k(\mathbf{v}; \mathbf{u}_n)$ is the linear form:⁵

$$k(\mathbf{v}; \mathbf{u}_n) = \int_{\Omega} \boldsymbol{\sigma}(\mathbf{u}_n) : \boldsymbol{\epsilon}(\mathbf{v}) \, dV \quad (3.25)$$

Finally, the linear form $b(\mathbf{v}; \mathbf{t}_{n+1-\alpha_f})_{\partial_t \Omega}$ becomes:

$$b(\mathbf{v}; \mathbf{t}_{n+1-\alpha_f})_{\partial_t \Omega} = (1 - \alpha_f)b(\mathbf{v}; \mathbf{t}_{n+1})_{\partial_t \Omega} + \alpha_f b(\mathbf{v}; \mathbf{t}_n)_{\partial_t \Omega} \quad (3.26)$$

Final variational problem. The time discretized variational formulation to solve becomes:

Find $\mathbf{u}_{n+1} \in \mathcal{U}$ such that :

$$\tilde{K}(\mathbf{u}_{n+1}, \mathbf{v}) = \tilde{l}(\mathbf{v})$$

(3.27)

where $\tilde{K}(\mathbf{u}_{n+1}, \mathbf{v})$ is the bi-linear form associated with the effective/equivalent stiffness matrix:

$$\tilde{K}(\mathbf{u}_{n+1}, \mathbf{v}) = \frac{1 - \alpha_m}{\beta \Delta t^2} M(\mathbf{u}_{n+1}, \mathbf{v}) + (1 - \alpha_f) K(\mathbf{u}_{n+1}, \mathbf{v}) \quad (3.28)$$

and $\tilde{l}(\mathbf{v}) = \tilde{l}(\mathbf{v}; \{\mathbf{b}, \mathbf{t}_n, \mathbf{t}_{n+1}, \mathbf{u}_n, \dot{\mathbf{u}}_n, \ddot{\mathbf{u}}_n\})$ is the following linear form:

$$\begin{aligned} \tilde{l}(\mathbf{v}) &= b(\mathbf{v}; \mathbf{b}) + b(\mathbf{v}; \mathbf{t}_{n+1-\alpha_f})_{\partial_t \Omega} + \frac{1 - \alpha_m}{\beta \Delta t^2} m(\mathbf{v}, \mathbf{u}_n) + \frac{1 - \alpha_m}{\beta \Delta t} m(\mathbf{v}; \dot{\mathbf{u}}_n) \\ &\quad \dots + \left(1 - \frac{1 - \alpha_m}{2\beta}\right) m(\mathbf{v}; \ddot{\mathbf{u}}_n) - \alpha_f k(\mathbf{v}; \mathbf{u}_n) \end{aligned} \quad (3.29)$$

3.3.3 Time discretized variational problem (Rayleigh damping)

The problem to solve is now:

Find $\mathbf{u}_{n+1} \in \mathcal{U}$ such that :

$$M(\ddot{\mathbf{u}}_{n+1-\alpha_m}, \mathbf{v}) + C(\dot{\mathbf{u}}_{n+1-\alpha_f}, \mathbf{v}) + K(\mathbf{u}_{n+1-\alpha_f}, \mathbf{v}) = b(\mathbf{v}; \mathbf{b}) + b(\mathbf{v}; \mathbf{t}_{n+1-\alpha_f})_{\partial \Omega} \quad \forall \mathbf{v} \in \mathcal{V}$$

(3.30)

where, following a simple Rayleigh formulation, the bi-linear form associated with the damping matrix can be written as:

$$C(\dot{\mathbf{u}}_{n+1-\alpha_f}, \mathbf{v}) = \eta_M M(\dot{\mathbf{u}}_{n+1-\alpha_f}, \mathbf{v}) + \eta_K K(\dot{\mathbf{u}}_{n+1-\alpha_f}, \mathbf{v}) \quad (3.31)$$

with (η_M, η_K) denoting two positive model parameters.

Now, using definitions (3.10), (3.11) and (3.12), $\dot{\mathbf{u}}_{n+1-\alpha_f}$ can be written as:⁶

$$\dot{\mathbf{u}}_{n+1-\alpha_f} = \frac{\gamma(1 - \alpha_f)}{\beta \Delta t} \mathbf{u}_{n+1} + (1 - \alpha_f) \dot{\mathbf{u}}_{n+1} - \frac{\gamma(1 - \alpha_f)}{\beta \Delta t} \bar{\mathbf{u}}_{n+1} + \alpha_f \dot{\mathbf{u}}_n \quad (3.33)$$

⁵More in general, given a field $\mathbf{a} = \mathbf{a}(\mathbf{x}) : \Omega \rightarrow \mathbb{R}^d$, $k(\mathbf{v}; \mathbf{a})$ denotes the linear form:

$$k(\mathbf{v}; \mathbf{a}) = \int_{\Omega} \boldsymbol{\sigma}(\mathbf{a}) : \boldsymbol{\epsilon}(\mathbf{v}) \, dV \quad (3.24)$$

⁶Using definitions (3.10), (3.11) and (3.12), the velocity field at time $t_{n+1-\alpha_f}$ reads:

$$\begin{aligned} \dot{\mathbf{u}}_{n+1-\alpha_f} &= (1 - \alpha_f) \dot{\mathbf{u}}_{n+1} + \alpha_f \dot{\mathbf{u}}_n \\ &= (1 - \alpha_f) \dot{\mathbf{u}}_{n+1} + \alpha_f \dot{\mathbf{u}}_n + \gamma \Delta t (1 - \alpha_f) \ddot{\mathbf{u}}_{n+1} \\ &= \frac{\gamma(1 - \alpha_f)}{\beta \Delta t} \mathbf{u}_{n+1} + (1 - \alpha_f) \dot{\mathbf{u}}_{n+1} - \frac{\gamma(1 - \alpha_f)}{\beta \Delta t} \bar{\mathbf{u}}_{n+1} + \alpha_f \dot{\mathbf{u}}_n \end{aligned} \quad (3.32)$$

or, using definitions (3.12), as:⁷

$$\dot{\mathbf{u}}_{n+1-\alpha_f} = \frac{\gamma(1-\alpha_f)}{\beta\Delta t}\mathbf{u}_{n+1} - \frac{\gamma(1-\alpha_f)}{\beta\Delta t}\mathbf{u}_n - \left[\frac{\gamma(1-\alpha_f)}{\beta} - 1 \right] \dot{\mathbf{u}}_n - \Delta t(1-\alpha_f) \left(\frac{\gamma}{2\beta} - 1 \right) \ddot{\mathbf{u}}_n \quad (3.35)$$

Bilinear and linear operators. Operator $M(\dot{\mathbf{u}}_{n+1-\alpha_f}, \mathbf{v})$ reads:

$$\begin{aligned} M(\dot{\mathbf{u}}_{n+1-\alpha_f}, \mathbf{v}) &= \frac{\gamma(1-\alpha_f)}{\beta\Delta t} M(\mathbf{u}_{n+1}, \mathbf{v}) - \frac{\gamma(1-\alpha_f)}{\beta\Delta t} m(\mathbf{v}; \mathbf{u}_n) \\ &\dots - \left[\frac{\gamma(1-\alpha_f)}{\beta} - 1 \right] m(\mathbf{v}; \dot{\mathbf{u}}_n) - \Delta t(1-\alpha_f) \left(\frac{\gamma}{2\beta} - 1 \right) m(\mathbf{v}; \ddot{\mathbf{u}}_n) \end{aligned} \quad (3.36)$$

Similarly, the stiffness contribution becomes:

$$\begin{aligned} K(\dot{\mathbf{u}}_{n+1-\alpha_f}, \mathbf{v}) &= \frac{\gamma(1-\alpha_f)}{\beta\Delta t} K(\mathbf{u}_{n+1}, \mathbf{v}) - \frac{\gamma(1-\alpha_f)}{\beta\Delta t} k(\mathbf{v}; \mathbf{u}_n) \\ &\dots - \left[\frac{\gamma(1-\alpha_f)}{\beta} - 1 \right] k(\mathbf{v}; \dot{\mathbf{u}}_n) - \Delta t(1-\alpha_f) \left(\frac{\gamma}{2\beta} - 1 \right) k(\mathbf{v}; \ddot{\mathbf{u}}_n) \end{aligned} \quad (3.37)$$

Final variational problem. Finally, the variational problem to solve reads:

$$\begin{aligned} &\text{Find } \mathbf{u}_{n+1} \in \mathcal{U} \text{ such that :} \\ &\tilde{\tilde{K}}(\mathbf{u}_{n+1}, \mathbf{v}) = \tilde{\tilde{l}}(\mathbf{v}) \quad \forall \mathbf{v} \in \mathcal{V} \end{aligned}$$

(3.38)

where $\tilde{\tilde{K}}(\mathbf{u}_{n+1}, \mathbf{v})$ is the bi-linear form associated with the effective stiffness matrix:

$$\begin{aligned} \tilde{\tilde{K}}(\mathbf{u}_{n+1}, \mathbf{v}) &= \tilde{\tilde{K}}(\mathbf{u}_{n+1}, \mathbf{v}) + \frac{\gamma(1-\alpha_f)}{\beta\Delta t} C(\mathbf{u}_{n+1}, \mathbf{v}) \\ &= \frac{1-\alpha_m}{\beta\Delta t^2} M(\mathbf{u}_{n+1}, \mathbf{v}) + \frac{\gamma(1-\alpha_f)}{\beta\Delta t} C(\mathbf{u}_{n+1}, \mathbf{v}) + (1-\alpha_f) K(\mathbf{u}_{n+1}, \mathbf{v}) \end{aligned} \quad (3.39)$$

with $C(\mathbf{u}_{n+1}, \mathbf{v})$ denoting the Rayleigh damping operator:

$$C(\mathbf{u}_{n+1}, \mathbf{v}) = \eta_M M(\mathbf{u}_{n+1}, \mathbf{v}) + \eta_K K(\mathbf{u}_{n+1}, \mathbf{v}) \quad (3.40)$$

and $\tilde{\tilde{l}}(\mathbf{v}) = \tilde{\tilde{l}}(\mathbf{v}; \{\mathbf{b}, \mathbf{t}_n, \mathbf{t}_{n+1}, \mathbf{u}_n, \dot{\mathbf{u}}_n, \ddot{\mathbf{u}}_n\})$ being the following linear form:

$$\begin{aligned} \tilde{\tilde{l}}(\mathbf{v}) &= \tilde{\tilde{l}}(\mathbf{v}) + \Delta t(1-\alpha_f) \left(\frac{\gamma}{2\beta} - 1 \right) c(\mathbf{v}; \ddot{\mathbf{u}}_n) \\ &\dots + \left[\frac{\gamma(1-\alpha_f)}{\beta} - 1 \right] c(\mathbf{v}; \dot{\mathbf{u}}_n) + \frac{\gamma(1-\alpha_f)}{\beta\Delta t} c(\mathbf{v}; \mathbf{u}_n) \end{aligned} \quad (3.41)$$

In previous equation we introduced the following notation:

$$c(\mathbf{v}; \mathbf{a}) = \eta_M m(\mathbf{v}; \mathbf{a}) + \eta_K k(\mathbf{v}; \mathbf{a}) \quad (3.42)$$

⁷Using definitions (3.12) one obtains:

$$\begin{aligned} \dot{\mathbf{u}}_{n+1-\alpha_f} &= \frac{\gamma(1-\alpha_f)}{\beta\Delta t} \mathbf{u}_{n+1} + (1-\alpha_f) [\dot{\mathbf{u}}_n + \Delta t(1-\gamma)\ddot{\mathbf{u}}_n] - \frac{\gamma(1-\alpha_f)}{\beta\Delta t} \left[\mathbf{u}_n + \Delta t \dot{\mathbf{u}}_n + \Delta t^2 \left(\frac{1}{2} - \beta \right) \ddot{\mathbf{u}}_n \right] + \alpha_f \dot{\mathbf{u}}_n \\ &= \frac{\gamma(1-\alpha_f)}{\beta\Delta t} \mathbf{u}_{n+1} + \left[1 - \frac{\gamma(1-\alpha_f)}{\beta} \right] \dot{\mathbf{u}}_n + (1-\alpha_f) \Delta t \left\{ 1 - \gamma \left[1 + \left(\frac{1-2\beta}{2\beta} \right) \right] \right\} \ddot{\mathbf{u}}_n - \frac{\gamma(1-\alpha_f)}{\beta\Delta t} \mathbf{u}_n \\ &= \frac{\gamma(1-\alpha_f)}{\beta\Delta t} \mathbf{u}_{n+1} - \frac{\gamma(1-\alpha_f)}{\beta\Delta t} \mathbf{u}_n - \left[\frac{\gamma(1-\alpha_f)}{\beta} - 1 \right] \dot{\mathbf{u}}_n - \Delta t(1-\alpha_f) \left(\frac{\gamma}{2\beta} - 1 \right) \ddot{\mathbf{u}}_n \end{aligned} \quad (3.34)$$

3.3.4 Implicit N- β and HHT- α method as special cases

Newmark. One can easily show that, the Newmark scheme is obtained by choosing $\alpha_m = \alpha_f = 0$.

Without damping, the stiffness matrix becomes:

$$\tilde{K}(\mathbf{u}_{n+1}, \mathbf{v}) = \frac{1}{\beta \Delta t^2} M(\mathbf{u}_{n+1}, \mathbf{v}) + K(\mathbf{u}_{n+1}, \mathbf{v}) \quad (3.43)$$

whereas the linear form simplifies as follows:

$$\begin{aligned} \tilde{l}(\mathbf{v}) &= b(\mathbf{v}; \mathbf{b}) + b(\mathbf{v}; \mathbf{t}_{n+1})_{\partial_t \Omega} + \frac{1}{\beta \Delta t^2} m(\mathbf{v}; \bar{\mathbf{u}}_{n+1}) \\ &= b(\mathbf{v}; \mathbf{b}) + b(\mathbf{v}; \mathbf{t}_{n+1})_{\partial_t \Omega} + \frac{1}{\beta \Delta t^2} \left[m(\mathbf{v}; \mathbf{u}_n) + \Delta t m(\mathbf{v}; \dot{\mathbf{u}}_n) + \Delta t^2 \left(\frac{1}{2} - \beta \right) m(\mathbf{v}; \ddot{\mathbf{u}}_n) \right] \end{aligned} \quad (3.44)$$

When Rayleigh damping is considered, the bi-linear operator $\tilde{\tilde{K}}(\mathbf{u}_{n+1}, \mathbf{v})$ becomes:

$$\tilde{\tilde{K}}(\mathbf{u}_{n+1}, \mathbf{v}) = \frac{1}{\beta \Delta t^2} M(\mathbf{u}_{n+1}, \mathbf{v}) + \frac{\gamma}{\beta \Delta t} C(\mathbf{u}_{n+1}, \mathbf{v}) + K(\mathbf{u}_{n+1}, \mathbf{v}) \quad (3.45)$$

whereas the linear form simplifies as follows:

$$\tilde{\tilde{l}}(\mathbf{v}) = \tilde{l}(\mathbf{v}) + \Delta t \left(\frac{\gamma}{2\beta} - 1 \right) c(\mathbf{v}; \ddot{\mathbf{u}}_n) + \left(\frac{\gamma}{\beta} - 1 \right) c(\mathbf{v}; \dot{\mathbf{u}}_n) + \frac{\gamma}{\beta \Delta t} c(\mathbf{v}; \mathbf{u}_n) \quad (3.46)$$

HHT. One can also show that HHT- α [12] method is recovered for $\alpha_m = 0$. Such formulation is not detailed in the following of this document, since it is less used than the classic Newmark approach.

3.3.5 Considerations on methods based upon operator splitting

In order to introduce predictor-correction, implicit-explicit and more in general schemes based upon operator splitting, one can rewrite displacement and velocity in a predictor-correction fashion as in (3.11) and (3.12), where (3.12) now defines predictors and (3.11) correctors (for more general information, the interested reader can refer to [15, 25]). For instance, a simple explicit predictor-corrector method can be obtained through solving problem (3.30) with $K(\bar{\mathbf{u}}_{n+1}, \mathbf{v})$ and $C((1 - \alpha_f)\bar{\mathbf{u}}_{n+1} + \alpha_f \mathbf{u}_n)$. Mixed implicit-explicit predictor-corrector methods can also be obtained through splitting Ω into two subdomains and using different time-integration schemes for solving the dynamic equilibrium problem on each of them.

3.4 Space discretization

Space discretization is performed according to the standard finite element method. The computational domain Ω is thus discretized into a mesh Ω^h comprising a finite number (n_{el}) of subdomains, the finite element Ω_e^h , such that $\Omega \approx \Omega^h = \cup_{e=1}^{n_{el}} \Omega_e^h$. Inside each element, the displacement field is interpolated based on nodal displacements (\mathbf{d}) through the shape functions matrix (\mathbf{N}), i.e., $\mathbf{u} \approx \mathbf{u}^h = \mathbf{N}(\mathbf{x})\mathbf{d}$. As usual, gradient terms are interpolated using the derivatives of the shape functions, i.e., $\boldsymbol{\epsilon} \approx \boldsymbol{\epsilon}^h = \mathbf{B}(\mathbf{x})\mathbf{d}$.

In a standard matrix format, after spatial discretization of the displacement field, the problem to solve can be written in the standard form as:

Find \mathbf{d}_{n+1} such that :

$$\begin{aligned} &\left[\frac{1 - \alpha_m}{\beta \Delta t^2} \mathbf{M} + (1 - \alpha_f) \mathbf{K} \right] \mathbf{d}_{n+1} \\ &= \mathbf{f}_{n+1-\alpha_f} + \mathbf{M} \left[\left(\frac{1 - \alpha_m}{2\beta} - 1 \right) \ddot{\mathbf{d}}_n + \frac{1 - \alpha_m}{\beta \Delta t} \dot{\mathbf{d}}_n + \frac{1 - \alpha_m}{\beta \Delta t^2} \mathbf{d}_n \right] - \alpha_f \mathbf{K} \mathbf{d}_n \end{aligned} \quad (3.47)$$

where \mathbf{M} and \mathbf{K} are now the mass and stiffness matrices. They are obtained through assembling (operator \mathbf{A}) the corresponding elemental operators over the finite element mesh as:

$$\begin{aligned}\mathbf{M} &= \sum_{e=1}^{n_{el}} \int_{\Omega_e} \rho \mathbf{N}^\top \mathbf{N} dV \\ \mathbf{K} &= \sum_{e=1}^{n_{el}} \int_{\Omega_e} \mathbf{B}^\top \mathbf{D} \mathbf{B} dV\end{aligned}\quad (3.48)$$

where \mathbf{D} is the material stiffness matrix defining the link between the stress and strain tensors (or between theirs rates of variation – more details are given in the next section).

When Rayleigh damping is considered the problem to solve is written as:

Find \mathbf{d}_{n+1} such that :

$$\begin{aligned}& \left[\frac{1 - \alpha_m}{\beta \Delta t^2} \mathbf{M} + \frac{\gamma(1 - \alpha_f)}{\beta \Delta t} \mathbf{C} + (1 - \alpha_f) \mathbf{K} \right] \mathbf{d}_{n+1} \\ &= \mathbf{f}_{n+1-\alpha_f} + \mathbf{M} \left[\left(\frac{1 - \alpha_m}{2\beta} - 1 \right) \ddot{\mathbf{d}}_n + \frac{1 - \alpha_m}{\beta \Delta t} \dot{\mathbf{d}}_n + \frac{1 - \alpha_m}{\beta \Delta t^2} \mathbf{d}_n \right] - \alpha_f \mathbf{K} \mathbf{d}_n \\ &+ \mathbf{C} \left\{ \Delta t (1 - \alpha_f) \left(\frac{\gamma}{2\beta} - 1 \right) \ddot{\mathbf{d}}_n + \left[\frac{\gamma(1 - \alpha_f)}{\beta} - 1 \right] \dot{\mathbf{d}}_n + \frac{\gamma(1 - \alpha_f)}{\beta \Delta t} \mathbf{d}_n \right\}\end{aligned}\quad (3.49)$$

where matrix \mathbf{C} is now defined as:

$$\mathbf{C} = \eta_M \mathbf{M} + \eta_K \mathbf{K} \quad (3.50)$$

3.5 Linear and nonlinear dynamic solvers

Elastodynamics is the simplest case one can encounter in structural mechanics. In that case, the space-time discretized linear system of equations is linear and finding the solution at any time t_{n+1} is straightforward. In most applications, however, material behavior is nonlinear since structural materials often dissipate energy and exhibit damage, permanent strains, etc. In that case, the resulting discretized problem to solve is nonlinear, and Newton–Raphson procedures can be used. In that case, the solution is found iteratively through solving a series of linearized problems.

3.5.1 Linear case - linear elastic material behavior

Let us start from the linear case first. Under small strains conditions, if the material is assumed isotropic linear elastic, the Cauchy's stress tensor reads $\boldsymbol{\sigma} = \lambda \text{tr}(\boldsymbol{\epsilon}) \mathbf{I} + 2\mu \boldsymbol{\epsilon}$, where $\boldsymbol{\epsilon} = (\nabla \mathbf{u} + \nabla^\top \mathbf{u})/2$ is the small strain tensor (i.e., the symmetric part of the displacement gradient $\nabla \mathbf{u}$), $\lambda = \lambda(\mathbf{x})$ and $\mu = \mu(\mathbf{x})$ are the Lame's parameters and $\mathbf{I} = \delta_{ij} \mathbf{e}_i \otimes \mathbf{e}_j$ denotes the second order identity tensor. As a consequence, the bi-linear form $K(\mathbf{u}_{n+1}, \mathbf{v})$ and the corresponding linear form $k(\mathbf{v}; \mathbf{u}_n)$ can be rewritten in a more explicit form as:

$$\begin{aligned}K(\mathbf{u}_{n+1}, \mathbf{v}) &= \int_{\Omega} \boldsymbol{\sigma}(\mathbf{u}_{n+1}) : \boldsymbol{\epsilon}(\mathbf{v}) dV = \int_{\Omega} [\lambda \text{tr} \boldsymbol{\epsilon}(\mathbf{u}_{n+1}) \mathbf{I} + 2\mu \boldsymbol{\epsilon}(\mathbf{u}_{n+1})] : \boldsymbol{\epsilon}(\mathbf{v}) dV = \int_{\Omega} \boldsymbol{\epsilon}(\mathbf{u}_{n+1}) : \mathbb{E} : \boldsymbol{\epsilon}(\mathbf{v}) dV \\ k(\mathbf{v}; \mathbf{u}_n) &= \int_{\Omega} \boldsymbol{\sigma}(\mathbf{u}_n) : \boldsymbol{\epsilon}(\mathbf{v}) dV = \int_{\Omega} [\lambda \text{tr} \boldsymbol{\epsilon}(\mathbf{u}_n) \mathbf{I} + 2\mu \boldsymbol{\epsilon}(\mathbf{u}_n)] : \boldsymbol{\epsilon}(\mathbf{v}) dV = \int_{\Omega} \boldsymbol{\epsilon}(\mathbf{u}_n) : \mathbb{E} : \boldsymbol{\epsilon}(\mathbf{v}) dV\end{aligned}\quad (3.51)$$

where \mathbb{E} is the fourth-order elastic stiffness tensor.

3.5.2 Nonlinear case - inelastic material behaviors (under implementation)

An iterative Newton–Raphson procedure is used to solve the nonlinear problem. The unknown displacement \mathbf{u}_{n+1} at global iteration $k + 1$ is written as $\mathbf{u}_{n+1}^{k+1} = \mathbf{u}_{n+1}^k + \delta \mathbf{u}_{n+1}^{k+1}$, where \mathbf{u}_{n+1}^k is the solution at iteration

k , and $\delta \mathbf{u}_{n+1}^{k+1}$ is the solution variation at iteration $k + 1$. The latter is computed from the resolution of a linearized system of equations.

For this purpose, the variational formulation (3.39) is first written in residual form as:

$$\boxed{\begin{aligned} & \text{Find } \mathbf{u}_{n+1}^{k+1} \in \mathcal{U} \text{ such that :} \\ & R(\mathbf{u}_{n+1}^{k+1}, \mathbf{v}) = \tilde{\tilde{K}}(\mathbf{u}_{n+1}^{k+1}, \mathbf{v}) - \tilde{\tilde{l}}(\mathbf{v}) = 0 \quad \forall \mathbf{v} \in \mathcal{V} \end{aligned}} \quad (3.52)$$

The residual(i.e., the out-of-balance force) is then linearized around solution \mathbf{u}_{n+1}^k as follows:

$$R(\mathbf{u}_{n+1}^{k+1}, \mathbf{v}) = r(\mathbf{v}; \mathbf{u}_{n+1}^k) + R'(\delta \mathbf{u}_{n+1}^{k+1}, \mathbf{v}; \mathbf{u}_{n+1}^k) \quad (3.53)$$

where $r(\mathbf{v}; \mathbf{u}_{n+1}^k) = r(\mathbf{v}; \{\mathbf{b}, \mathbf{t}_n, \mathbf{t}_{n+1}, \mathbf{u}_n, \dot{\mathbf{u}}_n, \ddot{\mathbf{u}}_n\}, \mathbf{u}_{n+1}^k)$ is the linear form corresponding to the out-of-balance forces at iteration k :

$$r(\mathbf{v}; \mathbf{u}_{n+1}^k) = \frac{1 - \alpha_m}{\beta \Delta t^2} m(\mathbf{v}; \mathbf{u}_{n+1}^k) + \frac{\gamma(1 - \alpha_f)}{\beta \Delta t} c(\mathbf{v}; \mathbf{u}_{n+1}^k) + (1 - \alpha_f) k(\mathbf{v}; \mathbf{u}_{n+1}^k) - \tilde{\tilde{l}}(\mathbf{v}) \quad (3.54)$$

and:

$$\begin{aligned} R'(\delta \mathbf{u}_{n+1}^{k+1}, \mathbf{v}; \mathbf{u}_{n+1}^k) &= \left[\frac{1 - \alpha_m}{\beta \Delta t^2} + \frac{\gamma(1 - \alpha_f)\eta_M}{\beta \Delta t} \right] M(\delta \mathbf{u}_{n+1}^{k+1}, \mathbf{v}) \\ &\quad + (1 - \alpha_f) \left(1 + \frac{\gamma\eta_K}{\beta \Delta t} \right) K_t(\delta \mathbf{u}_{n+1}^{k+1}, \mathbf{v}; \mathbf{u}_{n+1}^k) \end{aligned} \quad (3.55)$$

with:

$$K_t(\delta \mathbf{u}_{n+1}^{k+1}, \mathbf{v}; \mathbf{u}_{n+1}^k) = \int_{\Omega} \boldsymbol{\epsilon}(\delta \mathbf{u}_{n+1}^{k+1}) : \mathbb{D}^k : \boldsymbol{\epsilon}(\mathbf{v}) \, dV \quad (3.56)$$

The fourth order stiffness tensor $\mathbb{D}^k = D_{ijkl}(\mathbf{e}_i \otimes \mathbf{e}_j \otimes \mathbf{e}_k \otimes \mathbf{e}_l)$ can be defined differently according to the chosen algorithm. For instance, if a standard Newton–Raphson formulation is chosen, $\mathbb{D}^k = \partial_{\boldsymbol{\epsilon}} \boldsymbol{\sigma}(\mathbf{u}_{n+1}^k)$ is the tangent stiffness operator at iteration k .

Finally, the discretized variational formulation to solve becomes:

$$\boxed{\begin{aligned} & \text{Find } \delta \mathbf{u}_{n+1}^{k+1} \in \mathcal{U}_{\delta} \text{ such that :} \\ & \left[\frac{1 - \alpha_m}{\beta \Delta t^2} + \frac{\gamma(1 - \alpha_f)\eta_M}{\beta \Delta t} \right] M(\delta \mathbf{u}_{n+1}^{k+1}, \mathbf{v}) + (1 - \alpha_f) \left(\frac{\gamma}{\beta \Delta t} \eta_K + 1 \right) K_d(\delta \mathbf{u}_{n+1}^{k+1}, \mathbf{v}; \mathbf{u}_{n+1}^k) \\ & = -r(\mathbf{v}; \mathbf{u}_{n+1}^k) \quad \forall \mathbf{v} \in \mathcal{V} \end{aligned}} \quad (3.57)$$

where \mathcal{U}_{δ} is the admissibility space of the displacement variations, and $-r(\mathbf{v}; \mathbf{u}_{n+1}^k)$ can now be interpreted as the difference between the pseudo-external forces (represented by the linear form $\tilde{\tilde{l}}(\mathbf{v})$) and the internal forces (first three terms of equation (3.54)).

3.6 Paraxial formulation for absorbing layers

When spatially unbounded (infinite) domains are represented through bounded computational domains, spurious wave reflections can be observed boundaries. Several techniques have been proposed in the literature to introduce proper treatments of the boundary conditions allowing to reproduce propagation processes in infinite one-phase and two-phase media artificially. Among the available formulations, one can cite the ones based upon using lumped dumpers [18], Perfectly Matched Layers (PML) [4] and paraxial boundaries [8, 6, 3, 19].

3.6.1 Standard formulation

Paraxial approximation constitutes a local boundary condition which permits diffracting waves to be evacuated from the computational domain. To introduce the formulation, let us consider a split of the total domain Ω^∞ into two subdomains Ω and Ω^E separated by a surface $\Sigma \in \mathbb{R}^d$ of outer normal \mathbf{m} (pointing from Ω to Ω^E). On surface Σ , the continuity condition of the displacement field read:

$$[\mathbf{u}] = \mathbf{u} - \mathbf{u}^E = 0 \quad \Sigma \times [0, T] \quad (3.58)$$

whereas the continuity of the traction vector reads:

$$[\boldsymbol{\sigma}] \cdot \mathbf{m} = (\boldsymbol{\sigma} - \boldsymbol{\sigma}^E) \cdot \mathbf{m} = \boldsymbol{\sigma} \cdot \mathbf{m} + \boldsymbol{\sigma}^E \cdot (-\mathbf{m}) = \mathbf{t} + \mathbf{t}^E = 0 \quad \Sigma \times [0, T] \quad (3.59)$$

In previous equations, symbol $[\bullet]$ is used to denote the jump of function \bullet across surface Σ , $\mathbf{u}^E = \mathbf{u}^E(\mathbf{x}, t) : \Omega^E \times [0, T] \rightarrow \mathbb{R}^d$ is the vector-valued displacement field on Ω^E , and $\boldsymbol{\sigma}^E = \boldsymbol{\sigma}^E(\mathbf{u}^E) : \Omega^E \times [0, T] \rightarrow \mathbb{R}^{d \times d}$ is the corresponding stress tensor.

Variational formulation

Given the traction continuity condition (3.59), the variational problem to solve on Ω reads:

Find $\mathbf{u} \in \mathcal{U}$ such that:

$$M(\ddot{\mathbf{u}}, \mathbf{v}) + C(\dot{\mathbf{u}}, \mathbf{v}) + K(\mathbf{u}, \mathbf{v}) = b(\mathbf{v}; \mathbf{b})_\Omega + b(\mathbf{v}; \mathbf{t})_{\partial_t \Omega} - b(\mathbf{v}; \mathbf{t}^E)_\Sigma \quad \forall \mathbf{v} \in \mathcal{V} \quad (3.60)$$

Using a zeroth-order paraxial approximation, the traction vector \mathbf{t}^E can be written as:

$$\mathbf{t}^E = A_0(\dot{\mathbf{u}}) = \rho c_p \dot{u}_m \mathbf{m} + \rho c_s \dot{u}_s \quad (3.61)$$

where (c_p, c_s) are the propagation velocities of compressional and shear waves, $\dot{u}_m = \dot{\mathbf{u}} \cdot \mathbf{m}$ is the velocity normal to Σ and $\dot{u}_s = \dot{\mathbf{u}} - \dot{u}_m \mathbf{m}$ its tangent counterpart.

More in general, given a vector-valued field \mathbf{a} (e.g., the displacement, velocity and acceleration fields), we write:⁸

$$A_0(\mathbf{a}) = \rho c_p (\mathbf{m} \otimes \mathbf{m}) \cdot \mathbf{a} + \rho c_s (\mathbf{I} - \mathbf{m} \otimes \mathbf{m}) \cdot \mathbf{a} = \rho [(c_p - c_s) m_i m_j + c_s \delta_{ij}] a_j \mathbf{e}_i \quad (3.62)$$

where symbol \otimes denotes the dyadic product between first order tensors (vectors).⁹

Time-discretization

After time discretization, equation (3.61) becomes:

$$\begin{aligned} b(\mathbf{v}; \mathbf{t}^E)_\Sigma &= \frac{\gamma(1-\alpha_f)}{\beta \Delta t} b(\mathbf{v}; A_0(\mathbf{u}_{n+1}))_\Sigma - \left[\frac{\gamma(1-\alpha_f)}{\beta} - 1 \right] b(\mathbf{v}; A_0(\dot{\mathbf{u}}_n))_\Sigma \\ &\dots - \Delta t(1-\alpha_f) \left(\frac{\gamma}{2\beta} - 1 \right) b(\mathbf{v}; A_0(\ddot{\mathbf{u}}_n))_\Sigma - \frac{\gamma(1-\alpha_f)}{\beta \Delta t} b(\mathbf{v}; A_0(\mathbf{u}_n))_\Sigma \end{aligned} \quad (3.66)$$

The variational problem to solve thus reads:

Find \mathbf{u}_{n+1} such that :

$$\tilde{\tilde{K}}(\mathbf{u}_{n+1}, \mathbf{v})(\mathbf{u}_{n+1}, \mathbf{v}) = \tilde{\tilde{l}}(\mathbf{v}) \quad \forall \mathbf{v} \in \mathcal{V} \quad (3.67)$$

⁸We recall that given three Euclidean vectors $\mathbf{v} \in \mathbb{R}^d$, $\mathbf{w} \in \mathbb{R}^d$ and $\mathbf{z} \in \mathbb{R}^d$, the dyadic product $\mathbf{v} \otimes \mathbf{w} \in \mathbb{R}^{d \times d}$ is the second order tensor defined by: $(\mathbf{v} \otimes \mathbf{w}) \cdot \mathbf{z} = (\mathbf{w} \cdot \mathbf{z})\mathbf{v}$. In components: $(\mathbf{v} \otimes \mathbf{w})_{ij} = v_i w_j$.

⁹Denoting (m_x, m_y, m_z) the components of vector \mathbf{m} in the reference system $R(O, \mathbf{e}_x, \mathbf{e}_y, \mathbf{e}_z)$, the components of $A_0(\mathbf{a})$ read:

$$(A_0(\mathbf{a}))_x = \rho [(c_p - c_s)m_x(m_x a_x + m_y a_y + m_z a_z) + c_s a_x] \quad (3.63)$$

$$(A_0(\mathbf{a}))_y = \rho [(c_p - c_s)m_y(m_x a_x + m_y a_y + m_z a_z) + c_s a_y] \quad (3.64)$$

$$(A_0(\mathbf{a}))_z = \rho [(c_p - c_s)m_z(m_x a_x + m_y a_y + m_z a_z) + c_s a_z] \quad (3.65)$$

where $\tilde{\tilde{K}}(\mathbf{u}_{n+1}, \mathbf{v})$ is:

$$\begin{aligned}\tilde{\tilde{K}}(\mathbf{u}_{n+1}, \mathbf{v}) &= \tilde{\tilde{K}}(\mathbf{u}_{n+1}, \mathbf{v}) + \frac{\gamma(1-\alpha_f)}{\beta\Delta t} b(\mathbf{v}; A_0(\mathbf{u}_{n+1}))_\Sigma \\ &= \frac{1-\alpha_m}{\beta\Delta t^2} M(\mathbf{u}_{n+1}, \mathbf{v}) + \frac{\gamma(1-\alpha_f)}{\beta\Delta t} C(\mathbf{u}_{n+1}, \mathbf{v}) + (1-\alpha_f) K(\mathbf{u}_{n+1}, \mathbf{v}) \\ &\quad \cdots + \frac{\gamma(1-\alpha_f)}{\beta\Delta t} b(\mathbf{v}; A_0(\mathbf{u}_{n+1}))_\Sigma\end{aligned}\quad (3.68)$$

and $\tilde{\tilde{l}}(\mathbf{v})$ is:

$$\begin{aligned}\tilde{\tilde{l}}(\mathbf{v}) &= \tilde{\tilde{l}}(\mathbf{v}) + \left[\frac{\gamma(1-\alpha_f)}{\beta} - 1 \right] b(\mathbf{v}; A_0(\dot{\mathbf{u}}_n))_\Sigma \\ &\quad \cdots + \Delta t(1-\alpha_f) \left(\frac{\gamma}{2\beta} - 1 \right) b(\mathbf{v}; A_0(\ddot{\mathbf{u}}_n))_\Sigma + \frac{\gamma(1-\alpha_f)}{\beta\Delta t} b(\mathbf{v}; A_0(\mathbf{u}_n))_\Sigma\end{aligned}\quad (3.69)$$

3.6.2 Accounting for incident waves

Let us now split the total displacement vector at Σ into its incident \mathbf{u}_{in} and radiant \mathbf{u}_r components:

$$\mathbf{u} = \mathbf{u}^E = \mathbf{u}_{in} + \mathbf{u}_r \quad (3.70)$$

and use the zeroth-order paraxial approximation for expressing the traction contribution to the traction vector \mathbf{t}^E due to the radiant field. The traction continuity condition (3.59), together with the linearity hypotheses at the vicinity of Σ , enables us to write:

$$\mathbf{t} = -\mathbf{t}^E(\mathbf{u}^E) = -\mathbf{t}^E(\mathbf{u}_{in}) - \mathbf{t}^E(\mathbf{u}_r) = -\mathbf{t}^E(\mathbf{u}_{in}) - A_0(\dot{\mathbf{u}}_r) = -\mathbf{t}^E(\dot{\mathbf{u}}_{in}) - A_0(\dot{\mathbf{u}}) + A_0(\dot{\mathbf{u}}_{in}) \quad (3.71)$$

here $\dot{\mathbf{u}}_{in}$ is known, whereas $\dot{\mathbf{u}}$ is the unknown velocity field.

The variational equation to solve now reads:

Find $\mathbf{u} \in \mathcal{U}$ such that :

$$\begin{aligned}M(\ddot{\mathbf{u}}, \mathbf{v}) + C(\dot{\mathbf{u}}, \mathbf{v}) + K(\mathbf{u}, \mathbf{v}) &= b(\mathbf{v}; \mathbf{b})_\Omega + b(\mathbf{v}; \mathbf{t})_{\partial_t \Omega} - b(\mathbf{v}; A_0(\dot{\mathbf{u}}))_\Sigma \\ &\quad \cdots - b(\mathbf{v}; \mathbf{t}_E(\dot{\mathbf{u}}_{in}))_\Sigma + b(\mathbf{v}; A_0(\dot{\mathbf{u}}_{in}))_\Sigma \quad \forall \mathbf{v} \in \mathcal{V}\end{aligned}\quad (3.72)$$

where the last two terms are the only novelty with respect to equation (3.60).

Chapter 4

Tutorials

Preliminaries

Before diving into the tutorials, here are some preliminaries that will help you guide easily through them.

- A PSD simulation is performed in three steps: preprocessing, solving, and postprocessing.
- Domain: denoted by Ω is a n -dimensional solid body such that $\Omega \subset \mathbb{R}^n$ with $n = 2$ for 2D problems or $n = 3$ for 3D problems.
- Finite element mesh: denoted by Ω^h with mesh size h . Mesh can be triangular in 2D and tetrahedral in 3D.
- MPI processes for simulation: denoted by N_p these are the total MPI ranks that will work in parallel to solve the problem.
- Partitioned mesh: denoted by $\{\Omega_i^h\}_{i=1}^{N_p}$ these are set of subdomains which are held by each MPI rank during a parallel simulation.

4.1 Linear Elasticity

Linear Elasticity is a mathematical approximation of solid object deformation caused by prescribed loading conditions. It is a simplification of the more general nonlinear theory of elasticity. PSD allows for solving Linear Elasticity problems both in sequential and in parallel. We shall discuss how to do so in details within this section.

PSD is a FEM based solver, to solve a given physics it heavily relies on the variational formulations of the underlying physics. Let us begin with writing the variational formulation of system of Elasticity in which the primary unknown is the displacements vector $\mathbf{u} = \{u_j\}_{j=1}^n$. In the Lagrangian FE framework for searching the unknown nodal displacements vector $\mathbf{u}^h = \{u_j^h\}_{j=1}^n$ the variational formulation of system of Elasticity reads,

$$\forall i \in \llbracket 1; N_p \rrbracket, \int_{\Omega_i^h} \boldsymbol{\sigma}(\mathbf{u}^h) : \boldsymbol{\varepsilon}(\mathbf{v}^h) = \int_{\partial\Omega_{i,N}^h} \mathbf{f} \cdot \mathbf{v}^h \quad \forall \mathbf{v}^h \in \mathbb{V}^h, \mathbf{u}^h \in \mathbb{V}^h, \quad (4.1)$$

here, \mathbf{u}^h is in fact the FE trial function and $\mathbf{v}^h = \{v_j^h\}_{j=1}^n$ is the FE test function.

$$\forall i \in \llbracket 1; N_p \rrbracket, \int_{\Omega_i^h} \lambda \nabla \cdot \mathbf{u}^h \nabla \cdot \mathbf{v}^h + \int_{\Omega_i^h} 2\mu \boldsymbol{\varepsilon}(\mathbf{u}^h) : \boldsymbol{\varepsilon}(\mathbf{v}^h) - \int_{\Omega_i^h} \mathbf{f} \cdot \mathbf{v}^h = 0, \quad \forall \mathbf{v}^h \in [H_0^1(\Omega_i^h)]^n \quad (4.2)$$

In these formulations λ and μ are the Lame's parameters, \mathbf{f} is the body force vector.

4.1.1 PSD simulation of 2D bar problem bending under own body weight

To showcase the usage of Linear elasticity, we shall discuss here an example of a 2D bar, which bends under its own load. The bar — $5 \times 1 \text{ m}^2$ in area— is made up of material with $\rho = 8\text{E}3$, $E = 200\text{E}9$, and $\nu = 0.3$.

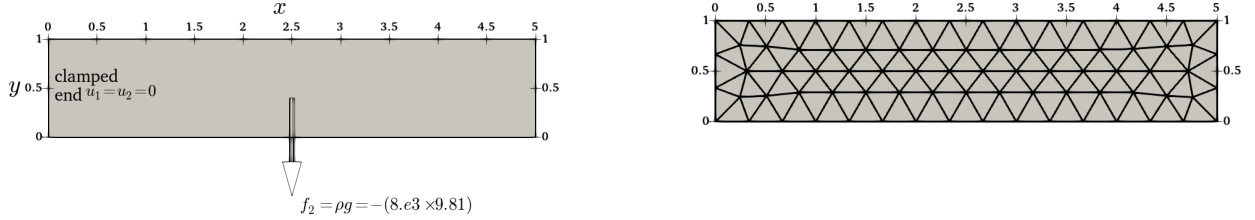


Figure 4.1: 2D bar clamped at left end and bending under own load. Geometry (left) and mesh (right).

Step 1: Preprocessing

First step in a PSD simulation is “PSD setup”, at this step you tell PSD what kind of physics, boundary conditions, approximations, mesh, etc are you expecting to solve. For “PSD setup” go to the PSD/Solver folder, launch `PSD_PreProcess` from the terminal, to do so run the following command.

```
PSD_PreProcess -dimension 2 -bodyforceconditions 1 -dirichletconditions 1 -postprocess u
```

After the “PSD setup” runs successfully you should see many `.edp` files in your PSD/Solver folder. *What do the arguments mean ?* `-dimension 2` means it is a 2D simulation, `-bodyforceconditions 1` with body force; `-dirichletconditions 1` says we have one Dirichlet border; and `-postprocess u` means we would like to have ParaView post processing files. The input properties “ E, ν ” can be mentioned in `ControlParameters.edp`, change $E = 200.\text{e}9$, and $\nu = 0.3$. The volumetric body force condition is mentioned in the same file via variable `Fbc0Fy -78480.0`, i.e $(\rho * g = 8.\text{e}3 * (-9.81) = -78480.0)$. In addition variable `Fbc0On 1` has to be provided in order to indicate the volume (region) for which the body force is acting, here 1 is the integer volume tag of the mesh. Dirichlet boundary conditions are also provided in `ControlParameters.edp`. To provide the clamped boundary condition the variables `Dbc0On 2`, `Dbc0Ux 0.`, and `Dbc0Uy 0.` are used, which means for Dirichlet border 2 (`Dbc0On 2`) where 2 is the clamped border label of the mesh Dirichlet constrain is applied and `Dbc0Ux 0.`, `Dbc0Uy 0` i.e., the clamped end condition ($u_x = u_y = 0$).

Step 2: Solving

As PSD is a parallel solver, let us use 4 cores to solve the 2D bar case. To do so enter the following command:

```
PSD_Solve -np 4 Main.edp
```

Here `-np 4` denote the argument used to enter the number of cores. `PSD_Solve` is a wrapper around `FreeFem++` or `FreeFem++-mpi`. Note that if your problem is large use more cores. PSD has been tested upto 13,000 cores, surely you will now need that many for the 2D bar problem.

Step 3: Postprocessing

PSD allows postprocessing of results in ParaView. After the step 2 mentioned above finishes. Launch ParaView and have a look at the `.pvda` file in the PSD/Solver/VTUs_DATE_TIME folder.

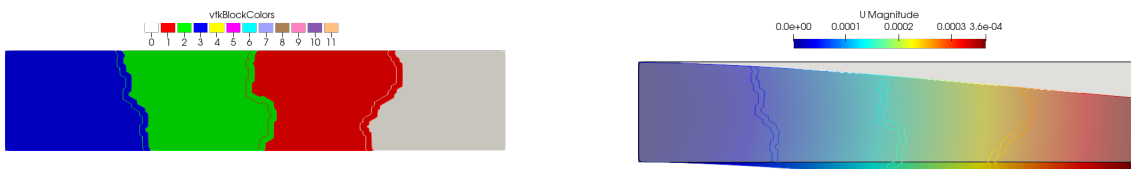


Figure 4.2: 2D clamped bar results. Partitioned mesh (left) and 1000X warped displacement field (right).

4.1.2 PSD simulation of 2D bar problem clamped at both ends

For this test the properties of the material are the same as used in section 4.1.1.

Step 1: Preprocessing

For “PSD setup” go to the PSD/Solver folder, launch the terminal there and run the following command.

```
PSD_PreProcess -dimension 2 -bodyforceconditions 1 -dirichletconditions 2 -postprocess u
```

Since basic nature of both the problems is same this is the exact same command used in preprocessing of section 4.1.1. The only difference of this problem compared to the one from section 4.1.1 is that an additional Dirichlet condition needs to be supplied, notified to PSD by `-dirichletconditions 2`. To provide Dirichlet conditions of the left clamped end ($u_x = u_y = 0$) in `ControlParameters.edp` set `Dbc0On 2`, `Dbc0Ux 0..`, and `Dbc0Uy 0..`. Similarly, for the right end set variables `Dbc1On 4`, `Dbc1Ux 0..`, and `Dbc1Uy 0`. Each one of these is a clamped border respectively labeled as 2 (`Dbc0On 2`) and 4 (`Dbc1On 4`) in the mesh.

Step 2: Solving

Let us now use 3 cores to solve this problem. To do so enter the following command:

```
PSD_Solve -np 3 Main.edp
```

Notice, that this is the exact same command used in solving of section 4.1.1, with only difference that we now use `-np 3` vs. `-np 4`.

Step 3: Postprocessing

Launch ParaView and have a look at the .pvda file in the PSD/Solver/VTUs_DATE_TIME folder.

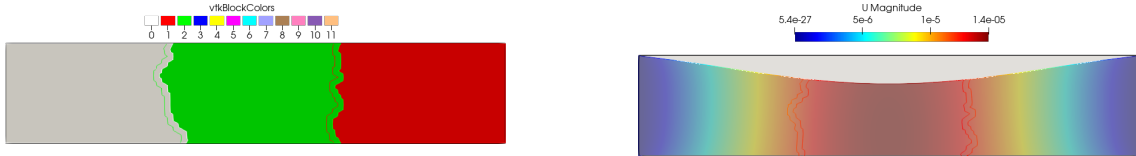


Figure 4.3: 2D clamped bar results. Partitioned mesh (left) and 20000X warped displacement field (right).

In fig. 4.3 there are only three subdomains in the partitioned mesh since only three cores were used.

Redoing the test on Jupiter and moon

Imagine, you wish to know how the test would compare if performed on Moon and Jupiter. The only thing that will change now is the gravitational pull, for Moon $g = 1.32$ and for Jupiter $g = 24.79$. To perform the moon test simply change `Fbc0Fy -10560.0` in `ControlParameters.edp` and redo step 2 and step 3. Similarly, for the Jupiter test `Fbc0Fy -198320.0` in `ControlParameters.edp` and redo step 2 and step 3.

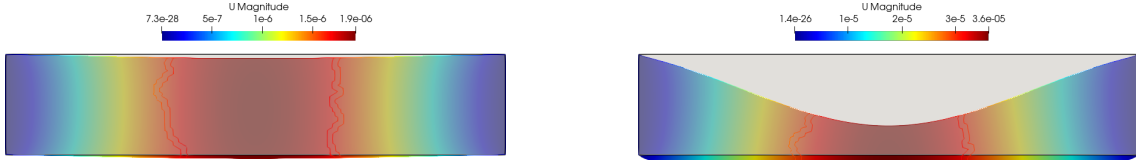


Figure 4.4: 2D clamped bar 20000X warped displacement fields. On moon (left) and on Jupiter (right).

4.1.3 PSD simulation of 2D bar problem clamped at one end while being pulled at the other end (Dirichlet-Dirichlet case)

In this section we showcase the 2D bar problem simulation with one end clamped while being pulled at the other end. Body force is neglected and the non clamped ends pull is approximated with Dirichlet displacement $u_1 = 1$. If this simulation is compared to the previous one from section 4.1.1, the only difference now is that no body force is applied and an additional Dirichlet condition is applied at the free end of the bar. Here is how PSD simulation of this case can be performed.

Step 1: Preprocessing

For "PSD setup" go to the PSD/Solver folder, launch the terminal there and run the following command.

```
PSD_PreProcess -dimension 2 -dirichletconditions 2 -postprocess u
```

In comparison to preprocessing from sections 4.1.1 and 4.1.2, notice that `-bodyforceconditions 1` is missing. This is due to the fact that for this problem we assume null body force. Just like in section 4.1.2 `-dirichletconditions 2`, which notifies to PSD that there are two Dirichlet borders —the clamped and the pulled ends of the bar— in this simulation. To provide these Dirichlet conditions of the two ends in `ControlParameters.edp` set the variables `Dbc0On 2`, `Dbc0Ux 0.`, and `Dbc0Uy 0.` signifying the clamped end ($u_x = 0, u_y = 0$ on mesh label 2) and `Dbc1On 4`, `Dbc1Ux 1.`, and `Dbc1Uy 0.` signifying the pulled end ($u_x = 1, u_y = 0$ on label 4). Note that here at border 4 we have explicitly set $u_2 = 0$ this means the bar is not allowed to shrink(compress) in y direction, however you might wish to allow the bar to compress. For such a simulation simply use `Dbc1On 4` and `Dbc1Ux 1.`, and remove the term `Dbc1Uy 0.` therefor asking PSD not to apply constrain in y direction on the pulled end.

Step 2: Solving

Let us now use 2 cores to solve this problem. To do so enter the following command:

```
PSD_Solve -np 2 Main.edp
```

Notice, that this is the exact same command used in solving of sections 4.1.1 and 4.1.2, with only difference that we now use `-np 2` vs. `-np 4` in section 4.1.1 and `-np 3` in section 4.1.2.

Step 3: Postprocessing

Launch ParaView and have a look at the `.pvf` file in the PSD/Solver/VTUs_DATE_TIME folder.

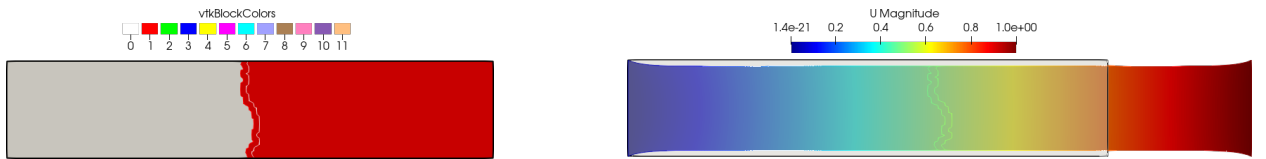


Figure 4.5: 2D bar results. Partitioned mesh (left) and 1.5X warped displacement field (right).

Note now in fig. 4.5 there are only two subdomains in the partitioned mesh since only three cores were used. As expected we see that the right end of the bar which is being pulled does not contract in y direction.

4.1.4 PSD simulation of 2D bar problem clamped at one end while being pulled at the other end (Dirichlet–Neumann case)

Similar simulation, as in section 4.1.3 is presented in this section. We showcase the 2D bar problem simulation with one end clamped while being pulled at the other end. Just like simulation from section 4.1.3 the body force is neglected, However now the non clamped ends pull is approximated with Neumann force $\int_{\partial\Omega_N^h} (\mathbf{t} \cdot \mathbf{v}^h)$. To simulate the pull we assume traction vector $\mathbf{t} = [t_x, t_y] = [10^9., 0]$ acting on the non clamped right end of the bar, i.e., force in x direction is 10 units. Here is how PSD simulation of this case can be performed.

Step 1: Preprocessing

For “PSD setup” go to the PSD/Solver folder, launch the terminal there and run the following command.

```
PSD_PreProcess -dimension 2 -dirichletconditions 1 -tractionconditions 1 -postprocess u
```

the commandline flag `-dirichletconditions 1`, notifies to PSD that there is one Dirichlet border —the clamped end of the bar—in this simulation. And the flag `-tractionconditions 1` notifies to PSD that there is one traction border —the right end of the bar—in this simulation. To provide the clamped boundary condition ($u_1 = 0, u_2 = 0$) set the variables `Dbc0On 2`, `Dbc0Ux 0.`, and `Dbc0Uy 0.` in `ControlParameters.edp`. In the same file traction boundary conditions are provided via the variables `Tbc0On 4` and `Tbc0Tx 1.e9`, which mean apply traction force $\mathbf{t} = [t_x, t_y] = [10^9., 0]$ on label number 4 (right) of the mesh. If user wishes to add traction force ,for instance $t_y = 100.$, simply add the missing macro `macro Tbc0Tx 1.e9 //.`

Step 2: Solving

Let us now use 5 cores to solve this problem. To do so enter the following command:

```
PSD_Solve -np 5 Main.edp
```

Notice, that this is the exact same command used in solving the previous bar problems from other sections, with only difference that we now use `-np 5`.

Step 3: Postprocessing

Launch ParaView and have a look at the .pvda file in the PSD/Solver/VTUs_DATE_TIME folder.



Figure 4.6: 2D bar results. Partitioned mesh (left) and 100X warped displacement field (right).

Note now in fig. 4.6 there are five subdomains in the partitioned mesh since five cores were used. Contrary to fig. 4.5, as expected, we see that the right end of the bar which is being pulled now contract in y direction. This is due to the fact that there is no Dirichlet condition at this end now.

4.1.5 PSD simulation of 2D bar problem clamped at one end while being pulled at the other end (Dirichlet-Neumann-Point boundary conditions case)

Similar simulations, as in sections 4.1.3 and 4.1.4 is presented in this section. We showcase the 2D bar problem simulation with one end clamped while being pulled at the other end. Contrary to simulation in sections 4.1.3 and 4.1.4, the clamped end just restricts x movement, i.e., $u_x = 0$. Just like simulation from sections 4.1.3 and 4.1.4 the body force is neglected. Just like simulation in section 4.1.4, the non clamped ends pull is approximated with Neumann force $\int_{\partial\Omega_N^h} (\mathbf{t} \cdot \mathbf{v}^h)$. To simulate the pull we assume traction vector $\mathbf{t} = [t_x, t_y] = [10^9, 0]$ acting on the non clamped right end of the bar, i.e., force in x direction is 10^9 units. Here is how PSD simulation of this case can be performed.

Step 1: Preprocessing

For "PSD setup" go to the PSD/Solver folder, launch the terminal there and run the following command.

```
PSD_PreProcess -dimension 2 -dirichletconditions 1 -tractionconditions 1 \
-dirichletpointconditions 1 -postprocess u
```

Additional flag `-dirichletpointconditions 1` now appears, this notifies to PSD that there is one Dirichlet point boundary condition. Edit the `ControlParameters.edp` to communicate the desired point boundary conditions, set the variables `PbcOUx 0.` and `PbcOUy 0.` to specify $u_x = 0, u_y = 0$, and variable `PbcCord = [[0. , 0.]]`; to specify the point coordinates $(x, y) = (0, 0)$. Via the flags we specified that `-dirichletconditions 1`, i.e., there is one Dirichlet border. To provide the Dirichlet condition ($u_x = 0$) set the variables `DbcOOn 2` and `DbcOUx 0.` in `ControlParameters.edp`. PSD understands that 4 is the mesh border label on which Dirichlet is applied and ($u_x = 0$) is the condition to be applied.

Step 2: Solving

Let us now use 6 cores to solve this problem. To do so enter the following command:

```
PSD_Solve -np 6 Main.edp
```

Notice, that this is the exact same command used in solving the previous bar problems from other sections, with only difference that we now use `-np 6`.

Step 3: Postprocessing

Launch ParaView and have a look at the `.pvda` file in the PSD/Solver/VTUs_DATE_TIME folder.



Figure 4.7: 2D bar results. Partitioned mesh (left) and 100X warped displacement field (right).

Note now in fig. 4.7 there are six subdomains in the partitioned mesh. As expected, we see that the right and the left end of the bar which is being pulled now contract in y direction, and the bar elongates in x direction.

4.1.6 PSD simulation of 3D bar problem clamped at one end while being pulled at the other end (Dirichlet-Neumann case)

In this section we present a 3D PSD simulation of a clamped bar which is being loaded in vertical direction at the non-clamped end. This simulation is like the one presented in section 4.1.4, however in 3D. The material properties are same as before, and at the non-clamped end traction $t_y = -10^9$ units. The 3D bar is $1 \times 1 \times 5 \text{ m}^3$.

Here is how PSD simulation of this case can be performed.

Step 1: Preprocessing

For "PSD setup" go to the PSD/Solver folder, launch the terminal there and run the following command.

```
PSD_PreProcess -dimension 3 -dirichletconditions 1 -tractionconditions 1 -postprocess u
```

The commandline flag **-dirichletconditions 1** notifies to PSD that there is one Dirichlet border —the clamped end of the bar— in this simulation; **-dimension 3** means the simulation is 3D. And the flag **-tractionconditions 1** notifies to PSD that there is one traction border —the right end of the bar— in this simulation. To provide Dirichlet conditions of the clamped end ($u_x = 0, u_y = 0, u_z = 0$) in **ControlParameters.edp** set **Dbc0On 1**, **Dbc0Ux 0.**, **Dbc0Uy 0.**, and **Dbc0Uz 0.**, where 1 being the surface mesh label of the clamped end. To add the traction boundary condition set **Tbc0On 2** and **Tbc0Ty -1.e9**, here the mesh label number of the right end is 2. For this end $\mathbf{t} = [t_x, t_y, t_z] = [0., 10^9, 0.]$, hence in **ControlParameters.edp** we only use **Tbc0Ty -1.e9**.

Step 2: Solving

Let us now use 4 cores to solve this problem. To do so enter the following command:

```
PSD_Solve -np 4 Main.edp
```

Notice, that this is the exact same command used in solving the previous bar problems from other sections.

Step 3: Postprocessing

Launch ParaView and have a look at the .pvda file in the PSD/Solver/VTUs_DATE_TIME folder.

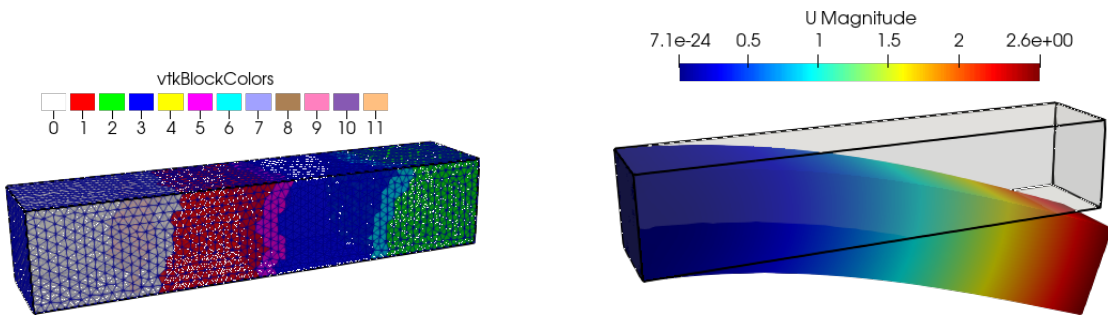


Figure 4.8: 3D bar results. Partitioned mesh (left) and 0.5X warped displacement field (right).

In fig. 4.8 there are four subdomains in the partitioned mesh since four cores were used.

4.1.7 PSD simulation of 3D mechanical piece (Dirichlet-Neumann case) with complex mesh

So far in the previous cases we only concentrated on bar simulations, which were more or less trivial cases. Moreover, the bar meshes are provided with the PSD solver. In this section we now turn towards 3D simulation of a mechanical piece, the geometry of which is shown in fig. 4.9. The left (small) hole is fixed: $u_1 = u_2 = u_3 = 0$, while as traction force $t_x = 10^9$ is applied on the large hole.

You can grab a copy of CAD geometry for the mechanical piece (the Gmsh .geo) your local Gmsh installation folder `gmsh/share/doc/gmsh/demos/simple_geo/piece.geo`. The listing of the file is also given in @. To generate the mesh `piece.msh` simply do

```
gmsh -3 piece.geo
```

Place the generated mesh `piece.msh` in `/PSD/Meshes/3D/piece.msh`. Now the PSD simulation can be performed.

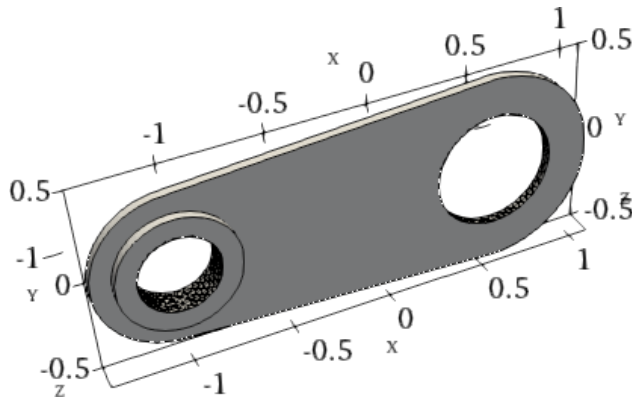


Figure 4.9: 3D mechanical piece.

Step 1: Preprocessing

For "PSD setup" go to the PSD/Solver folder, launch the terminal there and run the following command.

```
PSD_PreProcess -dimension 3 -dirichletconditions 1 -tractionconditions 1 -postprocess u
```

Here, by using these parameters we have generated one Dirichlet condition and one traction condition, respectively to be applied to the small and the large holes in the mesh. Further, by using `-dimension 3` we have let PSD know that the problem is 3D .In the `/PSD/Meshes/3D/piece.msh` generated, the label 4 (resp. 3) corresponds to the Dirichlet (resp. traction) border. To provide Dirichlet conditions on label number 4 ($u_x = 0, u_y = 0, u_z = 0$) in `ControlParameters.edp` use set `Dbc0On 4`, `Dbc0Ux 0..`, `Dbc0Uy 0..`, and `Dbc0Uz 0..` To add the values and label numbers of the traction borders edit the `ControlParameters.edp`, set `Tbc0On 3` and `Tbc0Ty -1.e9`. For this end $\mathbf{t} = [t_x, t_y, t_z] = [0., 10^9, 0.]$. Finally we use steel properties for the material, so in `ControlParameters.edp` the parameters `real E = 200.e9`; and `real nu = 0.3`; should be used. These represent E and ν , respectively. With all the properties and boundary conditions set we now use `string ThName = "../Meshes/3D/piece"`; in the `ControlParameters.edp` file, this notifies PSD about the name of the mesh used for this simulation.

Step 2: Solving

Let us now use 2 cores to solve this problem. To do so enter the following command:

```
PSD_Solve -np 2 Main.edp
```

Step 3: Postprocessing

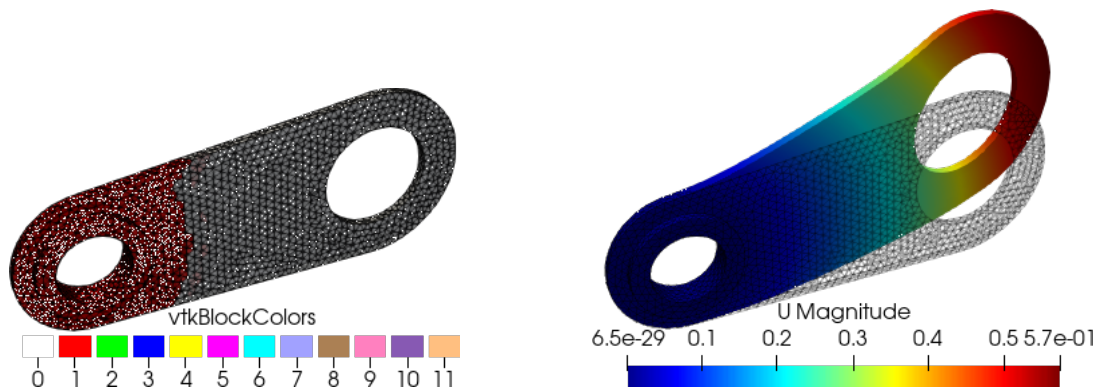


Figure 4.10: Mechanical piece test results. Partitioned mesh (left) and warped displacement field (right).

Launch ParaView and have a look at the .pvda file in the PSD/Solver/VTUs_DATE_TIME folder.

Redoing the test with different conditions

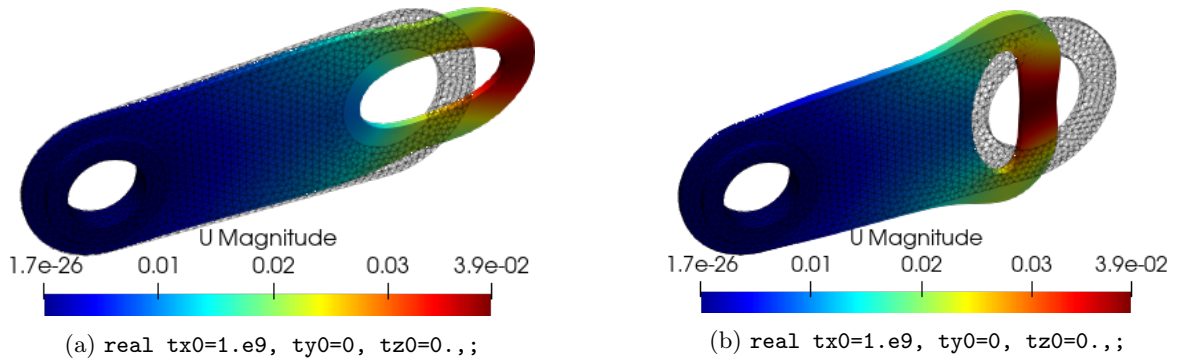


Figure 4.11: Mechanical piece test results.

4.2 Damage mechanics

4.2.1 Hybrid phase-field for damage

On a meshed domain $\Omega^h \in \Omega \subset \mathbb{R}^n$, for damage mechanics the mixed finite element variational formulation in the Lagrangian framework for searching the unknown nodal displacements vector $\mathbf{u}^h = [u_1, u_2, u_3]^\top$ reads,

$$\begin{aligned} & \text{search } \mathbf{u}^h \in \mathbb{V}^h \text{ that satisfies } \forall t \in [0, T] : \\ & \int_{\Omega^h} [(1 - d^h)^2 + \kappa] \boldsymbol{\sigma}(\mathbf{u}^h) : \boldsymbol{\varepsilon}(\mathbf{v}^h) \, dv = \int_{\partial\Omega_N^h} \bar{\mathbf{t}} \cdot \mathbf{v}^h \, ds \quad \forall \mathbf{v}^h \in \mathbb{V}^h, \end{aligned} \quad (4.3)$$

where $\kappa \ll 1$ is a model parameter to prevent numerical singularity when $d \rightarrow 1$. In this formulation, the notation “ $:$ ” is used for the double contraction between tensors (i.e., component-wise tensor product) and \mathbb{V}^h is a mixed third order vector valued finite element functional space to approximate vector test function \mathbf{v}^h and vector trial function \mathbf{u}^h :

$$\mathbb{V}^h = \{ \mathbf{u}^h \in [H^1(\Omega^h)]^3 \mid \forall t \in [0, T] \mid \forall \mathbf{x} \in \partial\Omega_D^h \mathbf{u}^h = \bar{\mathbf{u}} \}, \quad (4.4)$$

with $H^1(\Omega^h)$ denoting a square integrable Sobolev functional space. Similarly, for the phase-field the standard finite element variational formulation for the unknown damage scalar d^h reads,

$$\begin{aligned} & \text{search } d^h \in V^h \text{ that satisfies } \forall t \in [0, T] : \\ & \int_{\Omega^h} \left[\frac{G_c}{l_0} + 2\mathcal{H}^+(\mathbf{u}^h) \right] d^h \theta^h \, dv + \int_{\Omega^h} G_c l_0 \nabla d^h \cdot \nabla \theta^h \, dv = \int_{\Omega^h} 2\mathcal{H}^+(\mathbf{u}^h) \theta^h \, dv \quad \forall \theta^h \in V^h, \end{aligned} \quad (4.5)$$

where, V^h denotes the scalar finite element functional space to approximate scalar test function θ^h and scalar trial function d^h :

$$V^h = \{ d^h \in H^1(\Omega^h) \mid \forall t \in [0, T] \mid d^h \in [0, 1] \}. \quad (4.6)$$

4.3 Elastodynamics

4.4 Soil dynamics

4.5 General list of examples

=====

Sequential 2D linear-elasticity

=====

```
./PSD_PreProcess -dimension 2 -bodyforceconditions 1 conditions 1 -sequential -dirichletconditions 1
PSD_Solve Main.edp -v 0 -ns -nw
```

=====

Sequential 3D linear-elasticity

=====

```
./PSD_PreProcess -dimension 3 -bodyforceconditions 1 -sequential -dirichletconditions 1
PSD_Solve Main.edp -v 0 -ns -nw
```

=====

Sequential 2D linear-elasticity fastmethod

=====

```
./PSD_PreProcess -dimension 2 -bodyforceconditions 1 -sequential -dirichletconditions 1 -fastmethod
PSD_Solve Main.edp -v 0 -ns -nw
```

=====

Sequential 3D linear-elasticity fastmethod

=====

```
./PSD_PreProcess -dimension 3 -bodyforceconditions 1 -sequential -dirichletconditions 1 -fastmethod
PSD_Solve Main.edp -v 0 -ns -nw
```

=====

Parallel 2D linear-elasticity

=====

```
./PSD_PreProcess -dimension 2 -bodyforceconditions 1 -dirichletconditions 1
ff-mpirun-np 2 Main.edp -v 0 -ns -nw
```

=====

Parallel 3D linear-elasticity

=====

```
./PSD_PreProcess -dimension 3 -bodyforceconditions 1 -dirichletconditions 1
ff-mpirun-np 2 Main.edp -v 0 -ns -nw
```

=====

Parallel 2D linear-elasticity fastmethod

=====

```
./PSD_PreProcess -dimension 2 -bodyforceconditions 1 -dirichletconditions 1 -fastmethod
ff-mpirun-np 2 Main.edp -v 0 -ns -nw
```

*=====

Parallel 3D linear-elasticity fastmethod

*=====

```
./PSD_PreProcess -dimension 3 -bodyforceconditions 1 -dirichletconditions 1 -fastmethod
ff-mpirun-np 2 Main.edp -v 0 -ns -nw
```

*=====

Sequential 2D phase-field fracture mechanics

*=====

```
./PSD_PreProcess -dimension 2 -problem damage -model hybrid-phase-field -sequential -dirichletconditions 2
PSD_Solve Main.edp -v 0 -ns -nw
```

*=====

Sequential 3D phase-field fracture mechanics

*=====

```
./PSD_PreProcess -dimension 3 -problem damage -model hybrid-phase-field -sequential -dirichletconditions 2
PSD_Solve Main.edp -v 0 -ns -nw
```

*=====

Parallel 2D phase-field fracture mechanics

*=====

```
./PSD_PreProcess -dimension 2 -problem damage -model hybrid-phase-field -dirichletconditions 2
PSD_Solve -np 2 Main.edp -v 0 -ns -nw
```

*=====

Parallel 3D phase-field fracture mechanics

*=====

```
./PSD_PreProcess -dimension 3 -problem damage -model hybrid-phase-field -dirichletconditions 2
PSD_Solve -np 2 Main.edp -v 0 -ns -nw
```

*=====

Parallel 2D phase-field fracture mechanics with vectorial FEM

*=====

```
./PSD_PreProcess -dimension 2 -problem damage -model hybrid-phase-field -vectorial -dirichletconditions 2
PSD_Solve -np 2 Main.edp -v 0 -ns -nw
```

*=====

Parallel 3D phase-field fracture mechanics with vectorial FEM

*=====

```
./PSD_PreProcess -dimension 3 -problem damage -model hybrid-phase-field -vectorial -dirichletconditions 2
PSD_Solve -np 2 Main.edp -v 0 -ns -nw
```

*=====

Sequential 2D phase-field fracture mechanics energydecomp

*=====

```
./PSD_PreProcess -dimension 2 -problem damage -model hybrid-phase-field -sequential -dirichletconditions 2
-energydecomp
PSD_Solve Main.edp -v 0 -ns -nw
```

*=====

Sequential 3D phase-field fracture mechanics energydecomp

*=====

```
./PSD_PreProcess -dimension 3 -problem damage -model hybrid-phase-field -sequential -dirichletconditions 2
-energydecomp
PSD_Solve Main.edp -v 0 -ns -nw
```

*=====

Parallel 2D phase-field fracture mechanics energydecomp

*=====

```
./PSD_PreProcess -dimension 2 -problem damage -model hybrid-phase-field -dirichletconditions 2
-energydecomp
PSD_Solve -np 2 Main.edp -v 0 -ns -nw
```

*=====

Parallel 3D phase-field fracture mechanics energydecomp

*=====

```
./PSD_PreProcess -dimension 3 -problem damage -model hybrid-phase-field -dirichletconditions 2
-energydecomp
PSD_Solve -np 2 Main.edp -v 0 -ns -nw
```

*=====

Parallel 2D phase-field fracture mechanics energydecomp & vectorial

*=====

```
./PSD_PreProcess -dimension 2 -problem damage -model hybrid-phase-field -vectorial -dirichletconditions 2
-energydecomp
PSD_Solve -np 2 Main.edp -v 0 -ns -nw
```

*=====

Parallel 3D phase-field fracture mechanics energydecomp

*=====

```
./PSD_PreProcess -dimension 3 -problem damage -model hybrid-phase-field -vectorial -dirichletconditions 2
-energydecomp
PSD_Solve -np 2 Main.edp -v 0 -ns -nw
```

*=====

Sequential 2D phase-field fracture mechanics with GFP

*=====

```
./PSD_PreProcess -dimension 2 -problem damage -model hybrid-phase-field -dirichletconditions 2
-sequential -useGFP

PSD_Solve Main.edp -v 0 -ns -nw
```

*=====

Sequential 3D phase-field fracture mechanics with GFP

*=====

```
./PSD_PreProcess -dimension 3 -problem damage -model hybrid-phase-field -dirichletconditions 2
-sequential -useGFP

PSD_Solve Main.edp -v 0 -ns -nw
```

*=====

Parallel 2D phase-field fracture mechanics with GFP

*=====

```
./PSD_PreProcess -dimension 2 -problem damage -model hybrid-phase-field -dirichletconditions 2 -useGFP

PSD_Solve -np 2 Main.edp -v 0 -ns -nw
```

*=====

Parallel 3D phase-field fracture mechanics with GFP

*=====

```
./PSD_PreProcess -dimension 3 -problem damage -model hybrid-phase-field -dirichletconditions 2 -useGFP

PSD_Solve -np 2 Main.edp -v 0 -ns -nw
```

*=====

Parallel 2D phase-field fracture mechanics with GFP & vectorial

*=====

```
./PSD_PreProcess -dimension 2 -problem damage -model hybrid-phase-field -vectorial -dirichletconditions 2
-useGFP

PSD_Solve -np 2 Main.edp -v 0 -ns -nw
```

*=====

Parallel 3D phase-field fracture mechanics with GFP & vectorial

*=====

```
./PSD_PreProcess -dimension 3 -problem damage -model hybrid-phase-field -vectorial -dirichletconditions 2
-useGFP

PSD_Solve -np 2 Main.edp -v 0 -ns -nw
```

*=====

Sequential 2D phase-field fracture mechanics with energydecomp & GFP

*=====

```
./PSD_PreProcess -dimension 2 -problem damage -model hybrid-phase-field -sequential -dirichletconditions 2
-energydecomp -useGFP

PSD_Solve Main.edp -v 0 -ns -nw
```

*=====

Sequential 3D phase-field fracture mechanics with energydecomp & GFP

*=====

```
./PSD_PreProcess -dimension 3 -problem damage -model hybrid-phase-field -sequential -dirichletconditions 2
-energydecomp -useGFP

PSD_Solve Main.edp -v 0 -ns -nw
```

*=====

Parallel 2D phase-field fracture mechanics with energydecomp & GFP

*=====

```
./PSD_PreProcess -dimension 2 -problem damage -model hybrid-phase-field -dirichletconditions 2
-energydecomp -useGFP

PSD_Solve -np 2 Main.edp -v 0 -ns -nw
```

*=====

Parallel 3D phase-field fracture mechanics with energydecomp & GFP

*=====

```
./PSD_PreProcess -dimension 3 -problem damage -model hybrid-phase-field -dirichletconditions 2
-energydecomp -useGFP

PSD_Solve -np 2 Main.edp -v 0 -ns -nw
```

*=====

Parallel 2D phase-field fracture mechanics with energydecomp, vectorial & GFP

*=====

```
./PSD_PreProcess -dimension 2 -problem damage -model hybrid-phase-field -vectorial -dirichletconditions 2
-energydecomp -useGFP

PSD_Solve -np 2 Main.edp -v 0 -ns -nw
```

*=====

Parallel 3D phase-field fracture mechanics with energydecomp, vectorial & GFP

*=====

```
./PSD_PreProcess -dimension 3 -problem damage -model hybrid-phase-field -vectorial -dirichletconditions 2
-energydecomp -useGFP

PSD_Solve -np 2 Main.edp -v 0 -ns -nw
```

*=====

Parallel 2D phase-field fracture mechanics with reaction-force, energydecomp, vectorial & GFP

*=====

```
./PSD_PreProcess -dimension 2 -problem damage -model hybrid-phase-field -vectorial -dirichletconditions 2
-getreactionforce -energydecomp -useGFP

PSD_Solve -np 2 Main.edp -v 0 -ns -nw
```

*=====

Parallel 3D phase-field fracture mechanics with reaction-force, energydecomp, vectorial & GFP

*=====

```
./PSD_PreProcess -dimension 3 -problem damage -model hybrid-phase-field -vectorial -dirichletconditions 2
-getreactionforce -energydecomp -useGFP

PSD_Solve -np 2 Main.edp -v 0 -ns -nw
```

*=====

Parallel 2D phase-field fracture mechanics with live reaction-force plotting, energydecomp, vectorial & GFP

*=====

```
./PSD_PreProcess -dimension 2 -problem damage -model hybrid-phase-field -vectorial -dirichletconditions 2
-getreactionforce -plotreactionforce -energydecomp -useGFP

PSD_Solve -np 2 Main.edp -v 0 -ns -nw
```

*=====

Parallel 3D phase-field fracture mechanics with live reaction-force plotting, energydecomp, vectorial & GFP

*=====

```
./PSD_PreProcess -dimension 3 -problem damage -model hybrid-phase-field -vectorial -dirichletconditions 2
-getreactionforce -plotreactionforce -energydecomp -useGFP

PSD_Solve -np 2 Main.edp -v 0 -ns -nw
```

*=====

Sequential 2D Elastodynamics

*=====

```
./PSD_PreProcess -dimension 2 -problem elastodynamics -sequential -dirichletconditions 1
-tractionconditions 1

PSD_Solve Main.edp -v 0 -ns -nw
```

*=====

Sequential 3D Elastodynamics

*=====

```
./PSD_PreProcess -dimension 3 -problem elastodynamics -sequential -dirichletconditions 1
-tractionconditions 1

PSD_SolveMain.edp -v 0 -ns -nw
```

*=====

Parallel 2D Elastodynamics

*=====

```
./PSD_PreProcess -dimension 2 -problem elastodynamics -dirichletconditions 1 -tractionconditions 1
ff-mpirun -np 2 Main.edp -v 0 -ns -nw
```

*=====

Parallel 3D Elastodynamics

*=====

```
*=====*
```

```
./PSD_PreProcess -dimension 3 -problem elastodynamics -dirichletconditions 1 -tractionconditions 1  
ff-mpirun -np 2 Main.edp -v 0 -ns -nw
```

```
*=====*
```

Sequential 2D Soildynamics

```
*=====*
```

```
./PSD_PreProcess -dimension 2 -problem soildynamics -sequential -dirichletconditions 1  
PSD_Solve Main.edp -v 0 -ns -nw
```

```
*=====*
```

Sequential 3D Soildynamics

```
*=====*
```

```
./PSD_PreProcess -dimension 3 -problem soildynamics -sequential -dirichletconditions 1  
PSD_Solve Main.edp -v 0 -ns -nw
```

```
*=====*
```

Parallel 2D Soildynamics

```
*=====*
```

```
./PSD_PreProcess -dimension 2 -problem soildynamics -dirichletconditions 1  
PSD_Solve -np 2 Main.edp -v 0 -ns -nw
```

```
*=====*
```

Parallel 3D Soildynamics

```
*=====*
```

```
./PSD_PreProcess -dimension 3 -problem soildynamics -dirichletconditions 1  
PSD_Solve -np 2 Main.edp -v 0 -ns -nw
```

Chapter 5

Validation

5.1 Linear elasticity solver validation and verification using method of manufactured solutions

The main aim of this write-up is to develop and implement the method of manufactured solutions (MMS) within the field of linear elasticity. A FEM solver is developed for solving linear elasticity problems. Within this note MMS is applied to verify and validate this solver.

Mathematical typesetting conventions

Unless specified, the mathematical typesetting conventions are as follows.

Typesetting	Example	Description
Bold uppercase	\mathbf{A}, \mathbf{M}	Matrices
Bold lowercase	$\mathbf{x}, \mathbf{b}, \mathbf{f}$	Vector
Lowercase Greek	α, β, λ	Scalars
Lowercase Roman	g	Scalars
Bold Greek	$\boldsymbol{\sigma}, \boldsymbol{\epsilon}$	Tensor
Blackboard bold style	\mathbb{R}	Number set

5.1.1 Introduction

In order to use the developed FEM solver to predict outcomes from previously unforeseen situations in linear elasticity, it is important to validate and verify the proposed solver. In other words, it is important to build trust on the solvers reliability and know its limits. This can be done by asserting whether the solver is able to reproduce analytical or experimental observations for certain linear elasticity problems. Another way is to compare against results of certain benchmark problems solved with other numerical tools, hence performing cross-validation. Other interesting option is the use of MMS.

Before progressing further, let us interpret what validation and verification means in the context of numerical modeling. Assuming that the mathematical model for a given physics is accurate, the process of *verification* investigates if an accurate numerical solution to the given mathematical model can be obtained via the numerical method which is being verified. By the process of verification the order of accuracy for the numerical methods can also be calculated. Whereas, the process of *validation* asserts if an appropriate mathematical model has been chosen to describe the physical phenomenon. More elaborate discussions on the process of validation and verification of numerical tools can be found in [21].

5.1.2 Verification tests with the method of manufactured solutions

The method of manufactured solutions is used by many numerical communities for solver (code) verification, see for example [23, 7, 22]. Concerning the solid mechanics solvers, studies such as ??? used the method of manufactured solutions for solver verification.

In the method of manufactured solutions, we start with an assumed explicit expression for the solution field (manufactured solution). Then, the solution is substituted in the concerned PDE model. This leads to a consistent set of source terms and/or initial conditions and/or boundary conditions. These terms are then used to solve the equation numerically, with the method (solver) that needs to be verified. Finally, by analyzing the error between the numerical solution and the manufactured solution, one can verify if the numerical method works. In addition, by analyzing how the error decreases when finer numerical discretization is considered, one can obtain the order of convergence for the numerical method.

Two-dimensional MMS test case

Let us assume a hypothetical solid material domain ($\Omega \in \mathbb{R}^2$) is acted upon by manufactured forcing vector $\hat{\mathbf{f}} = [\hat{f}_1, \hat{f}_2]^\top$. This causes the body to deform:

$$\begin{aligned}\hat{u}_1 &= x^3 + x^2y, \\ \hat{u}_2 &= xy^2 + x^2y.\end{aligned}\tag{5.1}$$

The equation (5.1) is our manufactured solution and has been explicitly assumed¹. The task now is to calculate the manufactured forcing vector $\hat{\mathbf{f}}$. In order to do so the following steps are applied.

- Using (5.1) for calculating $\nabla \cdot \hat{\mathbf{u}}$:

$$\begin{aligned}\partial_x \hat{u}_1 &= 3x^2 + 2xy, & \partial_y \hat{u}_1 &= x^2, \\ \partial_x \hat{u}_2 &= y^2 + 2xy, & \partial_y \hat{u}_2 &= x^2 + 2xy,\end{aligned}\tag{5.2}$$

then

$$\nabla \cdot \hat{\mathbf{u}} = \nabla \cdot [\hat{u}_1 \quad \hat{u}_2]^\top = 4(x^2 + xy).\tag{5.3}$$

- Using (5.2) for calculating the manufactured stain tensor $\hat{\boldsymbol{\varepsilon}}$ components $\hat{\varepsilon}_{ij}$:

$$\hat{\varepsilon}_{ij}(\hat{\mathbf{u}}) = \frac{1}{2} (\partial_j \hat{u}_i + \partial_i \hat{u}_j),$$

then

$$\begin{aligned}\hat{\varepsilon}_{11} &= 3x^2 + 2xy, & \hat{\varepsilon}_{12} &= \frac{1}{2}(x^2 + y^2 + 2xy), \\ \hat{\varepsilon}_{21} &= \frac{1}{2}(x^2 + y^2 + 2xy), & \hat{\varepsilon}_{22} &= x^2 + 2xy.\end{aligned}\tag{5.4}$$

- Using (5.3) and (5.4) for calculating the manufactured stress tensor $\hat{\boldsymbol{\sigma}}$ components $\hat{\sigma}_{ij}$:

$$\hat{\sigma}_{ij} = \lambda \delta_{ij} \nabla \cdot \hat{\mathbf{u}} + 2\mu \hat{\varepsilon}_{ij}(\hat{\mathbf{u}})$$

then

$$\begin{aligned}\hat{\sigma}_{11} &= 4\lambda(x^2 + xy) + 2\mu(3x^2 + 2xy), & \hat{\sigma}_{12} &= \mu(x^2 + y^2 + 2xy), \\ \hat{\sigma}_{21} &= \mu(x^2 + y^2 + 2xy), & \hat{\sigma}_{22} &= 4\lambda(x^2 + xy) + 2\mu(3x^2 + 2xy).\end{aligned}\tag{5.5}$$

- Finally, using (5.4) for calculating the manufactured force vector $\hat{\mathbf{f}}$ components \hat{f}_i :

$$\begin{aligned}\hat{f}_1 &= -\partial_x \hat{\sigma}_{11} - \partial_x \hat{\sigma}_{12}, \\ \hat{f}_2 &= -\partial_x \hat{\sigma}_{21} - \partial_x \hat{\sigma}_{22},\end{aligned}$$

¹One could chose other expressions, as long as small strain limiting condition is obeyed: $\|\boldsymbol{\varepsilon}\| = \{0.2 \times 10^{-2}; 0.5 \times 10^{-2}\}$

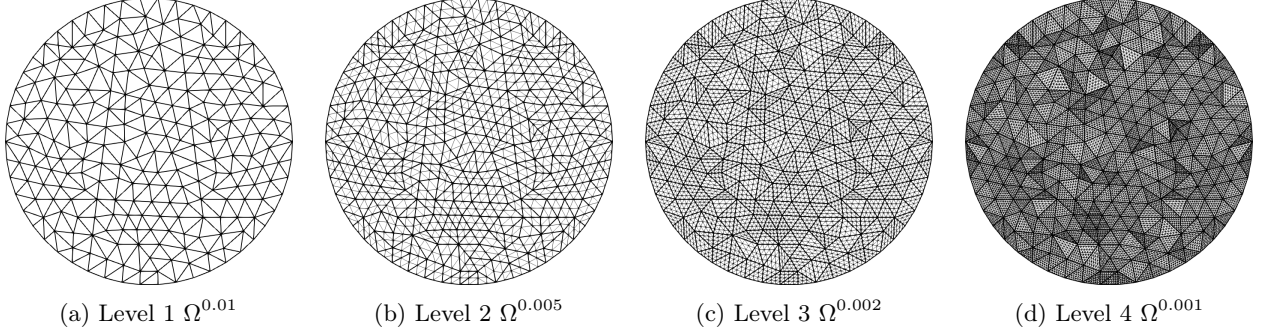


Figure 5.1: Finite element meshes.

then

$$\begin{aligned}\hat{f}_1 &= -x(8\lambda + 14\mu) - y(4\lambda + 6\mu), \\ \hat{f}_2 &= -x(6\lambda + 4\mu) - y(2\mu).\end{aligned}\tag{5.6}$$

Now all we need is a FEM solver that can solve the elasticity system given the manufactured forcing vector (5.6). Error analysis between the displacement solution vector \mathbf{u}^h from the FEM solver and the manufactured solution $\hat{\mathbf{u}}$, can then be used to validate and verify the solver. In addition the error analysis will help in assessing the convergence order.

5.1.3 FEM solving model

Assuming Ω^h be the bi-dimensional tessellated reference configuration for the hypothetical solid material, or in other words the finite element mesh defined with size parameter h . Finite element variational formulation in the Lagrangian framework for the unknown displacements vector \mathbf{u}^h then reads,

$$\left| \begin{array}{l} \text{find } \mathbf{u}^h \in [H_0^1(\Omega^h)]^2 : \\ \int_{\Omega^h} \lambda \nabla \cdot \mathbf{u}^h \nabla \cdot \mathbf{v}^h + \int_{\Omega^h} 2\mu \boldsymbol{\varepsilon}(\mathbf{u}^h) : \boldsymbol{\varepsilon}(\mathbf{v}^h) + \int_{\Omega^h} \hat{\mathbf{f}} \cdot \mathbf{v}^h = 0, \quad \forall \mathbf{v}^h \in [H_0^1(\Omega^h)]^2, \\ \text{given } \mathbf{u}^h = \hat{\mathbf{u}} \text{ on } \partial\Omega_D^h. \end{array} \right. \tag{5.7}$$

Notice in this equation the essential Dirichlet boundary conditions² are provided by the known manufactured displacement field $\hat{\mathbf{u}}$ from equation (5.1). Please refer to the other note "The Krylov subspace based CG solver for linear elasticity", in order to know how the finite element linear system $\mathbf{Ax} = \mathbf{b}$ is assembled and then solved iteratively to derive the displacement field $\hat{\mathbf{u}} : \hat{\mathbf{u}} = \mathbf{x}^{(m)}$, where m is the converged iteration number for the CG iterative solver.

-	Level 1	Level 2	Level 3	Level 4
N_v	244	923	3,589	14,153
N_e	486	1,844	7,176	28,304
h_{\min}	0.0102	0.0051	0.0026	0.00013

Table 5.1: Characteristics of different FEM meshes used for error analysis.

5.1.4 The FEM solver

To numerically solve equation (5.7), a mixed finite element space based solver is developed using a DSL FreeFem++ [11]. The space discretization kernel of FreeFem++ uses unstructured (triangular or tetrahedral) mesh inputs. Further, for the linear algebra backend the CG solver provided within FreeFem++.

²For unique solution of the elasticity problem one needs the Dirichlet boundary conditions.

has the capabilities to mix \mathbb{P}_1 , \mathbb{P}_2 , and \mathbb{P}_3 finite element spaces, for approximating \mathbf{u} . For the sake of simplicity we will only use mixed \mathbb{P}_1 spaces, i.e. in order to solve (5.7) a mixed finite element space $\mathcal{V}^h := \mathcal{V}^h \times \mathcal{V}^h$ is defined, such that

$$\mathbf{u}^h = [u_1^h, u_2^h]^\top \in \mathcal{V}^h \quad \text{and} \quad \mathbf{v}^h = [v_1^h, v_2^h]^\top \in \mathcal{V}^h.$$

where,

$$\mathcal{V}^h(v^h) = \{v^h \in [H_0^1(\Omega^h)], v^h \in \mathbb{P}_1 : v^h = \hat{u} \text{ on } \partial\Omega_D^h\}.$$

Let us now asses if the developed solver is any good and asses its convergence order. We assume Ω to be a circle³ of radius 0.1 m and made of a material with modulus of elasticity $E = 100$ GPa and Poissons ratio $\nu = 0.2$. Let us call this test MMS-test 1.

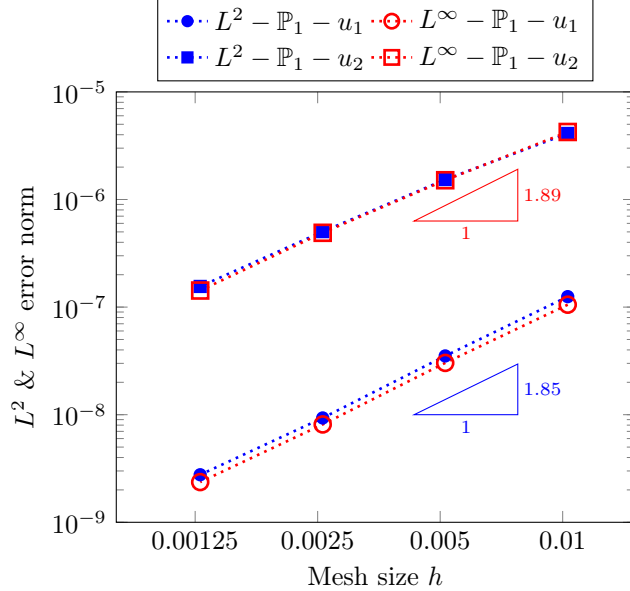


Figure 5.2: Error between the FEM and manufactured solution. Note that the mesh size h is infact the minimum element size h_{\min} that exists within a mesh Ω^h .

To solve this elasticity problem with FEM, four hierarchical meshes are produced using BMAG: Bidimensional Anisotropic Mesh Generator [10]. Hierarchy of refined meshes are obtained by splitting each triangle in the coarse level mesh by four. The split operation is followed to ensure that coarse solutions live in the fine ones. The four hierarchical meshes are presented in figure 5.1. For elaborated characteristics of these meshes refer to table 5.1.

Using the four hierarchical meshes, four simulations of MMS-test 1 were performed. Note, to avoid numerical error discrepancies from the linear solver, the CG iteration was stopped when the relative unpreconditioned residual was lower than 10^{-13} . The mixed FEM solution for the solver was then compared to the manufactured one and L^2 and L^∞ errors were calculated:

$$L^2(\mathbf{u}) = \left(\int_{\Omega^h} (\hat{\mathbf{u}} - \mathbf{u}^h)^2 \right)^{\frac{1}{2}} \quad \text{and} \quad (5.8)$$

$$L^\infty(\mathbf{u}) = \max(|\hat{\mathbf{u}} - \mathbf{u}^h|), \quad (5.9)$$

these are plotted in figure 5.2.

Error analysis plot provided in figure 5.2 proves that the developed FEM solver has approximately second order convergence rate. More precisely, the L^2 error analysis reveled that the FEM solver has the order of

³Circular domain is just an assumption, given the mathematics developed in section 5.1.2 one could use any 2D geometry of choice.

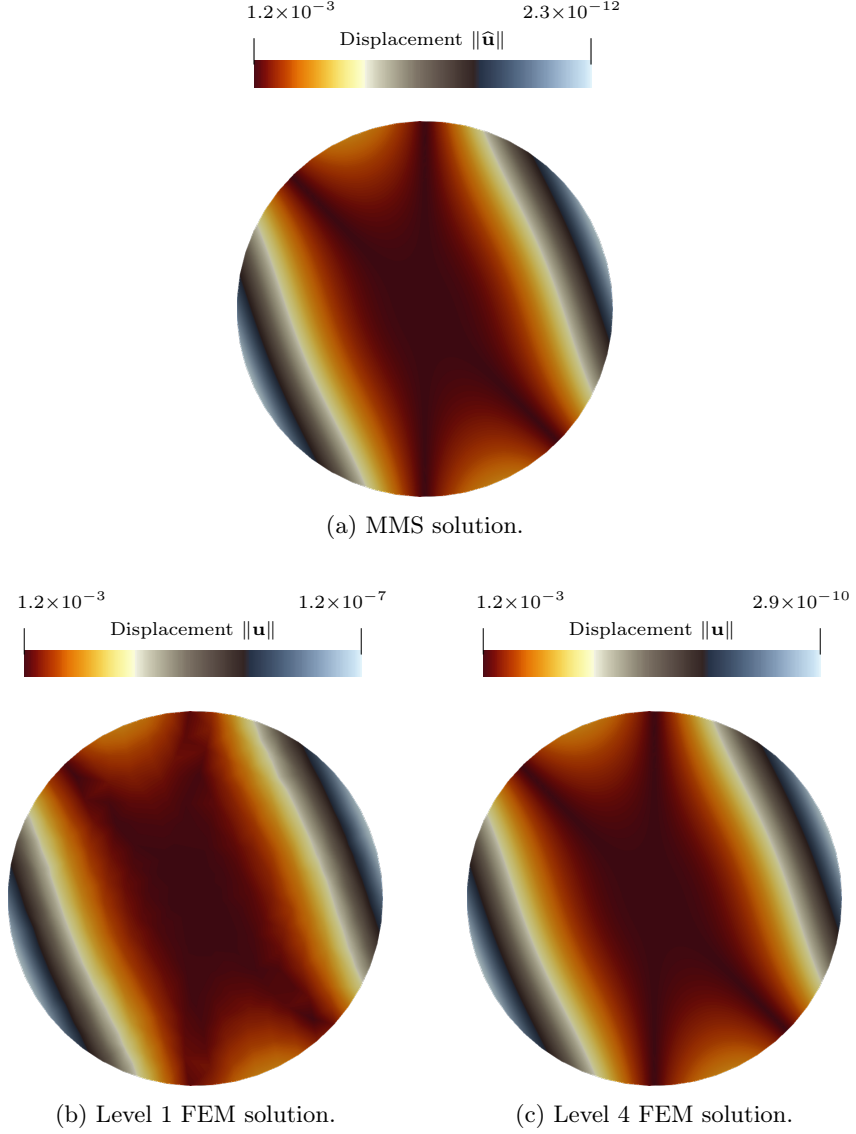


Figure 5.3: Displacement field magnitude visualization.

convergences given by 1.85, against theoretical value of 2. Similarly, the L^∞ error analysis reveled that the FEM solver has the order of convergences given by 1.89, against theoretical value of 2. To investigate further the displacement field magnitudes for the MMS solution and the FEM solutions have been visualized in figure 5.3. Notice how solution improves from the coarsest level mesh (level 1) to the finest one (level 4). It is fair to say that even the coarse level solution is approximating the displacement field well. To investigate further in figure 5.4 the point wise error field is visualized. One can clearly observe how the error reduces when using ore refined meshes. Moreover, notice that error is zero at the borders, this is due to the fact that all border are Dirichlet borders.

5.2 Damage mechanics solver validation

A commonly used numerical test from literature (see e.g., [1, 17, 16, 13] to cite but a few), the two-dimensional (2D) single-edge notched tensile fracture test, is considered as the benchmark problem in this subsection. From here-forth this test is referenced as test 1 in the text.

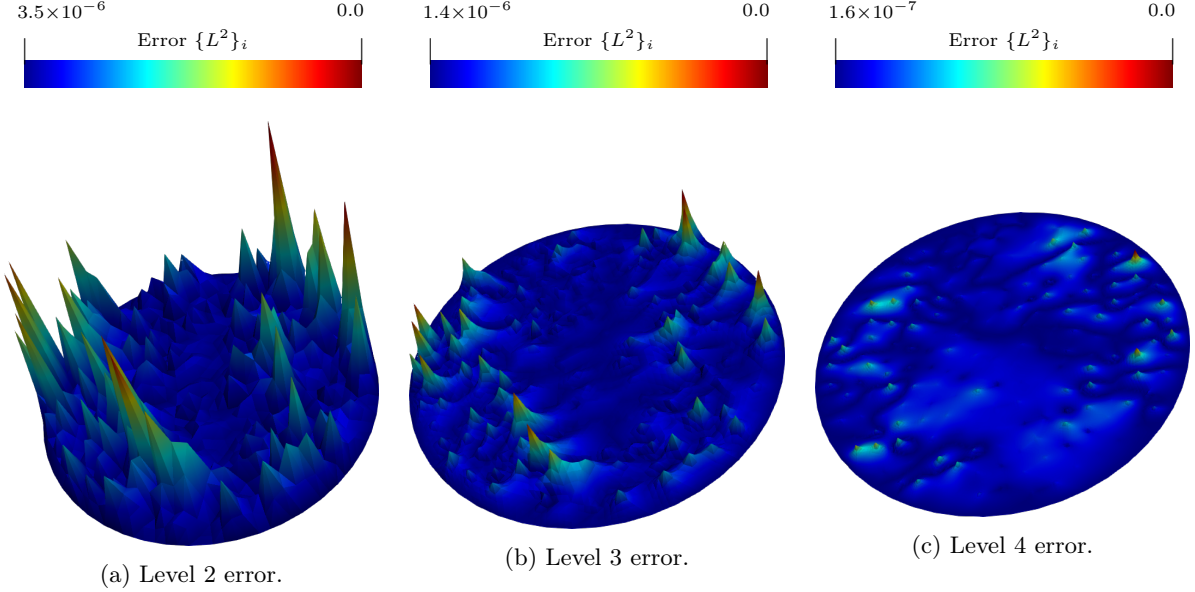


Figure 5.4: Warped error field visualization. The warp fields have been magnified a million times for better visualization.

Problem setting

The domain of interest is an initially cracked square plate $(x, y) \in \Omega = [0 \text{ cm}, 1 \text{ cm}]^2$ (fig. 5.5a). With an initial crack and a constrained bottom edge $\partial\Omega_D(x, y : y = 0)$, the plate is subject to increasing displacements on its top edge $\partial\Omega_D(x, y : y = 1)$ until the plate fully cracks open. The initial crack is placed at the center of the plate, i.e., $\partial\Omega_D(x : 0 \leq x \leq 0.5, y : y = 0.5)$. These boundary conditions are also illustrated in fig. 5.5a. The plate material is characterized by $\lambda = 121.15 \text{ kPa}$, $\mu = 80.77 \text{ kPa}$, and $G_c = 2.7 \text{ kN mm}^{-1}$.

Concerning the computational specifications of test 1, the displacement discontinuity imposed by the initial crack was modeled by nearly overlapping (tolerance $\delta y = 10^{-7} \text{ m}$) Dirichlet nodes placed along the cracks edge $\partial\Omega_D^h(x : 0 \leq x \leq 0.5, y : y = 0.5 \pm \delta y)$ within Ω^h . For illustration proposes, a coarse grid featuring Dirichlet nodes for the initial crack of test 1 is presented in fig. 5.5b. The displacement Dirichlet condition on the top edge is applied with an increment of $\Delta\bar{u}_2 = 1 \cdot 10^{-5} \text{ mm}$ up to $u_2 = 5 \cdot 10^{-3} \text{ mm}$ and $\Delta\bar{u}_2 = 1 \cdot 10^{-6} \text{ mm}$ up to failure of the specimen. For the lower edge, the constrained displacement Dirichlet conditions $\bar{u}_1 = \bar{u}_2 = 0$ are applied. Further, for test 1 and for all the simulations that appear in this study, parameter κ is set to $1 \cdot 10^{-6}$ and l_0 is assumed equal to $2h$, where h is the characteristic size of the mesh Ω^h .

The unstructured Delaunay (triangular) meshes generated with Gmsh are used for solving the finite element problem of test 1. To establish mesh convergence, test 1 has been solved multiple times by varying the level of mesh refinements, details of these meshes are provided in table 5.2. The hierarchy of mesh refinements were generated by dividing each triangle in Ω^h into four equal triangles. As such in table 5.2, we observe that with every refinement, the mesh size h halves and the number of triangles quadruple. The initial crack fields for the three mesh refinements (visualized using damage-field d) are presented in fig. 5.6.

Solver validation

Using the test 1 we cross-validate and compare our PSD solver (sequential and parallel) against benchmark solutions of this test available in the literature. In fig. 5.7, the top surface reaction force F_y versus applied displacements is plotted for various mesh refinement levels (detailed in table 5.2) and compared to a reference anisotropic phase-field solution from [2].

In fig. 5.7, the mesh convergence is evidenced from the improving PSD solutions (solid lines) towards the

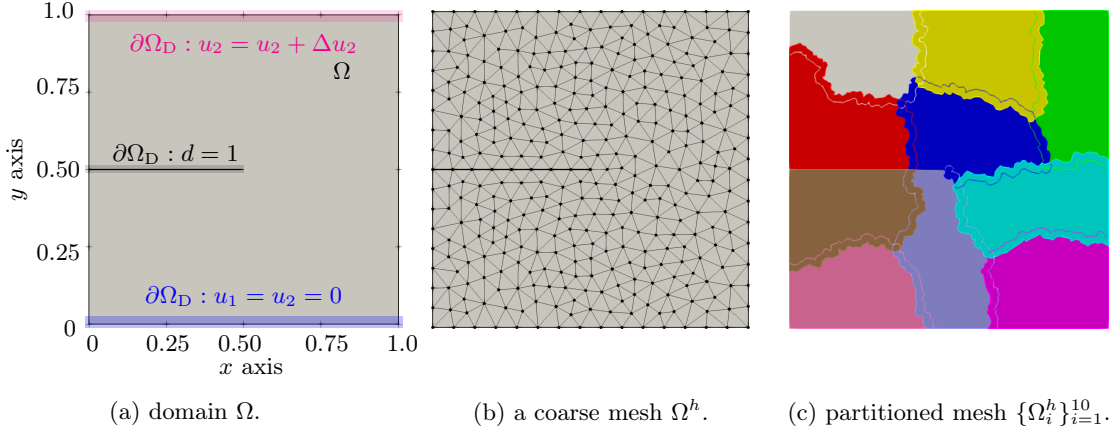


Figure 5.5: domain Ω , mesh Ω^h , and partitioned mesh $\{\Omega_i^h\}_{i=1}^{10}$ for test 1. (a) also illustrates the boundary conditions applied to test 1. (b) represents a coarse unstructured finite element mesh with ‘nearly’ duplicate Dirichlet nodes for the initial crack.

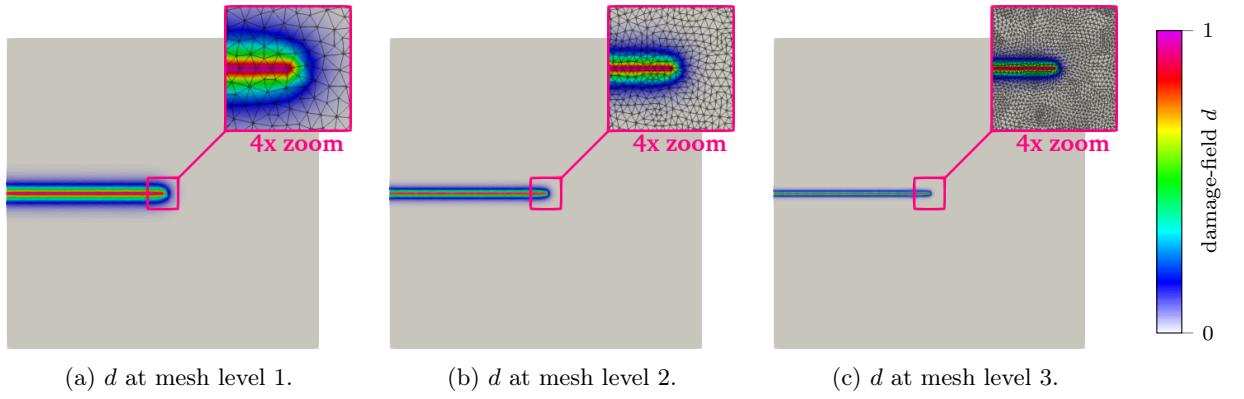


Figure 5.6: initial crack visualization of test 1 via damage-field d at different mesh levels.

reference solution, hence validating the PSD solver. Our computations (at level 3) are in good agreement with the results provided in [2]. This simulation was executed using 10 processes on the desktop PC. The parMETIS partitioned mesh with 10 subdomains is presented in fig. 5.5c.

To further validate the PSD solver, we compare the errors in computing the maximum reaction-force $\max(F_y)$ obtained from our solver against two different reference solutions provided in [1] and [2]. The last two columns of table 5.1 enumerate these errors. At finest mesh level 3, these errors decrease down to less than 1%. Alongside the plot in fig. 5.7, four instantaneous snapshots of the calculated damage-fields are presented. These damage-fields are obtained from the simulation of test 1 at the finest mesh level 3. Damage-field evolution, crack initiation, and propagation can be observed in these snapshots. As expected, under extreme tensile loading, the crack can be seen to travel along a (almost) straight line dividing the square specimen into two (almost) equal halves. Note that for additional validation, other literature comparative tests (mode I, mode II, and mode III fracture) were also performed but these are not shown here for the sake of conciseness.

Table 5.2: characteristics and computational details for the different finite element meshes used for test 1. $E1_{\max(F_y)}$ and $E2_{\max(F_y)}$ are the maximum reaction force errors computed against references [2] and [1], respectively.

mesh	nodes	triangles	h	N_{DOF}	N_{nz}	$E1_{\max(I)}$	$E2_{\max(I)}$
level 1	8,353	16,384	0.0156	25,059	520,425	17.82%	19.22%
level 2	33,089	65,536	0.0078	99,267	2,073,033	5.68%	8.12%
level 3	131,713	262,144	0.0039	395,139	8,274,825	0.45%	0.61%

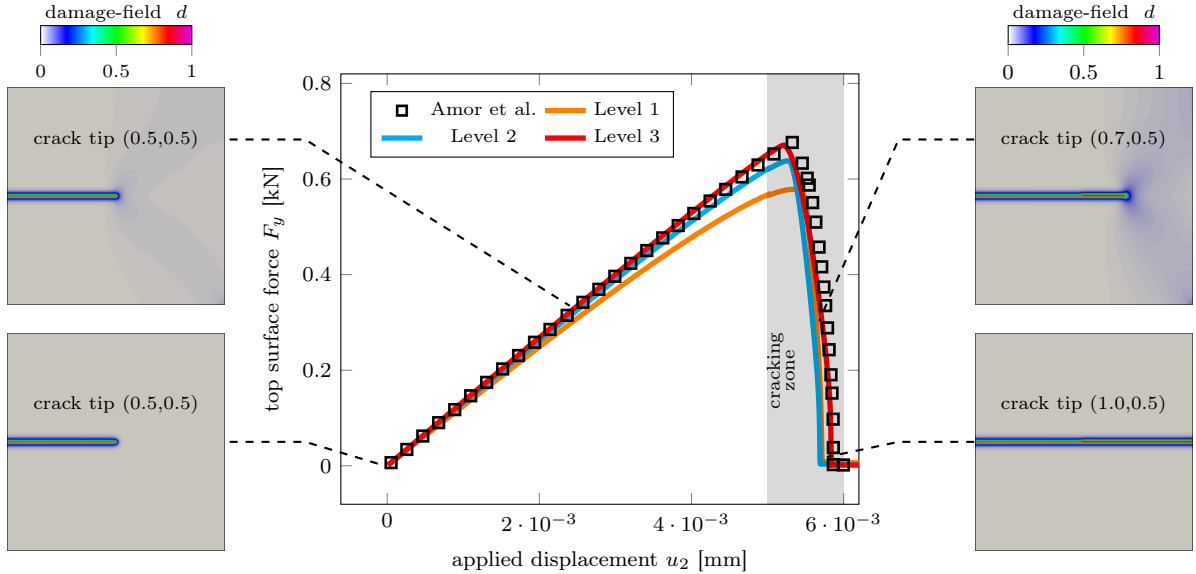


Figure 5.7: mesh convergence demonstrated via force-displacement plot for the two-dimensional single-edge notched tensile fracture simulation, test 1. The solid lines (Level 1 to 3) refers to our PSD solution for different mesh refinements and the square markers denote the reference solution (obtained by the anisotropic phase-field method) presented by [2].

5.3 Validating the PSD soil-dynamic solver with paraxial boundary conditions

In this subsection we would compare the paraxial absorbing elements implemented in PSD against other absorbing boundary conditions available in CAST3M⁴. This document also serves as a naive cross validation of the PSD solvers parallel/sequential kernel developed for soil-dynamics.

5.3.1 Numerical experiment 1: A two-dimensional square

The geometry is considered to be a square with 50 m side, meshed with 1 m elements. This test is inspired by the validation tests performed in the paper of Bambeger et al. 1988. The paraxial conditions (resp. absorbing boundary conditions) apply to the bottom, left, and right borders for the PSD simulation (resp. for the CAST3M simulation). Figure 5.8 illustrates the geometry, red borders depict the absorbing (paraxial) borders and the green one depicts the free boundary condition.

The essential algorithmic parameters concerning time discretization are enlisted below, while the material properties are tabulated in table 5.3.

- Time step used for the generalized- α scheme is $dt = 0.01$ sec

⁴The CAST3M numerical experiments are performed by Reine Fares - Research Engineer - CEA/SEMT.

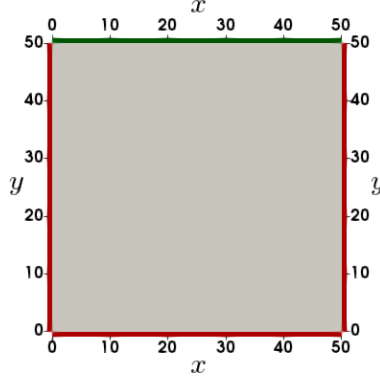


Figure 5.8: The two-dimensional geometry with paraxial borders in red and the free field border in green.

- The generalized- α parameters read $\alpha_m = 0.0$ and $\alpha_f = 0.0$. Note that these null values for α_m and α_f transforms the generalized- α time discretization scheme into a Newmark- β time discretization scheme. Hence, a Newmark- β is used both in PSD and CAST3M.
- The simulation is run for $t = 4.0$ seconds, hence requiring 400 iterations of the solver.

Case	ρ [kg m $^{-3}$]	E [Pa]	ν
Test 1	2500	6.62E6	0.45

Table 5.3: Parameters for the seismic test.

Before proceeding to the simulation comparison it is notified that meshes used by PSD and CASTEM, are triangular and quad type, respective. Figure 5.9 illustrates the difference between the PSD and the CASTEM meshes.

5.3.2 Test 1: top loading of the square

We test how the solvers behave when the free boundary is loaded.

- Concerning the loading, on the center region of the top border we apply a small sinusoidal excitation spread over 1 seconds. The applied force reads:

$$\int_{\partial\Omega} (\sigma \cdot \mathbf{n}) \cdot \mathbf{v} = \int_{\partial\Omega} (\rho c_p (\sin(2\pi t/1.0)) \mathbb{1}_{[x>20 \text{ \& } x<30 \text{ \& } y=50]} \times \mathbb{1}_{[t \leq 1]}) v_1$$

5.3.3 Test 2: bottom loading of the square

We test how the solvers behave when one of the paraxial (absorbing) boundary is loaded.

- Concerning the loading, on the center region of the bottom border we apply a small sinusoidal excitation spread over 1 seconds. The applied force reads:

$$\int_{\partial\Omega} (\sigma \cdot \mathbf{n}) \cdot \mathbf{v} = \int_{\partial\Omega} (\rho c_p (\sin(2\pi t/1.0)) \mathbb{1}_{[x>20 \text{ \& } x<30 \text{ \& } y=0]} \times \mathbb{1}_{[t \leq 1]}) v_1$$

5.3.4 Numerical experiment 2: 3D case with complex geometry

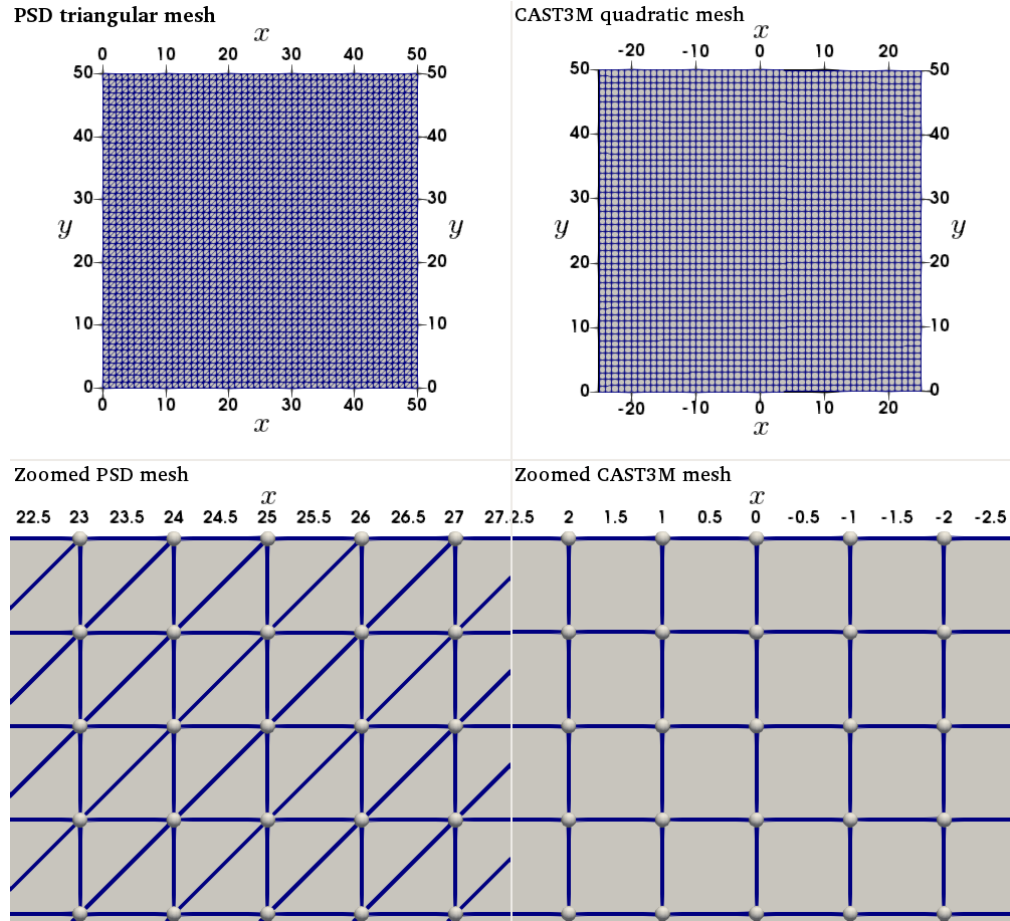


Figure 5.9: Meshes used by CAST3M (right) and PSD (left).

Case	package	version	time	boundary
Test 1	PSD	sequential	96	paraxial
Test 1	PSD	sequential-opt.	45	paraxial
Test 1	PSD	parallel	9	paraxial
Test 1	CAST3M	sequential	180	Lysmer-type

Table 5.4: CPU time comparison of CAST3M and PSD for different test/versions. CPU time is given in seconds, PSD version sequential-opt. means PSD with the GFP library (GoFastPlugins), by default the GFP library is used for PSD parallel version. As the mesh is tiny, only 4 MPI processes are used in the PSD parallel version.

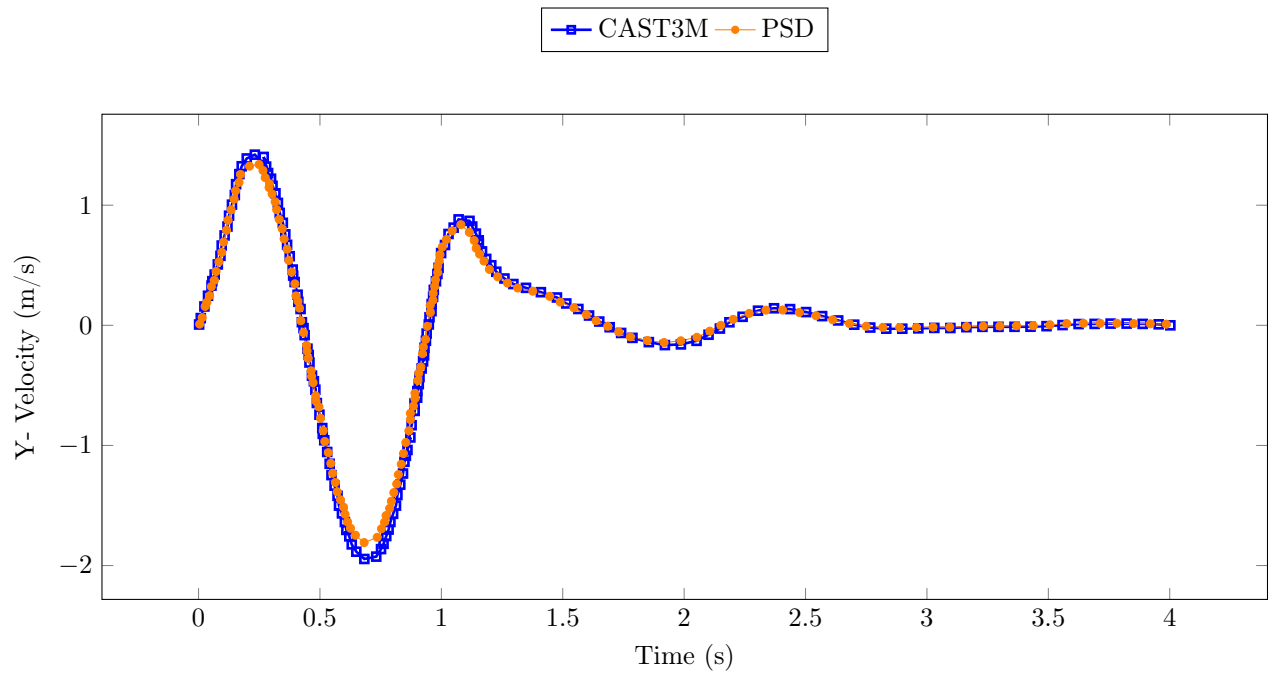


Figure 5.10: Test 1 results. Comparison of Y-velocities of a point $\mathbf{x} = (25, 50)$ obtained by CAST3M and PSD for a 4 second simulation with 1 second sinusoidal wave excitation.

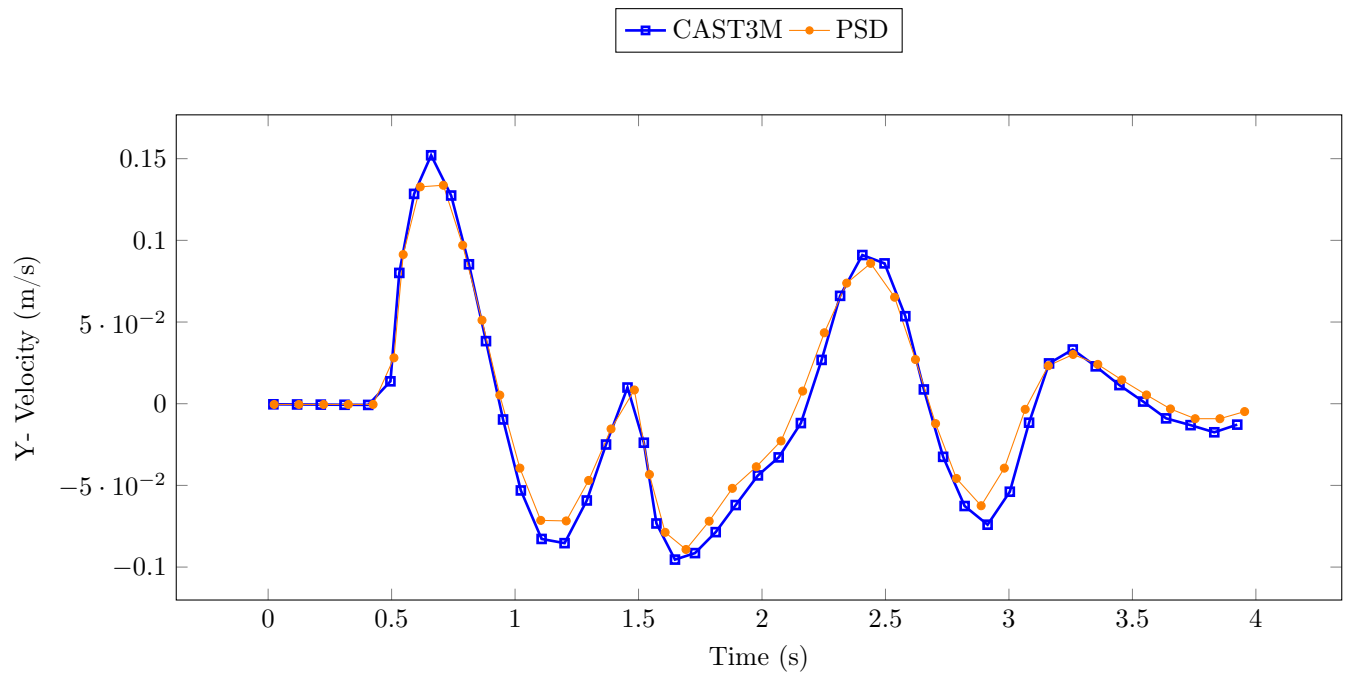


Figure 5.11: Test 1 results. Comparison of Y-velocities of a point $\mathbf{x} = (25, 0)$ obtained by CAST3M and PSD for a 4 second simulation with 1 second sinusoidal wave excitation.

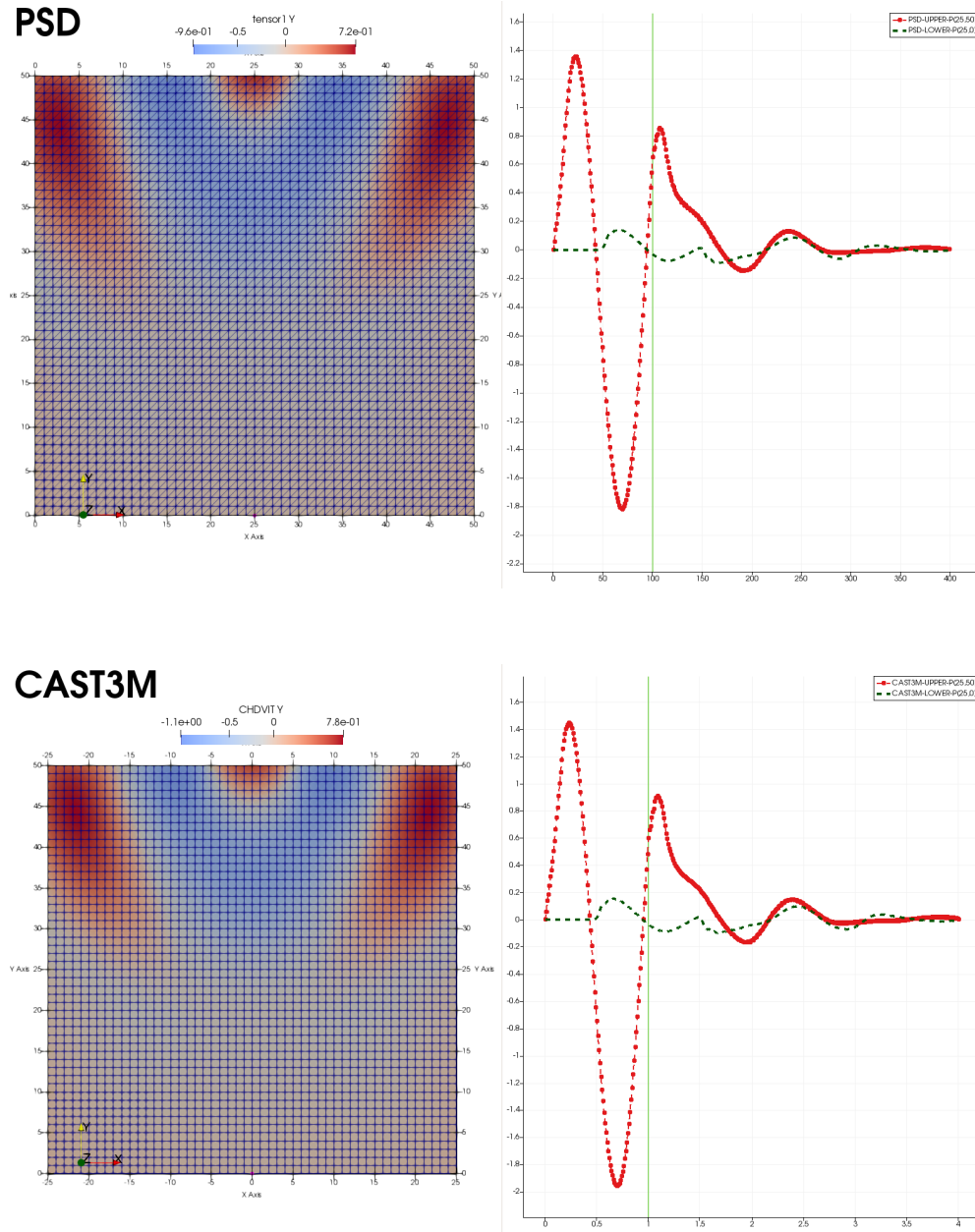


Figure 5.12: Comparison of simulations performed in CAST3M and PSD. Left: Y-velocity field snapshot at $t = 1.0$ second. Right: Top and bottom border point ($x = 25$) time history for Y-velocities.

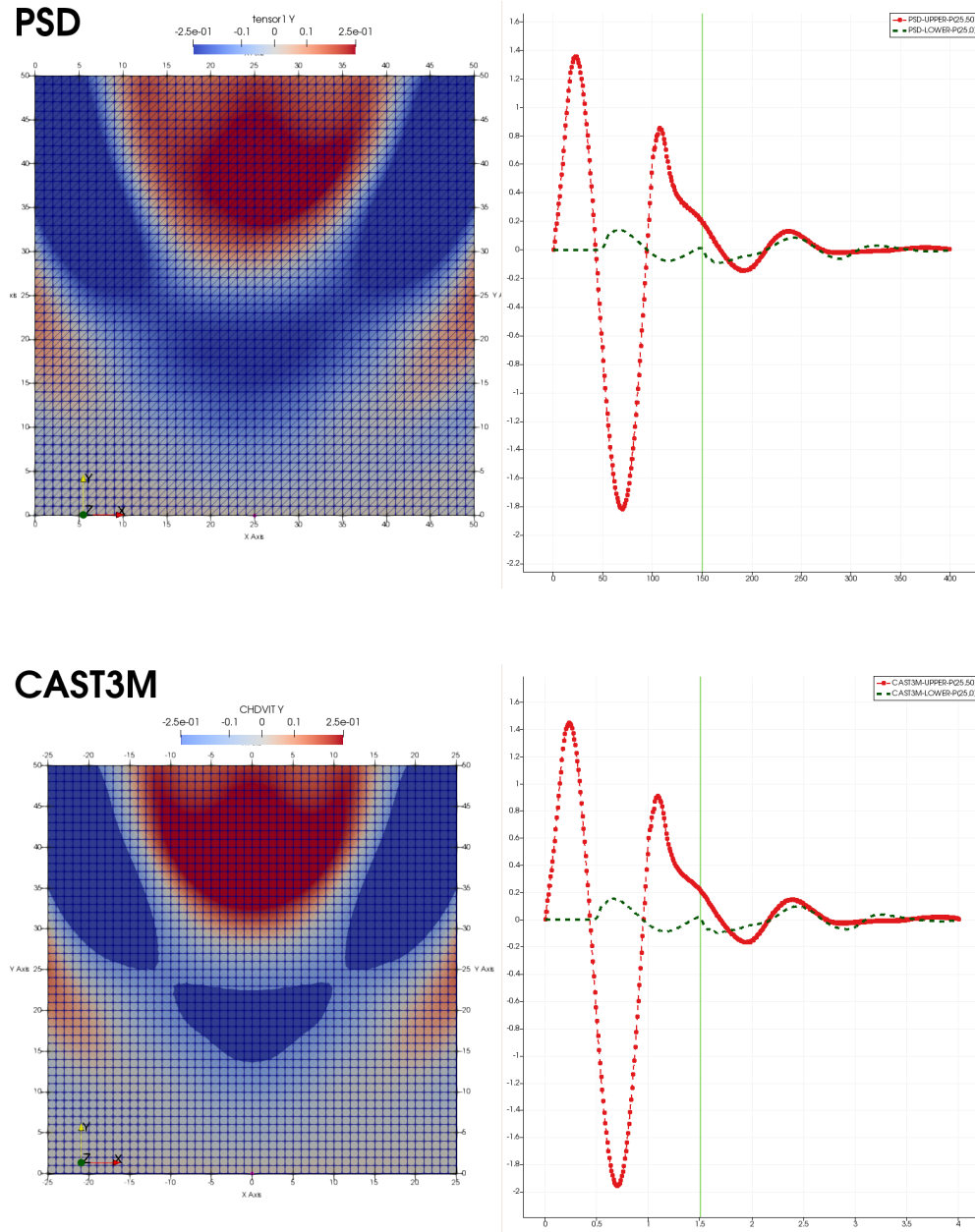


Figure 5.13: Comparison of simulations performed in CAST3M and PSD. Left: Y-velocity field snapshot at $t = 1.5$ second. Right: Top and bottom border point ($x = 25$) time history for Y-velocities.

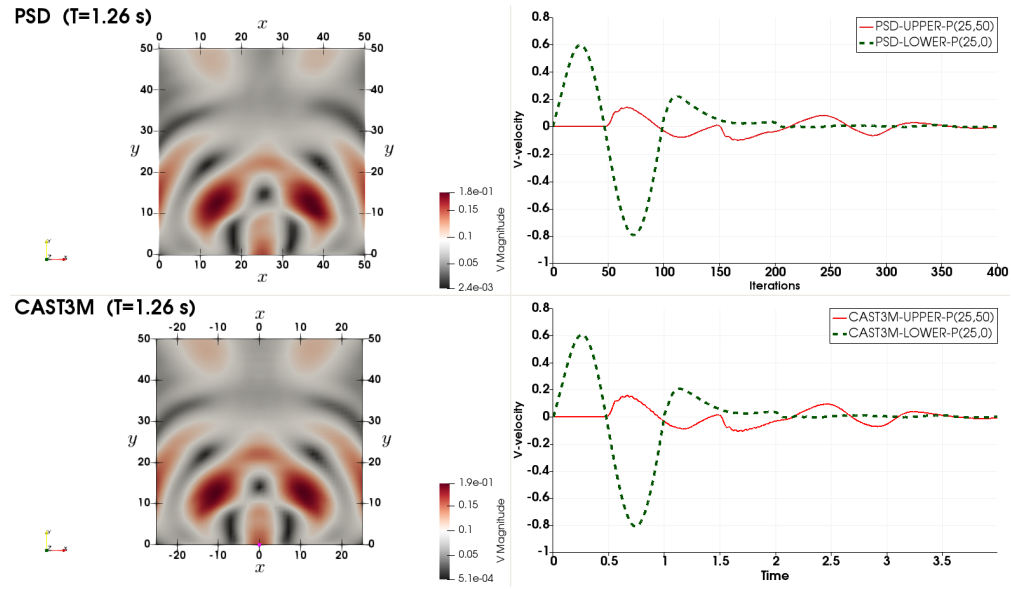


Figure 5.14: Comparison of simulations performed in CAST3M and PSD. Left: Y-velocity field snapshot at $t = 1.26$ second. Right: Top and bottom border point ($x = 25$) time history for Y-velocities.

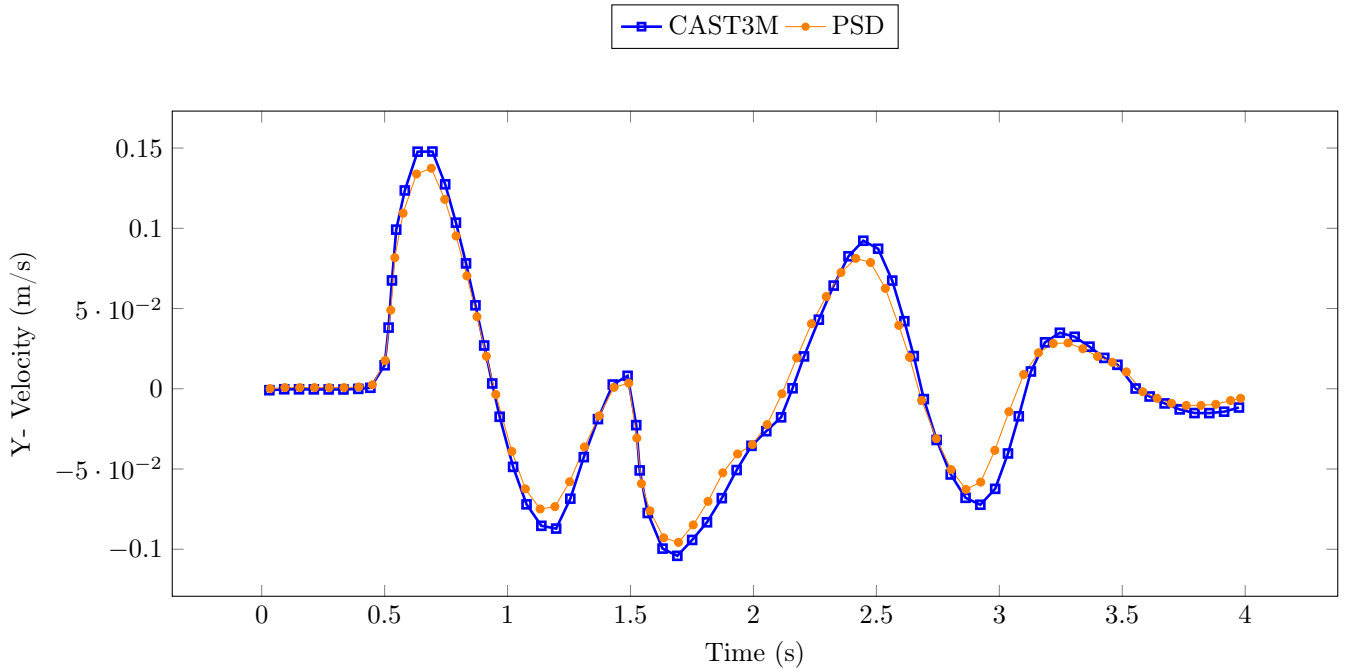


Figure 5.15: Test 2 results. Comparison of Y-velocities of a point $\mathbf{x} = (25, 50)$ obtained by CAST3M and PSD for a 4 second simulation with 1 second sinusoidal wave excitation.

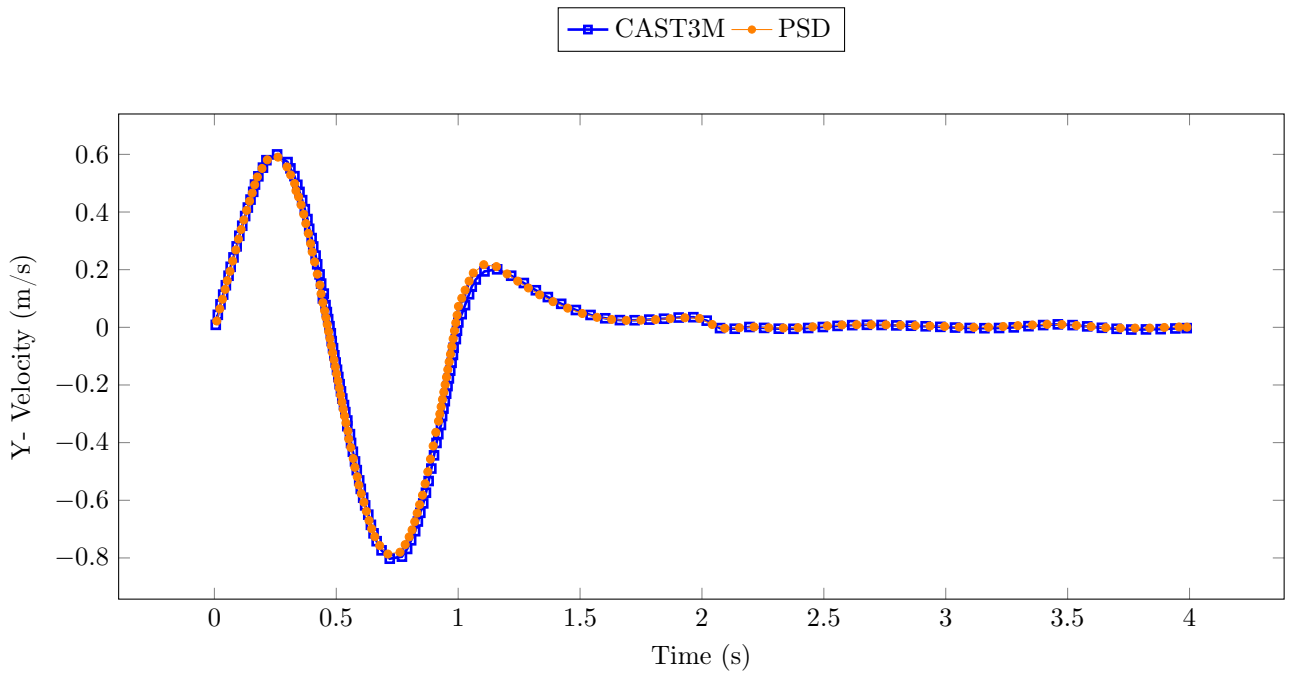


Figure 5.16: Test 2 results. Comparison of Y-velocities of a point $x = (25, 0)$ obtained by CAST3M and PSD for a 4 second simulation with 1 second sinusoidal wave excitation.

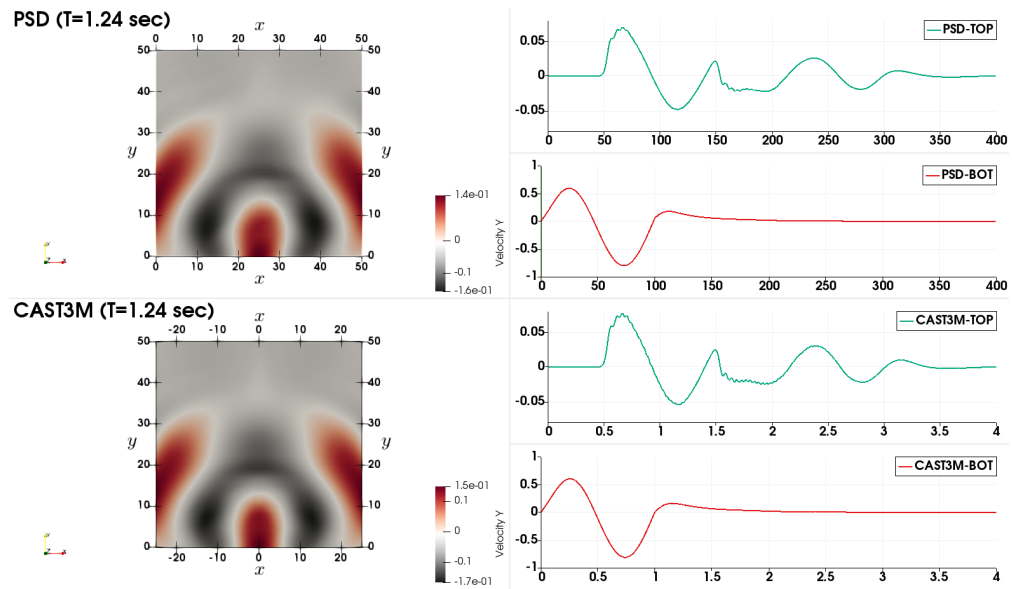


Figure 5.17: Comparison of simulations performed in CAST3M and PSD. Left: Y-velocity field snapshot at $t = 1.26$ second. Right: Top and bottom border point ($x = 25$) time history for Y-velocities.

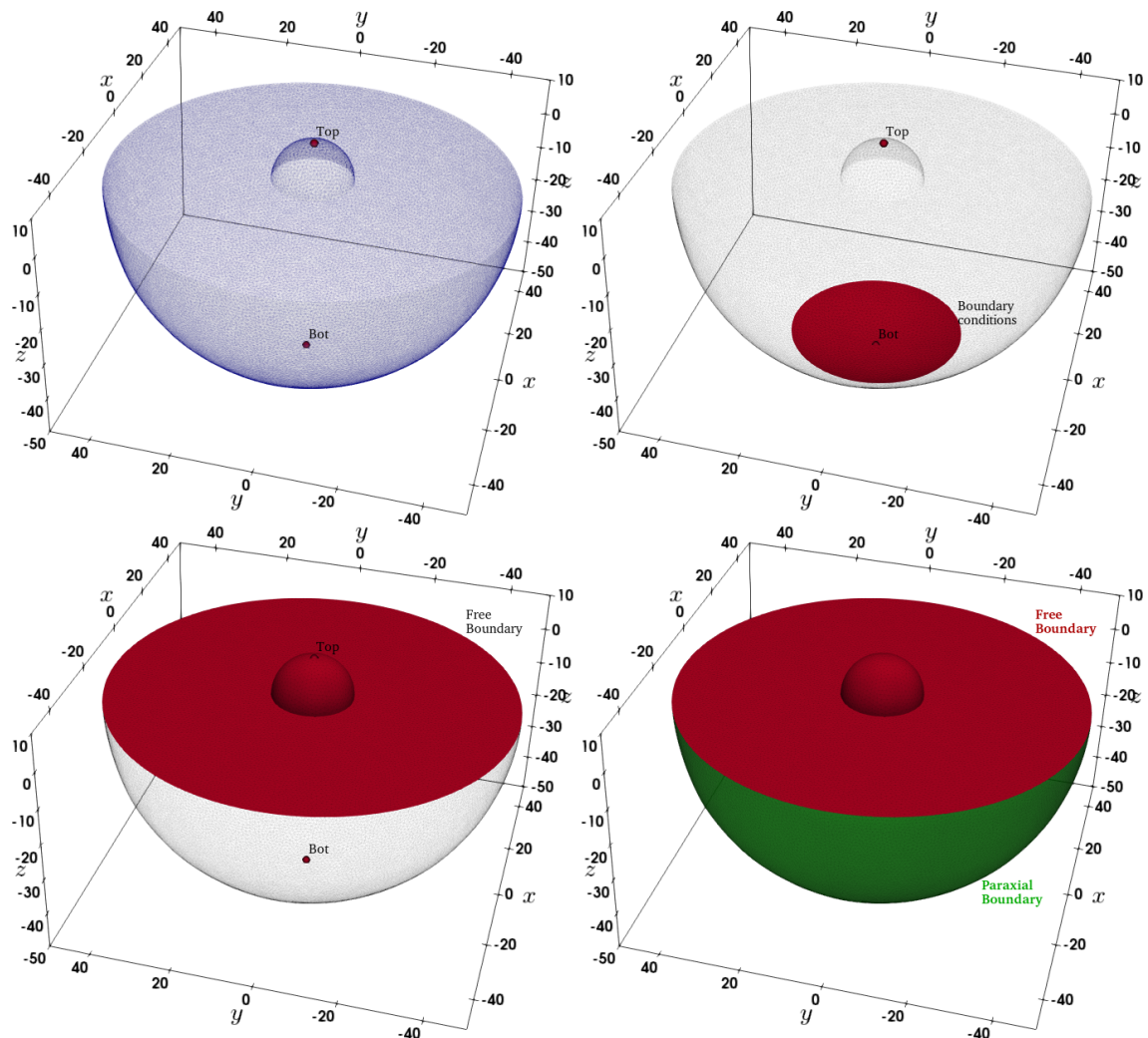


Figure 5.18: Seismic 3D cased with complex geometry and boundary conditions.

CAST3M Vs. PSD 3D Test

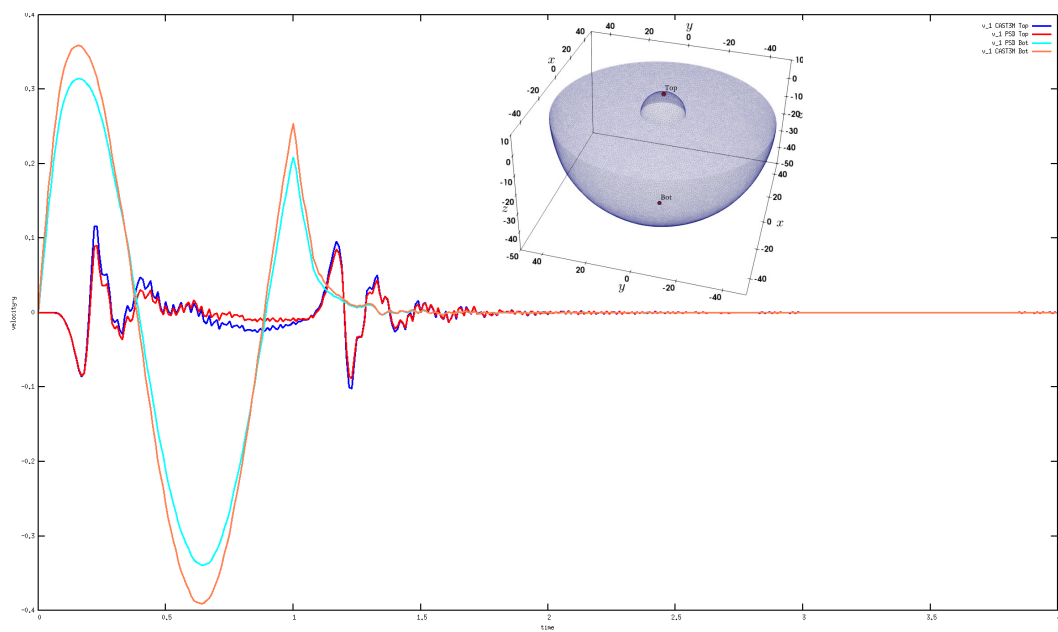


Figure 5.19: Comparison of 3D simulations performed in CAST3M and PSD.

Chapter 6

Functions and descriptions

6.1 Flags for PSD _ PreProcess

The PSD _ PreProcess relies heavily on command line flags for user interaction. These flags become a medium of communication between the user and the PSD solver. Three types of flags can be used i) **int** type : these are integer type flags which expect an integer argument, ii) **string** type : these flags expect a string argument, and iii) **bool** type : these are boolean type flags with no argument.

6.1.1 Integer type flags used for PSD _ PreProcess

-dirichletpointconditions	Number of Dirichlet points. Default 0.
-dirichletconditions	Number of Dirichlet boundaries. Default 0.
-bodyforceconditions	Number of regions to which body force is applied. Default 0.
-tractionconditions	Number of Neumann/traction boundaries. Default 0.
-parmetis_worker	Active when mesh partitioner is parmetis.
-dimension	Dimension of problem. 2 for 2D 3 for 3D. Default 2.
-lagrange	Lagrange order used for building FE space. Default 1 for P1.

6.1.2 String type flags used for PSD _ PreProcess

-timediscretization	Time discretization type. Use generalized-alpha newmark-beta hht-alpha central-difference.
-nonlinearmethod	Nonlinear method type. Use Picard Newton-Raphson.
-partitioner	Mesh partitioner. Use metis scotch parmetis.
-postprocess	Indicate postprocessing quantity. Use u v a phi uphi uva.
-doublecouple	Soil dynamics double couple boundary condition. Use force-based displacement-based.
-reactionforce	Reaction force calculation method. Use stress-based variational-based.
-problem	Interested problem. Use linear-elasticity damage elastodynamics soildynamics.
-model	Interested model. Use hybrid-phase-field Mazar pseudo-nonlinear.

6.1.3 Bool type flags used for PSD _ PreProcess

<code>-help</code>	Helping message on the terminal.
<code>-debug</code>	OpenGL plotting routine for displaying solution.
<code>-useGFP</code>	Activate use of GoFastPlugins. A suite of C++ plugins.
<code>-timelog</code>	To setup time logging for various phases of the solver.
<code>-useRCM</code>	Mesh level renumbering via Reverse Cuthill McKee.
<code>-vectorial</code>	Generate vectorial space solver for non-linear.
<code>-sequential</code>	To generate a sequential PSD solver.
<code>-fastmethod</code>	Produce a fast solver (more optimized).
<code>-pointprobe</code>	Setup a point probe to record variables.
<code>-energydecomp</code>	Hybrid phase-field energy decomposition.
<code>-top2vol-meshing</code>	top-ii-vol point source meshing for soil-dynamics.
<code>-getreactionforce</code>	Extraction reactions at surface.
<code>-plotreactionforce</code>	Live pipe plotting using GnuPlot.

6.2 Flags as per physics

Linear Elasticity	Damage Mechanics	Elastodynamics	Soildynamics
<p>INT TYPE</p> <ul style="list-style-type: none"> <code>-dirichletpointconditions</code> <code>-dirichletconditions</code> <code>-bodyforceconditions</code> <code>-tractionconditions</code> <code>-parmetis_worker</code> <code>-dimension</code> <code>-lagrange</code> <p>STRING TYPE</p> <ul style="list-style-type: none"> <code>-partitioner</code> <code>-postprocess</code> <code>-problem</code> <p>BOOL TYPE</p> <ul style="list-style-type: none"> <code>-sequential</code> <code>-fastmethod</code> <code>-timelog</code> <code>-useGFP</code> <code>-useRCM</code> <code>-debug</code> <code>-help</code> 	<p>INT TYPE</p> <ul style="list-style-type: none"> <code>-dirichletpointconditions</code> <code>-dirichletconditions</code> <code>-bodyforceconditions</code> <code>-tractionconditions</code> <code>-parmetis_worker</code> <code>-dimension</code> <code>-lagrange</code> <p>STRING TYPE</p> <ul style="list-style-type: none"> <code>-nonlinearmethod</code> <code>-reactionforce</code> <code>-partitioner</code> <code>-postprocess</code> <code>-problem</code> <code>-model</code> <p>BOOL TYPE</p> <ul style="list-style-type: none"> <code>-plotreactionforce</code> <code>-getreactionforce</code> <code>-energydecomp</code> <code>-sequential</code> <code>-vectorial</code> <code>-timelog</code> <code>-useGFP</code> <code>-useRCM</code> <code>-debug</code> <code>-help</code> 	<p>INT TYPE</p> <ul style="list-style-type: none"> <code>-dirichletpointconditions</code> <code>-dirichletconditions</code> <code>-bodyforceconditions</code> <code>-tractionconditions</code> <code>-parmetis_worker</code> <code>-dimension</code> <code>-lagrange</code> <p>STRING TYPE</p> <ul style="list-style-type: none"> <code>-timediscretization</code> <code>-partitioner</code> <code>-postprocess</code> <code>-problem</code> <code>-model</code> <p>BOOL TYPE</p> <ul style="list-style-type: none"> <code>-sequential</code> <code>-timelog</code> <code>-useGFP</code> <code>-useRCM</code> <code>-debug</code> <code>-help</code> 	<p>INT TYPE</p> <ul style="list-style-type: none"> <code>-dirichletpointconditions</code> <code>-dirichletconditions</code> <code>-bodyforceconditions</code> <code>-tractionconditions</code> <code>-parmetis_worker</code> <code>-dimension</code> <code>-lagrange</code> <p>STRING TYPE</p> <ul style="list-style-type: none"> <code>-doublecouple</code> <code>-postprocess</code> <code>-partitioner</code> <code>-postprocess</code> <code>-problem</code> <code>-model</code> <p>BOOL TYPE</p> <ul style="list-style-type: none"> <code>-top2vol-meshing</code> <code>-sequential</code> <code>-timelog</code> <code>-useGFP</code> <code>-useRCM</code> <code>-debug</code> <code>-help</code>

6.3 Functions in gofastplugins.cpp

6.3.1 GFPeigen

`GFPeigen(A,Eval,Evec);`

A is a matrix, Eval is vector returning eigenvalues, Evec is the matrix returning eigenvectors.

This is a call by reference pointer-based function of GFP library. It is used for computation of the eigenvalues and eigenvectors of a real symmetric matrix (upper triangular). This function inturn uses LAPACK libraries `dsyev_` for calculation of eigenvalues and eigenvectors.

The function `GFPeigen` which can be called from PSD is coded as `lapack_dsyevIn` function within the `gofastplugins.cpp`. this function argument 1: `A` is the supplied symmetric matrix, argument 2: `vp` are the output eigenvalues and argument 3: `vectp` are the output eigenvectors.

```

1 long lapack_dsyev (KNM<double> *const &A, KN<double> *const &vp, KNM<double> *
2   const &vectp)
3 {
4     intblas n = A->N();
5     KNM<double> mat(*A);
6
7     .
8     .
9     dsyev_(&JOBZ, &UPLO, &n, mat, &n, *vp, w, &lw, &info);
10    .
11    .
12    *vectp = mat;
}
```

6.3.2 GFPeigenAlone

`GFPeigen(A,Eval,Evec);` `A` is a matrix, `Eval` is vector returning eigenvalues.

This is a call by reference pointer based function of GFP library. It is used for computation of the eigenvalues of a real symmetric matrix (upper triangular). This function inturn uses LAPACK library for calculation of eigenvalues. The function `GFPeigenAlone` which can be called from PSD is coded as `lapack_dsyevAlone` function within the `gofastplugins.cpp`. In this function argument 1: `A` is the supplied symmetric matrix and argument 2: `vp` is the output eigenvalues of matrix `A` .

```

1 long lapack_dsyevAlone (KNM<double> *const &A, KN<double> *const &vp)
```

6.3.3 GFPmaxintwoFEfields

This is a call by reference pointer based function of GFP library. It is used to find out max between two real numbers `f` and `f1` (two 1D arrays). The max is stored in array `f`.

```

1 double GFPmaxintwoP1(KN<double> *const & f, KN<double> *const & f1)
```

Chapter 7

Gallery

This chapter showcases some test cases that have been performed with PSD.

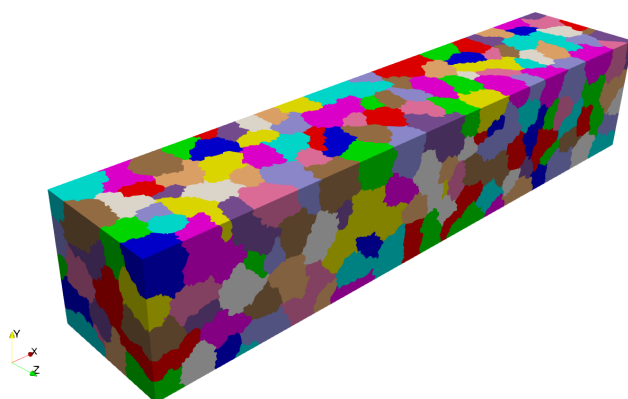


Figure 7.1: 90 M dof with 400 partitions.

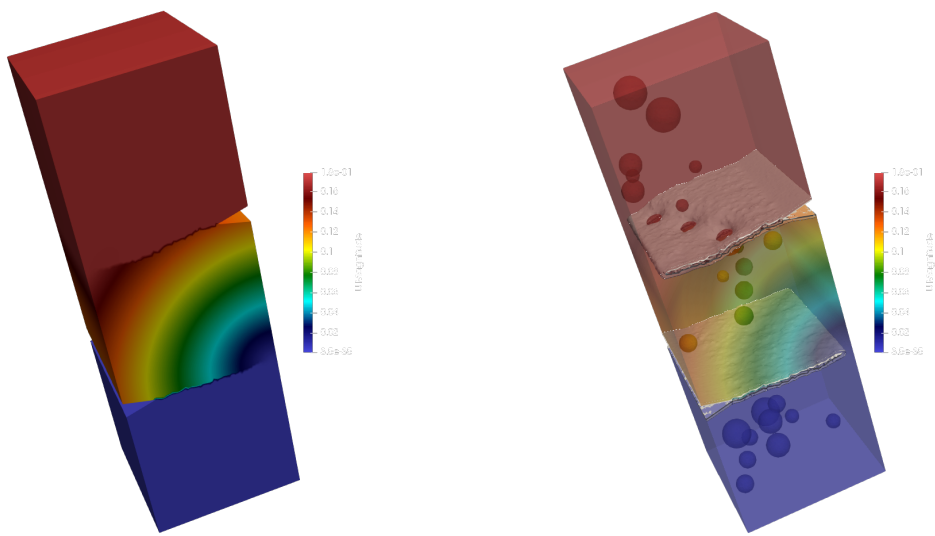


Figure 7.2: Perforated concrete bar cracking.

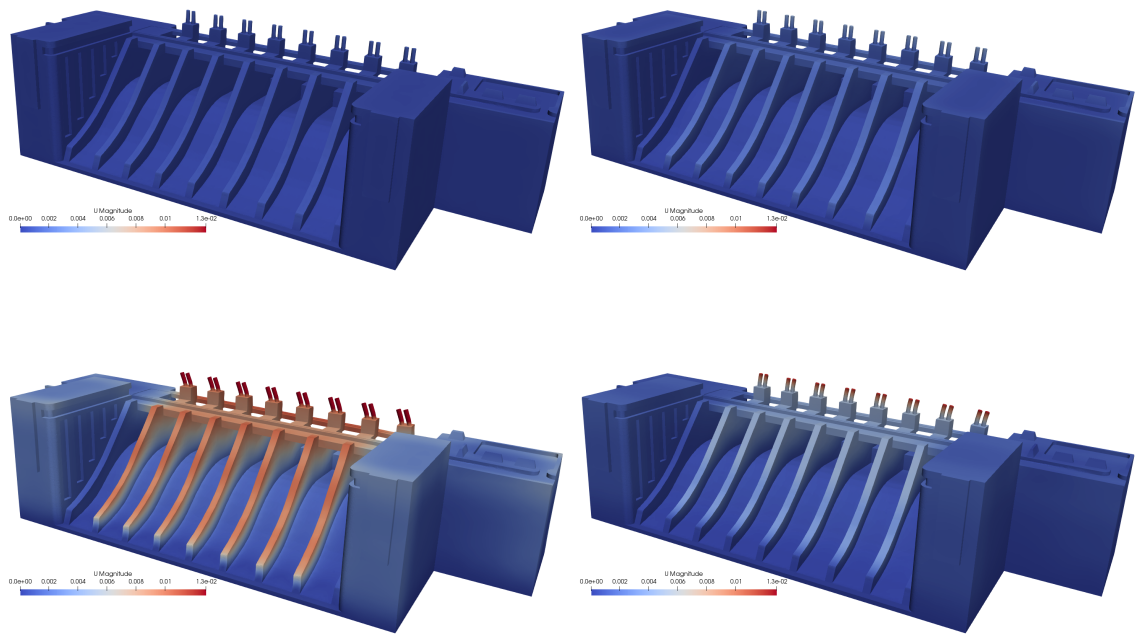


Figure 7.3: Full scale dam under seismic load.

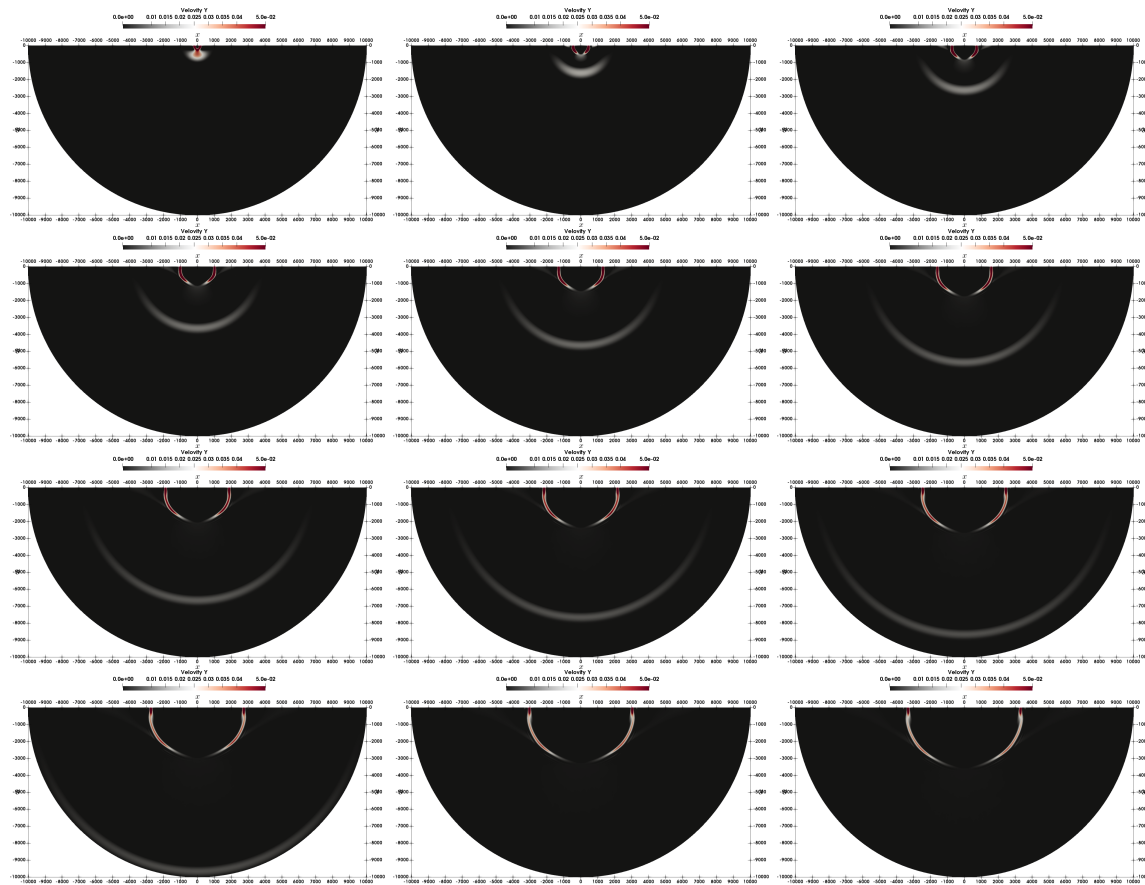


Figure 7.4: Seismic signal dispersion in soil.

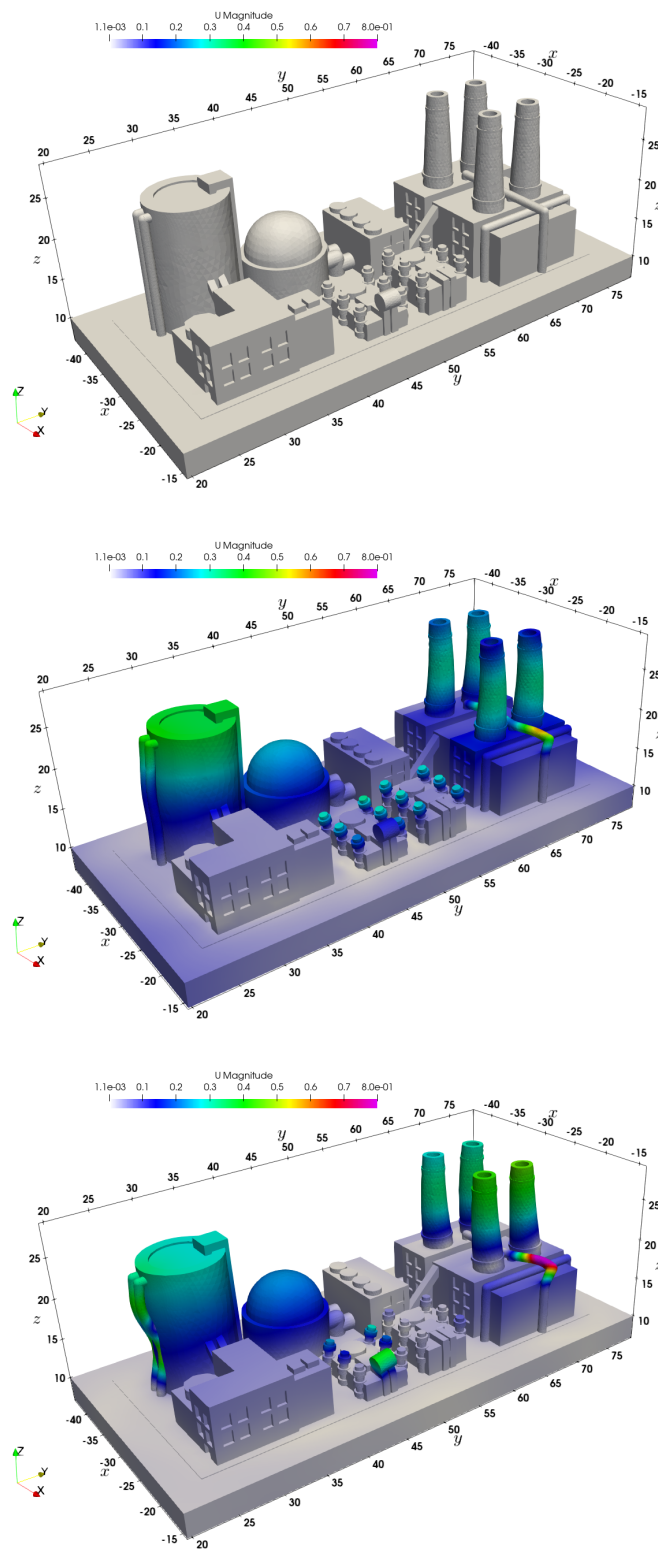


Figure 7.5: Seismic signal on nuclear site.

Bibliography

- [1] Marreddy Ambati, Tymofiy Gerasimov, and Laura De Lorenzis. “A review on phase-field models of brittle fracture and a new fast hybrid formulation”. In: *Computational Mechanics* 55.2 (2014), pp. 383–405.
- [2] Hanen Amor, Jean-Jacques Marigo, and Corrado Maurini. “Regularized formulation of the variational brittle fracture with unilateral contact: Numerical experiments”. In: *Journal of the Mechanics and Physics of Solids* 57.8 (2009), pp. 1209–1229.
- [3] D Aubry et al. “Local amplification of a seismic incident field through an elastoplastic sedimentary valley”. In: *International conference on numerical methods in geomechanics*. 1985, pp. 1343–1350.
- [4] Jean-Pierre Berenger. “A perfectly matched layer for the absorption of electromagnetic waves”. In: *Journal of computational physics* 114.2 (1994), pp. 185–200.
- [5] Jintai Chung and GM1223971 Hulbert. “A time integration algorithm for structural dynamics with improved numerical dissipation: the generalized- α method”. In: (1993).
- [6] Robert Clayton and Björn Engquist. “Absorbing boundary conditions for acoustic and elastic wave equations”. In: *Bulletin of the seismological society of America* 67.6 (1977), pp. 1529–1540.
- [7] Luis Eça et al. “Verification of RANS solvers with manufactured solutions”. In: *Engineering with computers* 23.4 (2007), pp. 253–270.
- [8] Björn Engquist and Andrew Majda. “Absorbing boundary conditions for numerical simulation of waves”. In: *Proceedings of the National Academy of Sciences* 74.5 (1977), pp. 1765–1766.
- [9] Silvano Erlicher, Luca Bonaventura, and Oreste S Bursi. “The analysis of the generalized- α method for non-linear dynamic problems”. In: *Computational Mechanics* 28.2 (2002), pp. 83–104.
- [10] Frédéric Hecht. “BAMG: bidimensional anisotropic mesh generator”. In: *User Guide. INRIA, Rocquencourt* (1998).
- [11] Frédéric Hecht. “New development in FreeFem++”. In: *Journal of numerical mathematics* 20.3-4 (2012), pp. 251–266.
- [12] Hans M Hilber, Thomas JR Hughes, and Robert L Taylor. “Improved numerical dissipation for time integration algorithms in structural dynamics”. In: *Earthquake Engineering & Structural Dynamics* 5.3 (1977), pp. 283–292.
- [13] Hirshikesh, Sundararajan Natarajan, and Ratna Kumar Annabattula. “A FEniCS implementation of the phase field method for quasi-static brittle fracture”. In: *Frontiers of Structural and Civil Engineering* 13.2 (2018), pp. 380–396.
- [14] C Hoff and PJ Pahl. “Development of an implicit method with numerical dissipation from a generalized single-step algorithm for structural dynamics”. In: *Computer Methods in Applied Mechanics and Engineering* 67.3 (1988), pp. 367–385.
- [15] Thomas JR Hughes. *The finite element method: linear static and dynamic finite element analysis*. Courier Corporation, 2012.
- [16] Heeyeong Jeong et al. “Phase field modeling of crack propagation under combined shear and tensile loading with hybrid formulation”. In: *Computational Materials Science* 155 (2018), pp. 483–492.
- [17] Guowei Liu et al. “Abaqus implementation of monolithic and staggered schemes for quasi-static and dynamic fracture phase-field model”. In: *Computational Materials Science* 121 (2016), pp. 35–47.
- [18] John Lysmer and Roger L Kuhlemeyer. “Finite dynamic model for infinite media”. In: *Journal of the Engineering Mechanics Division* 95.4 (1969), pp. 859–878.

- [19] Hormoz Modaressi and Ikhlef Benzenati. “Paraxial approximation for poroelastic media”. In: *Soil Dynamics and Earthquake Engineering* 13.2 (1994), pp. 117–129. ISSN: 0267-7261. DOI: [https://doi.org/10.1016/0267-7261\(94\)90004-3](https://doi.org/10.1016/0267-7261(94)90004-3). URL: <http://www.sciencedirect.com/science/article/pii/0267726194900043>.
- [20] Nathan Mortimore Newmark et al. “A method of computation for structural dynamics”. In: American Society of Civil Engineers. 1959.
- [21] William L Oberkampf, Timothy G Trucano, and Charles Hirsch. “Verification, validation, and predictive capability in computational engineering and physics”. In: *Applied Mechanics Reviews* 57.5 (2004), pp. 345–384.
- [22] Shawn D Pautz. *Verification of transport codes by the method of manufactured solutions: the ATTILA experience*. Tech. rep. Los Alamos National Lab., NM (US), 2001.
- [23] Patrick J Roache. “Verification of codes and calculations”. In: *AIAA journal* 36.5 (1998), pp. 696–702.
- [24] WL Wood, M Bossak, and OC Zienkiewicz. “An alpha modification of Newmark’s method”. In: *International Journal for Numerical Methods in Engineering* 15.10 (1980), pp. 1562–1566.
- [25] Olgierd C Zienkiewicz and Robert L Taylor. *The finite element method, ; volume 1: basic formulation and linear problems*. 1994.